CERAMIC/CARBON-BASED COMPOSITE MATERIALS FOR THE CONTAINMENT OF MOLTEN CHLORIDES FOR THERMAL ENERGY STORAGE

by

Elizabeth Laskowski

A Thesis

Submitted to the Faculty of Purdue University

In Partial Fulfillment of the Requirements for the degree of

Master of Science in Materials Engineering

School of Materials Engineering

West Lafayette, Indiana

December 2020

THE PURDUE UNIVERSITY GRADUATE SCHOOL
STATEMENT OF COMMITTEE APPROVAL

Dr. Kenneth Sandhage, Chair

School of Materials Engineering

Dr. John Blendell

School of Materials Engineering

Dr. Kevin Trumble

School of Materials Engineering

Approved by:

Dr. David Bahr

To My Darling Husband-

Your endless love and support are forever my anchor. May this chapter be just one of many on our journey through this beautiful life.

ACKNOWLEDGMENTS

It is with deep gratitude that I thank Dr. Kenneth Sandhage for extending multiple opportunities to me, for providing precious scientific guidance throughout my entire experience at Purdue, and for being so supportive during my transition to a master's degree. Thank you for your encouragement, for creating a space that offers stability, structure to grow, and ultimately the freedom to explore a diverse range of research.

Thank you to Dr. Liangjuan Gao for her assistance and insight throughout the entire project, especially for sharing her SEM sample preparation and analysis expertise. Thank you to Dr. Mario Caccia for his guidance in the final stretch and to Dr. Saeed Bagherzadeh for his support in designing a safe pressure vessel. Thank you to the MIT team and WAM corporation for their partnership in tackling this engineering challenge and to the Department of Energy for their financial support and rigorous oversight of the project. Finally, thank you to Purdue University for the multiple resources extended to support my studies as a student and a researcher.

I also express deep gratitude to my previous advisor Dr. Elizabeth Glogowski for her steadfast support on my journey and priceless mentorship. Thank you for taking a chance on me and for introducing me to the beautiful world of research.

Additionally, I would like to thank my family for their unwavering support. To my mother for the countless encouraging phone calls, for being instrumental in sparking my curiosity from a young age, and for showing me that all things can blossom and heal when showered in love. And to my late father, thank you for believing in me, always pushing me to work harder, and perhaps most importantly for showing me that life has multiple seasons that are meant to be enjoyed to their fullest.

To my friends for their support, especially Jordan for being a pillar of sanity and motivation, and Shannon for always refreshing my soul and reminding me that life is meant to be colorful.

It is also with a thankful heart that I acknowledge the daily guidance from my Lord and Savior Jesus Christ, and the unwavering peace of knowing that my life is in his hands.

And finally, to my darling husband, Ivan, thank you for putting the sunshine in my soul, for providing a sanctuary from the daily storms, and for always passionately supporting my dreams. Thank you for putting your life on hold so I might enrich mine, and above all else, thank you for your love. May my work be a love letter to you.

TABLE OF CONTENTS

LIST OF TABLES

LIST OF FIGURES

LIST OF ABBREVIATIONS

Ar- Argon

CA- Calcium Monoaluminate

CA_2- Calcium Dialuminate

CA_6- Calcium Hexaluminate

CA_6C- Calcium Hexaluminate Based Castable

CSP- Concentrated Solar Power

DOE- Department of Energy

EDX- Energy dispersive X-ray analysis

LCOE- Levelized Cost of Electricity

MIT- Massachusetts Institute of Technology

MKN- Magnesium/Potassium/Sodium salt mixture

OD- Outer Diameter

p_{O2}- Oxygen Partial Pressure

ppm- part per million

RPM- Rotations per Minute

SEM- Scanning Electron Microscopy

TES- Thermal Energy Storage

WAM- Westmoreland Advanced Materials

XRD- X-ray Diffraction

ABSTRACT

The desire to mitigate climate change and reduce energy dependence on fossil fuels has launched global efforts towards finding renewable energy solutions. According to the U.S. Department of Energy, within the United States, solar sources account for about 1% of the electricity supply, a number that is expected to grow to 14% by 2030 and 27% by 2050. Such growth will be dependent on lowering the cost of concentrated solar power (CSP), which is a large-scale solar technology that concentrates the sun's heat rather than photovoltaic conversion. CSP offers relatively easy grid integration, and most importantly, can be naturally paired with thermal energy storage that allows electricity to be produced on demand even when the sun is not shining and has been the most cost-effective energy storage to date. Lowering the cost of CSP requires raising the operating temperatures above 700^{o}C. At these temperatures, traditionally used nitrate-based salts are no longer stable, and efforts have focused on using chloride-based salts, which offer high-temperature stabilities, low viscosities, and relatively high heat capacities. Additionally, seawater-derived chlorides ($CaCl_2$, $MgCl_2$, NaCl, and KCl) are cheap, plentiful, and nontoxic. However, such chlorides are especially corrosive, and finding a long term containment solution that is not corroded nor wet and penetrated by the molten chlorides has proved to be one of the most significant challenges to using chloride salts in CSP. The approach of this study is to combine the nonwetting behavior of carbonaceous materials with cost-effective castable ceramics. By evaluating the effectiveness of these carbon-ceramic systems, effective containment solutions for molten chlorides have been identified for low-cost thermal energy storage for CSP so as to enable CSP as a competitive alternative to fossil fuels.

1. INTRODUCTION

1.1 Global Energy Challenges

The desire to mitigate climate change and reduce energy dependence on fossil fuels has launched global efforts towards finding renewable energy solutions. Fossil fuel resources are not distributed equally worldwide and are partially responsible for the release of carbon dioxide and the resulting greenhouse gas effect. According to the EIA (U.S Energy Information Administration), global energy demands are projected to increase 48% by 2040, increasing the use of petroleum and other liquid fuels to over 121 million barrels per day [1]. Such energy demands are required for continued growth and sustain global prosperity but require the development of renewable sources that can meet such energy demands at an economical price, provide energy security, and mitigate environmental impact.

Renewable energy is the fastest-growing source of electricity, with growth at an average of 2.6% every year (compared to coal-derived power, which grows at just 0.6%) and is expected to increase from 22% of the global supply to 29% in 2040 [1]. Within the United States, renewable energy provided approximately 12% of the country's electricity supply in 2019, with about 1% coming from solar sources [2], which is an impressive increase from just 0.1% being provided by solar 10 years earlier [3]. While a small contribution to date, solar power has enormous technical potential. The amount of solar energy available to the United States in just 1 hour of noontime summer sun is almost equal to the annual U.S. electricity demand [3].

The U.S. Department of Energy (DOE) has research programs dedicated to improving electricity-generating technologies' performance to aggressively reduce the cost and emissions associated with the U.S. power sector [4]. In 2011, the DOE launched the SunShot Initiative with the goal to make solar electricity cost-competitive with conventional electricity by 2020, with serious efforts to reduce costs by 70% to raise solar production to meet 14% of the U.S. electricity demand by 2030 and 27% by 2050 [5]. Perhaps the most significant challenge solar energy faces is the intermittent nature of sunlight, which requires the energy to be collected and stored efficiently for consistent production. Concentrated solar power (CSP), a solar technology that concentrates the sun's heat rather than utilizing photoelectric conversion, offers the ability to

naturally integrate thermal energy storage and offer higher efficiencies, low operating costs, and good scale-up potential compared to other solar energy technologies [6].

1.2 Concentrated Solar Power

Concentrated solar power (CSP) is a particularly attractive electricity-generation solution due to its ability to be naturally paired with thermal energy storage, overcoming the daily and seasonally intermittent nature of solar power. Integrating high-temperature thermal energy storage offers one of the lowest-cost forms of energy storage that can be used for both short-term and long term storage and has demonstrated over 97% round-trip efficiencies [6] [7]. Additionally, CSP can offer higher capacities and better scalability compared to other renewable sources. However, CSP currently has a higher levelized cost of energy (LCOE) compared to other utility-scaled renewable options, as shown in the high/low LCOE comparison for subsidized and unsubsidized energy sources in Figure 1.1.

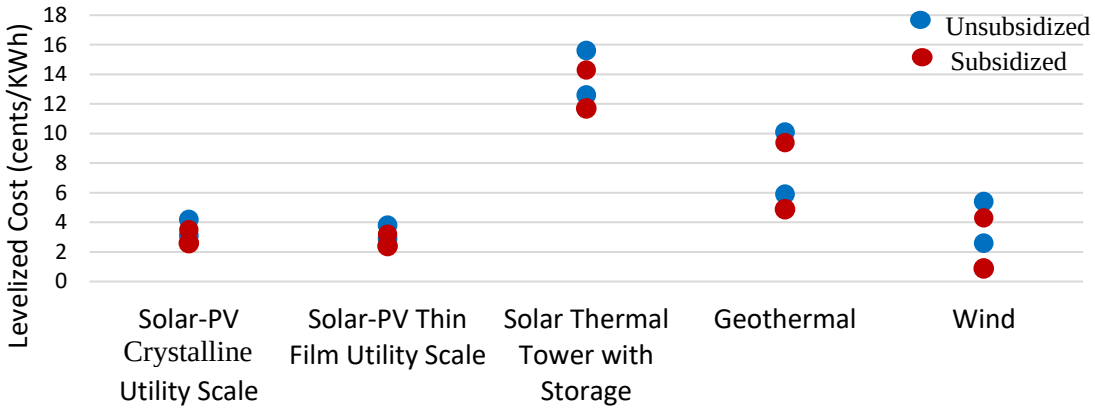

Figure 1.1. Levelized Cost of Energy (LCOE) Comparison for 2020 with and without U.S. Federal Tax Subsidies showing CSP as the highest costing utility-scale renewable option [8].

The high cost is the main challenge to implementing CSP as a competitive source of energy. The DOE SunShot initiative addresses this challenge with the set goal to reach 6 cents/kWh for CSP and 14 hours of thermal energy storage by 2020, a goal that was not met (reaching only 10 c/kWh in 2020 estimates) and has been revised to 5 cents/kWh and at least 12 hours of storage by 2030 [4], as shown in Figure 1.2.

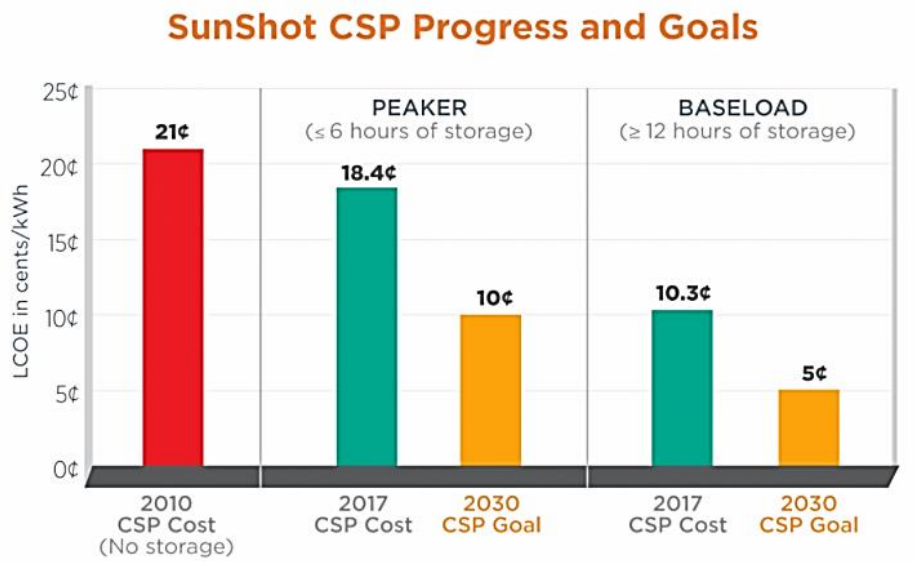

Figure 1.2. The progress and goals of lowering the LCOE of CSP from 2010 to 2030 [4].

Lowering costs requires increasing the thermal-to-electric conversion efficiency of CSP, which may be achieved by operating at higher temperatures, but which is a challenge that requires materials and components to be stable and function above 700^{o}C [9].

A CSP plant is composed of 4 core elements: solar concentrators, a high-temperature solar receiver, a fluid transport system, and a power generation block (e.g., Brayton cycle) [10]. The concentration of the solar heat is generally achieved through the use of sun-tracking mirrors that focus sunlight onto a solar receiver. The receiver can have several configurations, including troughs or dishes. However, the DOE third-generation demonstration site will use a receiving tower, referred to as a solar power tower [9]. The power tower heats a heat transfer fluid, which is then either pumped to a heat storage tank or directly to a heat exchanger, which transfers the heat to a working fluid, such as steam or supercritical CO_2, which powers turbines to generate electricity.

As mentioned, what makes CSP particularly powerful, is the ability to incorporate thermal energy storage into its design, which is achieved through a two-tank storage concept that uses a hot and cold tank to store the heat transfer fluid. A schematic illustration of the power tower and duel tank storage concept is shown in Figure 1.3.

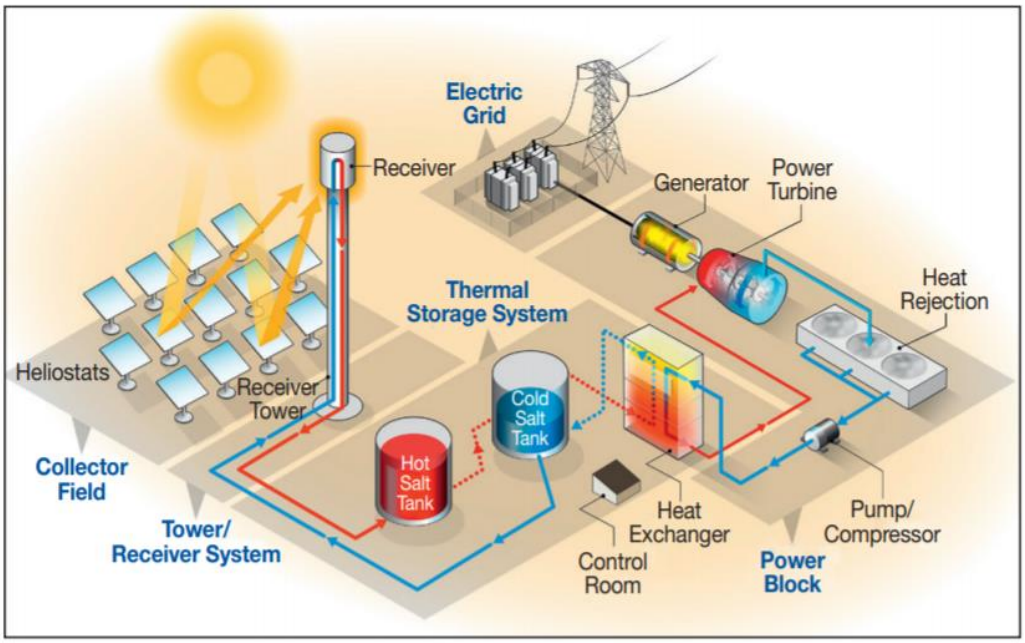

Figure 1.3. Schematic illustration of a concentrated solar power design with a molten salt power tower and direct thermal energy storage of heated molten salt in tanks [9].

Certain molten salts are considered among the best materials for CSP heat transfer fluids due to their stability at high temperatures, non-flammability, low viscosity, and low vapor pressure. [10]. The need for CSP operating temperatures above 700°C is incompatible with traditionally used nitrate-based salts, which are not stable at such temperatures [11] [12]. Thus, efforts have focused on the use of chloride-based salts, which offer higher temperature stability, low viscosity, and relatively high heat capacity [13]. Additionally, sea-derived chlorides ($CaCl_2$, $MgCl_2$, NaCl, and KCl) are cheap, plentiful, and nontoxic [14] [13]. The ternary chloride blend of 40/40/20 mole% $MgCl_2$/KCl/NaCl (MKN salt) has become a primary candidate of interest as a heat transfer and thermal energy storage media for CSP and has the potential to lower the cost of CSP enough to make it a competitive source of energy. While not the eutectic composition, this MKN salt composition still has a melting temperature of about 400°C and can be prepared with a cost-effective purification method using industrially-sourced salt [15].

1.3 Chloride Containment Material Considerations and Challenges

While chloride salt mixtures can promise low cost and good thermal storage, achieving cost-effective and long-term storage of molten salts at temperatures above 700°C has proven to be the largest barrier to implementing such molten chloride use in CSP [13]. Certain chloride salts are

especially corrosive due to their hydrophilic nature, which encourages the presence of corrosive impurities, such as MgOHCl and HCl, and their subsequent reactions with containment materials [11]. It is well accepted that the use of a low p_{O2} and low p_{H2O} cover gas is needed to suppress the formation of corrosive species in molten chlorides [11] [12] [13]. Maintaining a low p_{O2} environment enables the possibility to use carbon-containing refractories, as discussed through the work in this thesis, in approaching the challenge to find a containment solution that is not corroded by, and that is not wetted and penetrated by, the molten chloride salt, while maintaining a low cost to be implemented in thermal energy storage of molten chlorides for CSP.

Metal candidates, such as dense (nonporous) stainless steel and nickel-based alloys, can successfully prevent molten salt penetration. However, corrosion rates with metals are particularly challenging to keep low while maintaining a low cost. Such chloride corrosion challenges with commonly used structural materials are discussed in "High-Temperature Corrosion and Materials Applications" by Lai, and a summary of the corrosion results with MKN based salts are shown in Figure 1.4 [16]. None of the alloys survived after 456 hours at 900°C under an N_2 atmosphere. The DOE has set the requirement for materials to adhere to a corrosion rate of 15 µm/year in order to meet the 30-year longevity requirements of storage tank designs [17] [18].

	Weight change, mg/cm^2	
Alloy	**144 h**	**456 h**
304	Disintegrated	…
316	Disintegrated	…
800	Disintegrated	…
800H	−310	Disintegrated
556	−250	Disintegrated
Nickel	Disintegrated	…
600	−280	Disintegrated
214	−120	Disintegrated
X	Disintegrated	…
N	Disintegrated	…
S	−400	Disintegrated
230	−300	Disintegrated
X-750	Disintegrated	…
R-41	−150	Disintegrated
188	Disintegrated	…

N_2-(0.1–1H_2O)-(1–10O_2) was used for the cover gas. Source: Ref 9

Figure 1.4. Weight change measurements for metal samples in NaCl-KCl-$MgCl_2$ at 900°C [16].

Ding, et al. (2018) also investigated the corrosion of common metal materials, and as shown in Table 1.1, none of the alloys met the required DOE rate of 15 μm/year [11], with the expectation of operation under vacuum, which is a condition that is difficult and expensive to achieve in a large CSP application.

Table 1.1. Modified table from Ding, et al. [11] showing average corrosion rates for metallic alloys in molten chloride salts

Molten salts/ wt.-%	Alloy	T/°C	Atmosphere	Corrosion Time (hr)	Corrosion rate μm/year
$CaCl_2/MgCl_2/NaCl$ 43.6/17.7/38.7	Inc 625	600	Air	504	121
	HaX	600	Air	504	153
	HaB-3	600	Air	504	144
$KCl/MgCl_2/NaCl$ 20.4/55.1/24.5	SS 304	450-500	Vacuum	1000	<10
	SS 316	450-500	Vacuum	1000	~10
	SS 347	450-500	Vacuum	1000	~120
	HaN	450-500	Vacuum	1000	~50
	SS 304	900	N_2*	144	Disintegrated
	SS 316	900	N_2*	144	Disintegrated
	In 800H	900	N_2*	144	23725
	Ha 230	900	N_2*	144	20345
$KCl/NaCl/VCl_2$ 53.3/41.7/5	SS 316L	750	Argon	6	54000
	SS316 Ti	750	Argon	6	6100
	SS321	750	Argon	6	22200
KCl/NaCl 56.1/43.9	SS 316L	750	Argon	80	~157
	SS316 Ti	750	Argon	80	~168
	SS 321	750	Argon	80	~225

While few studies have measured the corrosion rate of ceramic refractories in these molten chlorides at 700-750°C, some studies have shown similar challenges in mitigating the corrosion of typically high performing ceramics (e.g., SiO_2-, Al_2O_3-, and MgO-based ceramics) in chloride melts [19] [20] [21]. Low-cost ceramics inherently have a porosity that must be considered; that is, a material that does not react may still be severely penetrated and fail to contain the molten chlorides [22]. While dense (sintered or fusion-cast) ceramic bricks are available, they require high-temperature/high-pressure treatment, transportation, and labor-intensive installation, which all increase their cost [23].

Castable ceramics can be a cost-effective option for large tanks due to their faster, easier, and cheaper installation compared to bricks [24]. The use of castable ceramics as refractories involves thermal treatment to remove the water and hydrates in the binding matrix, which increases

the porosity of conventional castable refractories to about 22-26% depending on aggregates used [24]. Such porosity and general strong wetting behavior of molten salts [25] [26] encourage penetration, which can drastically reduce the tank liner's effectiveness. As shown in this thesis, such wetting and penetration needs to be addressed if castable ceramics are to be used as tank lining materials for molten chloride salts.

Carbonaceous materials have shown resistance to wetting and penetration of molten chlorides [27] [28]. Pure graphite blocks could serve as a nonwetting, inert containment material but are easily eroded in moving fluid systems (such as CSP, where salt is continually being pumped in and out of the storage tanks). Thus, the approach of this thesis is to combine the erosion resistance of a castable ceramic with the nonwetting behavior of carbonaceous materials to create cost-effective, penetration-resistant designs for the containment of molten chloride salts. Two carbon-castable ceramic systems are explored: (i) the direct incorporation of carbon into a castable cement liner through pitch infiltration and subsequent thermal treatment to remove low-temperature volatiles, and (ii) a multiwall approach that uses a graphite particle bed protected by a thin castable ceramic wall to contain the molten salt.

By evaluating the effectiveness of combining nonwetting carbonaceous materials with castable ceramics, a potential cost-effective, reliable containment solution for molten chlorides can be found, enabling low-cost thermal energy storage for CSP to serve as a competitive alternative to fossil fuels.

2. MATERIALS AND METHODS

Experimental details for the two carbon-castable ceramic systems are grouped by similar topics. Sections 2.1-2.3 describe the experimental details of items needed to support both the pitch infiltration and packed-graphite bed methods, including details about the furnaces, MKN salt, and graphite components. Sections 2.4-2.8 describe experimental details that support the general motivation to use carbon-containing refractories, including chemical compatibility screening, the infiltration of MKN salt into a carbon-free crucible, and a wetting study with MKN salt on a graphite disk. Sections 2.9-2.12 describe the experimental details pertaining to the single-pitch infiltration and multi-pitch infiltration studies with the MKN salt, and Sections 2.12-2.18 include the experimental details pertaining to the multiwall-packed graphite powder bed studies.

2.1 Furnaces

A single zone tube furnace (STT-1500C-3-36, Sentro Tech, Strongsville, OH, USA) equipped with a 3 in. diameter stainless steel tube, and a three-zone tube furnace (STT-1500C-6-36, Sentro Tech, Strongsville, OH, USA) equipped with a 6 in. diameter stainless steel tube (SCH 10 6.63 in. OD 304 SS, Northern Manufacturing, Oak Harbor, OH, USA) were used for all tests performed under flowing argon (e.g., chemical compatibility screening, salt infiltration studies of pitch infiltrated samples from Servsteel, MKN salt preparation, and graphite powder preparation). These furnaces were used with industrial-grade Ar ($p_{O2} \leq 100$ ppm). The furnaces were purged for 1 hr with an Ar flow of 140 cm^3/min to achieve low p_{O2} in the tube before lowering the flow rate to 30-70 cm^3/min throughout the entirety of experiments involving the furnace. A schematic

illustration of the STT-1500C-6-36 furnace assembly with flowing Ar over the sample is shown in Figure 2.1.-a.

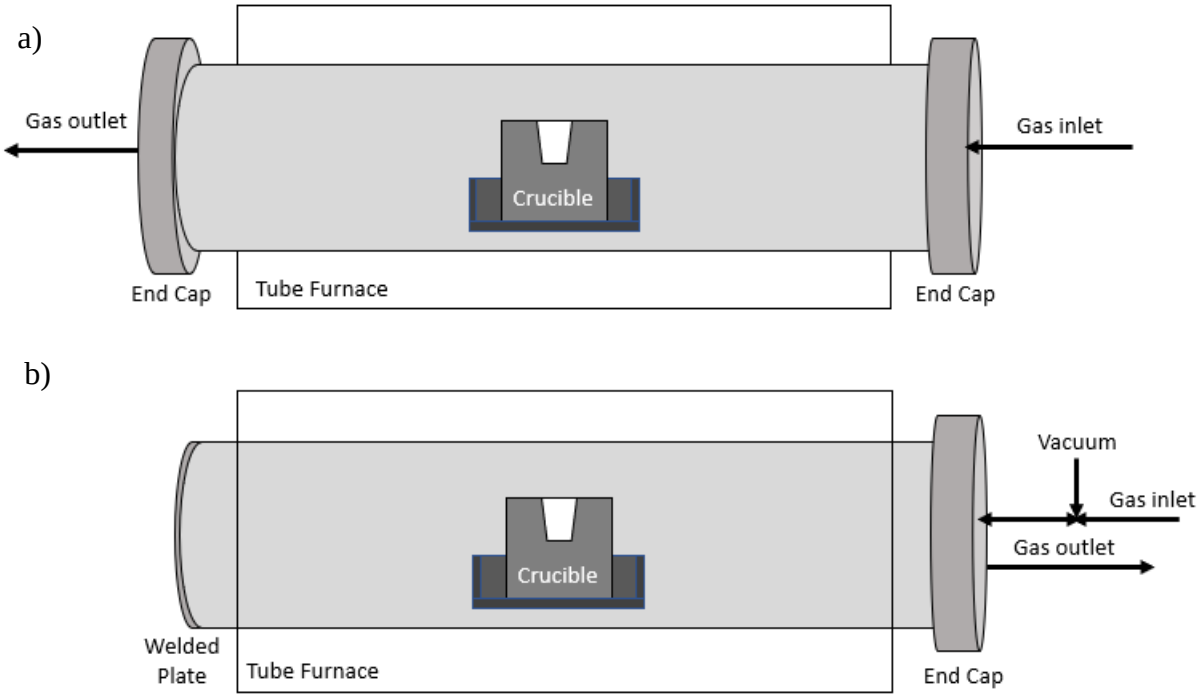

Figure 2.1. Schematic illustration of the STT-1500C-6-36 tube furnace with a) a stainless steel tube equipped with two end caps and flowing Ar gas over the sample and b) a pressure vessel with one end welded closed and equipped with one endcap and a vacuum/Ar gas inlet valve for the purging of O_2 from the tube.

The STT-1500C-6-36 furnace was also equipped with a pressure vessel (see Section 3.5.1) made from a one-end-closed stainless steel plate (316 stainless steel pipe with 6.63 in. OD, 0.28 in. thickness, with a stainless steel plug welded on one end). A schematic illustration of the STT-1500C-6-36 furnace with the pressure vessel assembly is shown in Figure 2.1.-b. A low p_{O2} was achieved by evacuating with a roughing pump (capable of achieving 30 mTorr), holding under vacuum for 2 min, and then backfilling with industrial-grade Ar ($p_{O2} \leq 100$ ppm) to 760 Torr. This purging and evacuating process was repeated three times before starting to heat the furnace. The Ar continued to flow at 140 cm^3/min for 1 hr before lowering the Ar flow to 30 cm^3/min throughout the entirety of experiments involving the furnace.

2.2 MKN Salt Preparation

$MgCl_2$ (anhydrous, 99.0% purity, Alfa Aesar, Ward Hill, MA, USA), KCl (ACS grade, 99.90-100.5% purity, Alfa Aesar), and NaCl (ACS grade, 99.0%-100.5%, BDH, Radnor, PA, USA) were used to prepare the 40/40/20 mole% $MgCl_2$-KCl-NaCl ternary salt mixture (MKN Salt). The $MgCl_2$, KCl, and NaCl were dried at 200°C under a roughing pump vacuum (about 23 Torr) for 12 hr, and the $MgCl_2$ was further dried in a tube furnace under flowing Ar (p_{O2}= 100 ppm, 30 cm^3/min) at 400°C for 4 hr to remove hydrates. These salts were immediately transferred to an Ar atmosphere-controlled glovebox (<10 ppm O_2 and 0.8 ppm H_2O) for storage. Salts were mixed in the glovebox to the desired composition of 40 mol% $MgCl_2$, 40 mol% KCl, and 20 mol% NaCl (MKN), then ground with a porcelain mortar and pestle for approximately 30 seconds and transferred to a graphite tray (AR-6, 6 in. x 3.5 in. x 1 in. cavity, Ohio Carbon Blank, Willoughby, OH, USA). The graphite tray with the mixed salt was heated to 750°C at 180°C/hr, then held for 12 hr at 750°C under 70 cm^3/min of flowing industrial-grade Ar (p_{O2}= 100 ppm) to achieve complete melting, homogenization of the salt mixture, and equilibrium with the low-oxygen gas atmosphere. The furnace was then cooled at 180°C/hr to room temperature. The solidified salt mixture was broken into smaller, irregular pieces (≤1 cm) with a cleaned chisel while in the Ar-atmosphere glovebox, characterized by XRD analysis, and stored in the Ar-atmosphere glovebox for later use.

2.3 Graphite Component Preparation

Graphite trays and crucibles were machined with a CNC router from graphite blanks (AR-6, Ohio Carbon Blank, Willoughby, OH, USA) to desired dimensions, then placed in an STT-1500C-6-36 three-zone tube furnace to be preheated at ≥750°C for ≥8 hr under Ar with a flow rate of 70 cm^3/min to outgas volatile impurities prior to use in subsequent experiments. K106 synthetic graphite powder (K106 grade, ≥99.0% purity, ≥89% with sizes between 100 mesh (149 μm) and 20 mesh (840 μm), Carbon Graphite Materials, Inc., Brocton, NY, USA) was placed in previously-fired graphite trays (6 x 3.5 x 1 in. cavities) to be heated under the same conditions: 750°C for 12 hr under industrial-grade Ar with a flow rate of 70 cm^3/min to outgas any volatile impurities.

2.4 Ceramic-MKN Compatibility Screening

Alumina (Al_2O_3) (lab grade, 100-200 mesh, Anhydrous Aluminum Oxide, Fisher Chemical, Hampton, NH, USA), calcium monoaluminate and dialuminate (CA/CA_2) (≥98.7% purity, 1.4-2.0 mm, Gorkal 70 Sintered Cement Grain, Gorka Cement, Trzebinia, Poland), calcium hexaluminate (CA_6) (≥99.2% purity, 3-6 mm, Bonite, Almatis International, Frankfurt, Germany) and Barium Sulfate ($BaSO_4$) (98% purity, Acros Organics, Fair Lawn, NJ, USA) grains were exposed to molten MKN salt at 750°C for 24 hr under Ar atmosphere to screen for their chemical compatibility. Grains were ground using a porcelain mortar and pestle until grains passed through a 25 mesh sieve, then placed on 304 stainless steel foil (McMaster-Carr 0.002 in. thick) to be predried at 750°C for 3 hr in Ar (30 cm^3/min, 100 ppm O_2). Once dried, the samples were transferred immediately to a controlled Ar-atmosphere glovebox (<10 ppm O_2, 0.8 ppm H_2O) for storage. The dried powder was characterized by XRD analysis, added to ground, purified MKN salt (from Section 2.2) to an approximate 1:1 ceramic: salt volumetric ratio using a leveled scoopula as a measure inside the glovebox. The combined powders were then mixed using a porcelain mortar and pestle for approximately 30 seconds. The resulting mixture was placed in a graphite crucible (1 in. diameter and 0.6 in. deep cavity), and the assembly was heated inside an STT-1500C-3-36 single-zone tube furnace under 30 cm^3/min flowing Ar. After exposure at 750°C for 24 hr, the resulting ceramic/salt mixture was ground using a porcelain mortar and pestle for approximately 30 sec, then characterized using XRD.

2.5 XRD Analysis of MKN Salt and Oxide Powder

X-Ray Diffraction (XRD, D2 phaser, Bruker) using Cu kα radiation (λ=1.54 Å) with a scanning rate of 0.06 degrees/s, an increment of 0.035 degrees, and a time of 0.6 s. Peaks were assigned with the use of Bruker Diffrac.suit software (equipped with ICDD PDF-2 2020 Powder diffraction database). Any materials that could fit the peaks but lacked a unique, unidentifiable peak were left unincluded in the final marking unless otherwise noted in the discussion. In labeling the spectra, peaks that fell below approximately 10% relative intensity to the most intense peak were left unmarked in figures unless needed to justify the presence of a low-intensity compound as one of its major peaks (≥ 50% relative intensity for the compound).

2.6 CA_6C Crucible Casting

Rubber plugs (EPDM #2 Stoppers: 0.8 in. upper diameter, 0.625 in. lower diameter, 1 in. height, WidgetCo Inc., Houston, TX, USA) for the pitch infiltration experiments and cast silicone plugs (2.2 x 2.2 x 2.5 in. and 0.8 x 0.8 x1.96 in.) Diamond Drive Liquid Rubber Silicone Mold Making Kit, Beckly-Amazon, Seattle, WA, USA) for the multiwall experiments, were glued onto laser cut acrylic sheets (0.75 in. thick cast acrylic, estreetplastics, Royse City, TX, USA) that were previously machined with a CNC router to create grooves for the acrylic pieces to fit together. The resulting molds allowed for the casting of 4 CA_6C (short for "calcium hexaluminate based castable" composition, by Westmoreland Advanced Materials) crucibles at a time. A photograph of such molds is provided in Figure 2.2.-b. Crucibles for the multiwall experiment were cast one at a time, and a photograph of the inner and outer molds are shown in Figure 2.3.

Molds were cured for at least 20 hr at room temperature before casting CA_6C crucibles. The CA_6C crucible wall thickness of 0.3 in. in the multiwall inner and outer crucibles was designed to accommodate the largest aggregate in the CA_6C mixture (~0.25 in. diameter), and in the case of crucibles for pitch infiltration studies, a wall thickness of 1 in. was used to satisfy a thickness >3x the largest aggregate size. A CA_6C castable precursor (overall molar ratio of Al_2O_3:CaO 5.9:1 with a predominate phase of CA_6, Westmoreland Advanced Materials, Charleroi, PA, USA) was cast using ultrafiltered water (18.2 MΩ·cm (25^{o}C), Milli-Q Direct, Millipore Sigma, Burlington, MA, USA) with a water: castable weight ratio of 8.02-8.20:100. Due to the small batch size relative to the mixing equipment, the water: castable ratio needed to be slightly higher than the recommended

6.5-7.5:100, in order to achieve the required vibration-casting consistency without the migration of small particles to the outer crucible edge.

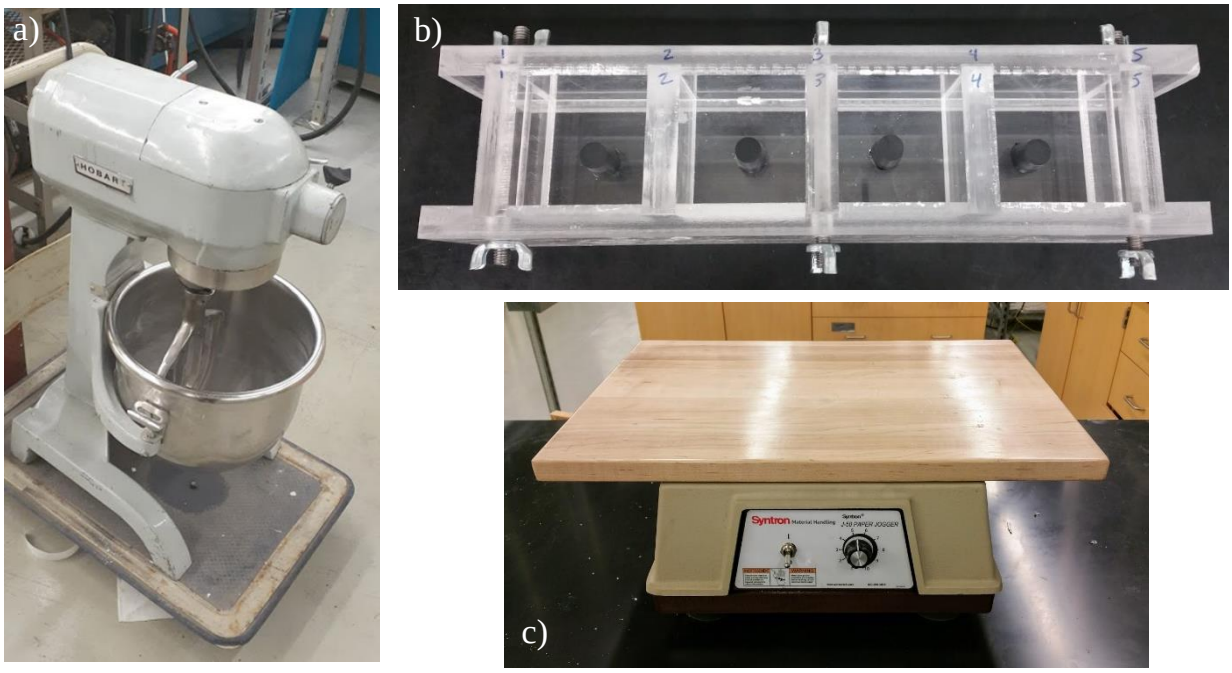

Figure 2.2. Photographs of a) the Hobart mixer, b) the acrylic molds for casting CA_6C crucibles, and c) the vibration deck jogger used in casting CA_6C samples.

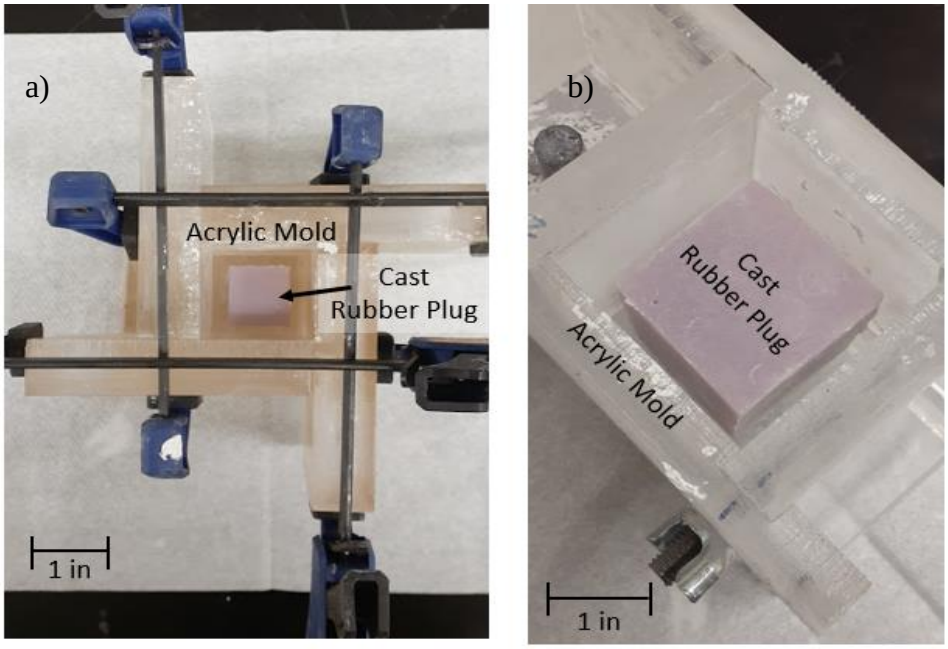

Figure 2.3. Photographs of a) the inner and b) the outer acrylic molds with silicone plugs for the casting of CA_6C inner and outer crucible, respectively, for the multiwall test.

To cast CA_6C crucibles, a 20-quart mixer (Hobart A-200, Hobart Co., Troy, OH, USA) at speed 1 (attachment speed of 61 RPM) and a Syntron J-50 flat deck jogger (J-50 flat deck jogger, Syntron Material Handling, South Saltillo, MS, USA) at speed 5 (~20 Hz), were used. Figure 2.2.-a and -c show photographs of the mixer and flat deck jogger, respectively. For casting each batch of CA_6C crucibles, 2.5 kilograms of CA_6C castable precursor was dry mixed in the Hobart 20 quart mixer for 30 sec. before being mixed with 200.47- 205.75 g of ultrafiltered water (Milli-Q Direct, 18.2 MΩ·cm (25^{o}C)) to a castable consistency as per WAM guidelines [29] and mixed for 2-4 min.

The CA_6C/water mixture was then cast into the acrylic molds and vibrated (~20 Hz) on the flat-deck jogger for 2 min. Samples were cured for 20 hr in a closed oven (Fisherbrand Isotemp Model 282A, Fisher Scientific, Hanover Park, IL, USA) at 35^{o}C and saturated humidity, which was achieved by placing an evaporation dish in the chamber with excess water and allowing for water evaporation for 1 hr at temperature prior to introducing samples into the chamber. Samples were then removed from the molds and returned to the same oven to cure at 110^{o}C for 24 hr in ambient air.

2.7 Weight Change Measurements of Salt Infiltrated Crucibles

2D-side view illustrations of a test crucible after each stage for global weight change measurements are provided in Figure 2.4. All samples were predried at 750^{o}C either under Ar (30 cm^3/min, industrial-grade, 100 ppm O_2) in the case of carbon-containing CA_6C crucible samples, or air in the case of carbon-free CA_6C crucible samples. A heating rate of 50^{o}C/hr and a cooling rate of 180^{o}C/hr were used. Samples were then reheated at 100^{o}C/hr for an additional 3-9 hr under the same atmosphere until the weight of the sample remained constant (±0.03 g as per the repeatability of the scale used) (Figure 2.4.-a). The crucible cavity was then filled with MKN salt (Figure 2.4.-b), placed in a graphite tray, then heated at 100^{o}C/hr to 750^{o}C in Ar, held for the respective test time, and then cooled at 180^{o}C/hr to room temperature. The mass change due to the salt's evaporation during the test was obtained by comparing the weight of the sample with the solidified MKN salt after heating to 750^{o}C (Figure 2.4.-c) to the MKN-loaded crucible before the thermal exposure (Figure 2.4.-b). The salt was then removed from the central cavity by carefully tapping a rubber mallet to a small flathead screwdriver, which served as a chisel. When salt could no longer be removed without damaging the crucible surface (and thereby removing graphite, which would affect the sample's weight change), cotton swabs soaked with ultrafiltered water were

used to dissolve away the remaining salt adhered to the cavity surface. The sample was then dried for 1 hr under vacuum (approx. 30 mTorr). The mass of the dried crucible after removing the non-infiltrated salt (Figure 2.4.-d) was compared to the starting weight of the sample (Figure 2.4.-a) to determine the mass of salt infiltrated into the crucible sample. The mass of the infiltrated salt was compared to the mass of salt added that did not evaporate to determine the percentage of the salt that had infiltrated into the crucible.

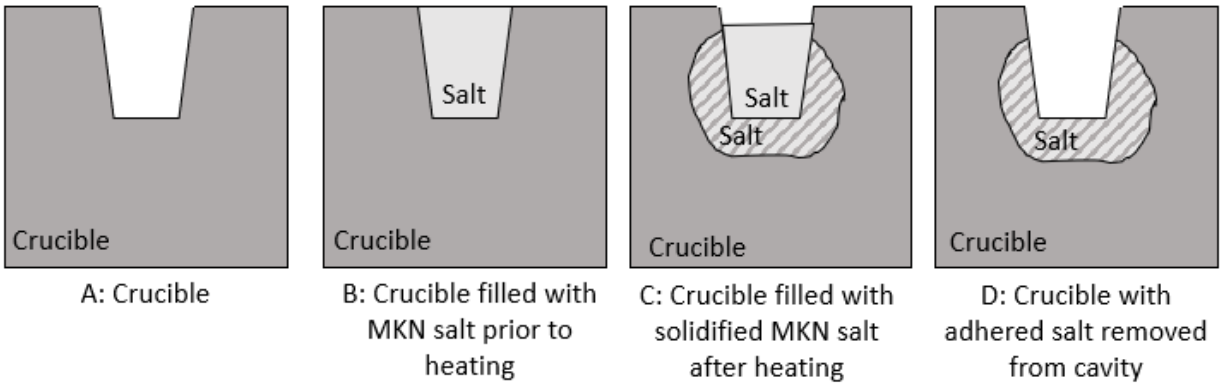

Figure 2.4. 2D side-view schematic illustrations of a crucible sample after each stage for weight change measurements of the salt infiltration process: A) a heat-treated CA_6C crucible, B) the crucible filled with the MKN prior to heating at 750°C, C) the crucible with solidified salt in the cavity after exposure to 750°C, where some salt has evaporated, and D) the crucible after removing the adhered salt from the crucible cavity walls.

2.8 Wetting of MKN Salt on a Graphite Disk

A graphite disk sample (1 in. diameter, 0.1 in. thickness) was polished with P-1200 SiC paper, then heated to 750°C for 12 hr under flowing industrial-grade Ar, as described in Section 2.3. MKN salt was pressed into a tablet using 200 kg/cm^2 of pressure, then placed on the center of the graphite disk. The graphite and salt were placed in a secondary graphite tray, then heated to 750°C for 30 min under 30 cm^3/min flowing industrial-grade Ar (100 ppm O_2). Once cooled to room temperature, the frozen salt was inspected for its contact angle with the salt. Once the salt was removed, the graphite disk was weighed and visually inspected for evidence of salt infiltration.

2.9 Pitch Infiltration

Proceeding the multi-pitch infiltrated samples used in Section 3.4.9, other pitch infiltration trials and a direct observation of the pitch in a vacuum oven with a window were necessary to

develop a procedure that successfully coated the CA_6C crucible with pitch. Such infiltration trails and observations are discussed in detail in Appendix B.

An aluminum cylinder (6061 aluminum, 5.25 in. diameter, 24 in. long, McMaster-Carr, Elmhurst, IL, USA) was machined with a CNC router to create three cavities (3 in. x 3 in. x3.5 in.) and to serve as a sample holder for pitch infiltration experiments (Figure 2.5). Such dimensions were designed to contain CA_6C crucibles with an additional 0.7-in. gap above the samples, which would allow a pitch volume >3x the estimated pore volume of the CA_6C crucible samples. A basket comprised of stainless steel mesh (316 stainless steel wire cloth, 9x9 mesh size, 0.088 in. opening size, McMaster-Carr, Elmhurst, IL, USA) was placed between the sample holder cavity and the CA_6C crucible to aid in the removal of the crucible after infiltration (Figure 2.6.-a). CTF-19 Pitch (a petroleum-based, coal-tar-free pitch with a melting point of 104-124^{o}C from Lone Star Specialties, LLC, Lone Star, TX, USA) was preheated to 120^{o}C for 1 hr, then poured over to the crucible (Figure 2.6.-b) to the top of the cavity (Figure 2.6.-c), to fully immerse the crucible in the liquid pitch.

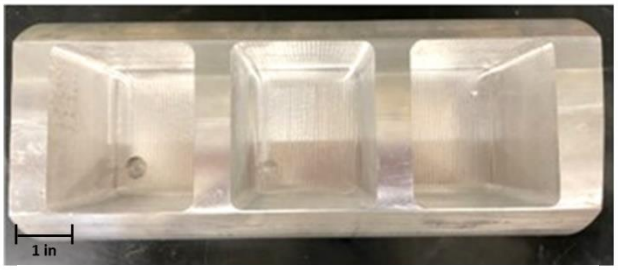

Figure 2.5. Photograph of the empty machined aluminum sample holder.

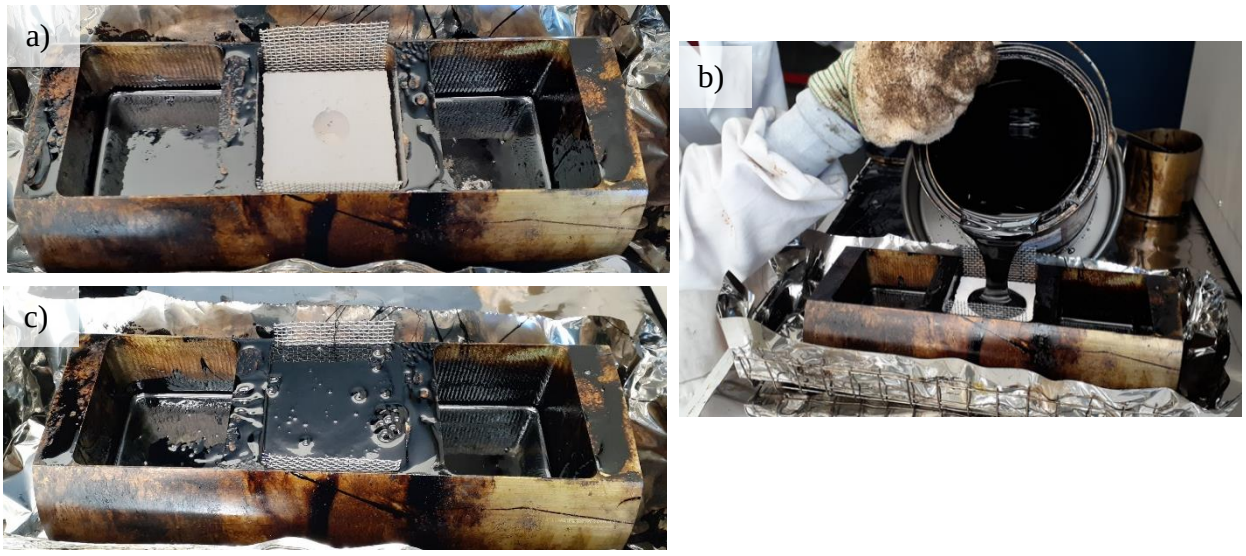

Figure 2.6. Photographs of a) the aluminum sample holder with the center cavity containing a cast and 850^{o}C fired CA_6C sample, b) 120^{o}C pitch being poured over the CA_6C sample in the central cavity, and c) the center cavity with the CA_6C crucible submerged in 120^{o}C pitch before entering the pressure vessel for infiltration.

The assembly was placed into the pressure vessel (the one end open stainless steel tube placed inside the STT-1500C-6-36 furnace). The end cap was sealed with a graphite gasket and stainless steel end cap, as shown in Figure 2.7., then heated at 180°C/hr to 120°C and held at 120°C for 1 hr. The furnace was pressurized to 60 psi with Ar to check for leaks at the endcap, then evacuated with a roughing pump (capable of reaching 30 mTorr) and backfilled to 1 atm with Ar 3 times. The furnace was then held under active vacuum and heated at 50°C/hr to 182°C, held for 45 min under the vacuum, then pressurized with the Ar to 60 psi. The vessel was held at 60 psi for 45 min, then remained under pressure as the furnace cooled to 100°C at 180°C/hr.

The pressure was then returned to 1 atm, and the crucible samples were removed from the sample holder cavities with the stainless steel baskets. The crucible samples were left to cool in ambient air on a stainless steel tray to room temperature over about 4 hr; then they were weighed and returned to the furnace to be heat treated at 850°C to remove low-temperature volatiles. Crucible samples were heated at 50°C/hr to 850°C, held at temperature for 11 hr, then cooled at 180°C/hr to room temperature all under an industrial-grade Ar atmosphere ($p_{O2} \leq 100$ ppm).

Figure 2.7. A photograph of the pressure vessel inside the furnace closed with an endcap and operating at 60 psi at 182°C for pitch infiltration.

2.10 He Pycnometry Measurement of Carbonaceous Material

The CTF-19 Pitch (Lone Star Specialties, LLC) was fired at 850°C for 11 hr in industrial-grade Ar ($p_{O2} \leq 100$ ppm) in a porcelain crucible. The resulting carbonaceous material was then

ground with a porcelain mortar and pestle for 30 sec. The solid volume of the powder was determined through Helium pycnometry (AccuPyc 1330, Micrometrics, with a 3.5 cm^3 AccuPyc calibration standard cup calibrated with 2.422872 cm^3 balls, Norcross, GA, USA) equipped with He gas (99.999% purity). The resulting density of the carbonaceous material was 1.89 g/cm^3.

2.11 CA_6C Apparent Porosity Measurement

WAM provided an apparent porosity of 27.4% for their CA_6C samples [30]. To confirm this value, the apparent relative porosity values of two cast and 850°C-fired CA_6C samples were obtained using the water absorption method (ASTM Standard C20-00). Samples were immersed in 1 liter of ultrafiltered water (Milli-Q Direct, 18.2 MΩ·cm (25°C)), boiled for 2 hr, and then soaked for 24 hr at room temperature. The water-saturated weight was compared to the dry weight to determine the weight of water absorbed by the sample and the resulting volume of the open pores. The exterior volume was obtained through an Archimedes measurement of the saturated sample. The volume of the pores was then compared to the volume of the sample to calculate the apparent porosity. The resulting porosities were 23.7% and 26.5% for the two samples or an average porosity of 25.1± 1.4%, which was not far from that reported by WAM.

2.12 Cross-Sectioning of Samples

Cross-sectioned crucible samples were prepared by cutting samples with a diamond wafering blade (#60-20075, Allied High-Tech Products, Inc., Rancho Dominguez, CA) on a slow speed saw (TechCut 4™, Allied High-Tech Products, Inc.) that were previously cleaned with soap and water followed by ethanol before use. Fresh mineral oil (Heavy LG, lab grade, Aldon Corp SE, Avon, NY, USA) was used as the cutting fluid for each sample. A photograph of the cross-sectioning arrangement for a pitch-infiltrated CA_6C sample is shown in Figure 2.8.

The large dimensions and heavy weight of the crucibles relative to the saw required rotating the sample and making multiple smaller cuts to look at a particular cross-section. The region of most interest was directly below the salt-bearing crucible cavity.

Crucible samples were then dried under vacuum at room temperature for up to 12 hr. If mineral oil was still detected, samples were heated to 80°C under vacuum (~28 mTorr) and held for up to 12 hrs. If mineral oil remained, dry acetone was prepared by swirling $MgSO_4$ (Anhydrous RG powder, lab grade, Aldon Corp SE, Avon, NY, USA) through acetone (99.5% purity, McMaster-Carr, Elmhurst, IL, USA) until hydrated $MgSO_4$ precipitated on the bottom of the vial (approximately 2 g per 20 ml of acetone). The $MgSO_4$ was then filtered with 11 µm filter cellulose filter paper (Whatman Qualitative 55 mm Diameter filter paper, Cytiva, Marlborough, MA, USA) and the acetone used immediately to rinse samples for approximately 10 seconds, which were then dried again under vacuum for 1-3 hours at room temperature. Small cross-sections were analyzed by scanning electron microscopy (Phenom Desktop SEM, Thermo Fisher Scientific, Waltham, MA, USA) equipped with energy dispersive X-ray spectroscopy (EDX).

Figure 2.8. Photograph of a pitch-infiltrated CA_6C crucible being cross-sectioned with a slow speed saw and diamond wafering blade.

2.13 Preparation of Multiwall CA_6C Components

To test the containment of molten MKN salt using a new multiwall tank design, inner and outer CA_6C crucibles were assembled with a packed graphite bed between these crucibles. A schematic illustration of the multiwall test crucibles (with dimensions for each layer) is shown in Figure 2.9.

CA_6C crucible components were cast in acrylic molds with a negative cavity to create pieces' dimensions. To create the negative cavity shape, silicone plugs were cast to the crucible cavity dimension using castable epoxy (2.2 x 2.2 x 2.5 in. and 0.8 x 0.8 x 1.96 in., Diamond Drive Liquid Rubber Silicone Mold Making Kit, Beckly-Amazon, Seattle, WA, USA) to the desired

dimensions and cured for at least 24 hr before use. A wall thickness of 0.3 in. was used for both the inner and outer crucibles to accommodate the largest aggregate (0.25 in.) in the CA_6C mixture.

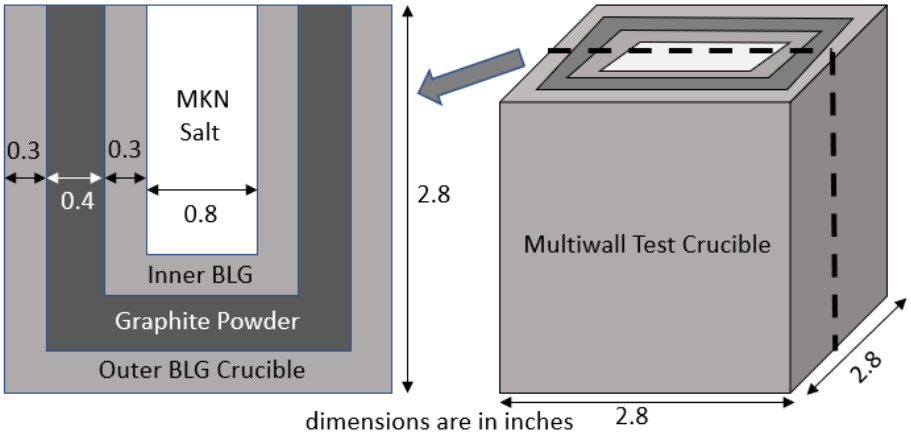

Figure 2.9. A schematic illustration of the multiwall test crucible and a cross-section showing the dimensions of each layer.

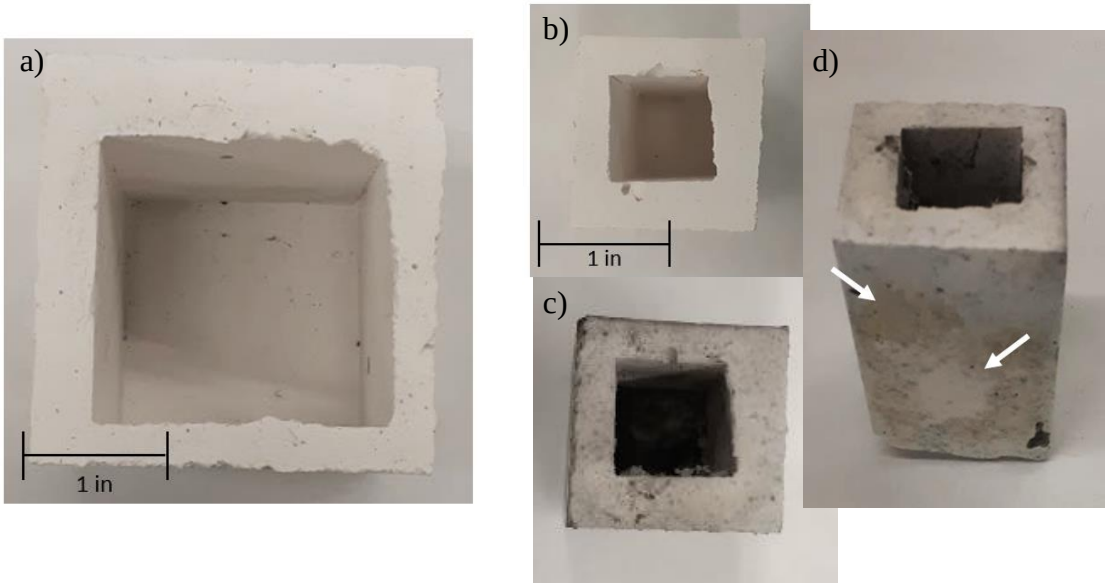

Figure 2.10. Top-down photographs of: a) a cast CA_6C outer crucible after firing for 10 hr at 750°C air, b) an inner crucible after firing for 10 hr at 750°C , and c) the inner crucible after premelting MKN salt in the crucible cavity for 2 hr at 750°C under Ar, c) A side view image of the same premelted inner crucible, showing that the salt had fully infiltrated through the walls of this crucible

CA_6C components were cast and cured using the same procedure described in Section 2.6. As with the pitch infiltration studies in Section 3.4.9, cast components were not fired to 1500°C to make the design more feasible for CSP application. Rather, components were fired at 750°C for

10 hr in air to remove free and chemically bound water. Photographs of a cast and 750°C-fired outer crucible and a cast and 750°C-fired inner crucible are provided in Figure 2.10-a, and -b, respectively.

2.14 Premelting of the MKN Salt in the Inner CA_6C Crucible

The inner pore volume was then calculated by measuring the crucible volume and assuming a relative porosity of 27.4% [30]. To ensure that enough salt was present to fully penetrate the inner crucible, the inner crucible was filled with MKN salt and premelted at 750°C under Ar for 2 hr. As shown in Figure 2.10.-d, there was a slight color change at certain locations along the external crucible surfaces that were consistent with complete salt penetration through the walls of the sample.

2.15 Graphite Powder Preparation

K106 graphite powder (K106 grade, ≥99.0% purity, ≥89% with sizes between 100 mesh (149 μm) and 20 mesh (840 μm), Carbon Graphite Materials, Inc., Brocton, NY, USA) was poured into a graphite tray that was previously fired at 750°C in Ar to remove volatile impurities. A secondary electron image of such powder is provided in Figure 2.11. The tray with the powder was then heated to 750°C under flowing industrial-grade Ar ($p_{O2} \leq$ 100 ppm) and held for 12 hr to remove volatile species. Upon cooling, the graphite powder was immediately transferred to an Ar atmosphere glovebox and stored in a closed container.

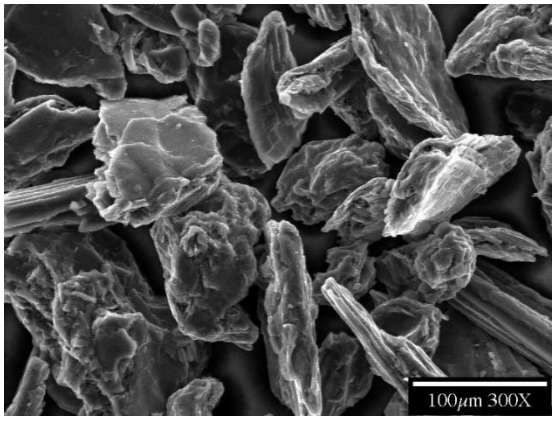

Figure 2.11. A secondary electron image of K106 graphite powder [31].

2.16 Graphite Packing Condition Determination

Graphite powder packing density was measured by placing 25 cc of graphite powder in a clear plastic graduated cylinder (25 ml, 0.5 ml resolution, Polypropylene, VWR, Radnor, PA, USA). The initial graphite bed was densified by vibration using a flat-deck jogger (Syntron J-50 flat deck jogger, Syntron Material Handling, South Saltillo, MS, USA) at different frequencies and holding times. The compacted packing density was measured by tracking the change in volume of the graphite particle column. The packed density was compared to graphite's theoretical density (2.26 g/cm^3) to determine the relative packing density. Three samples were used in each time and frequency measurement. The average and standard deviation of each trial are plotted against vibration time in Figure 2.12.

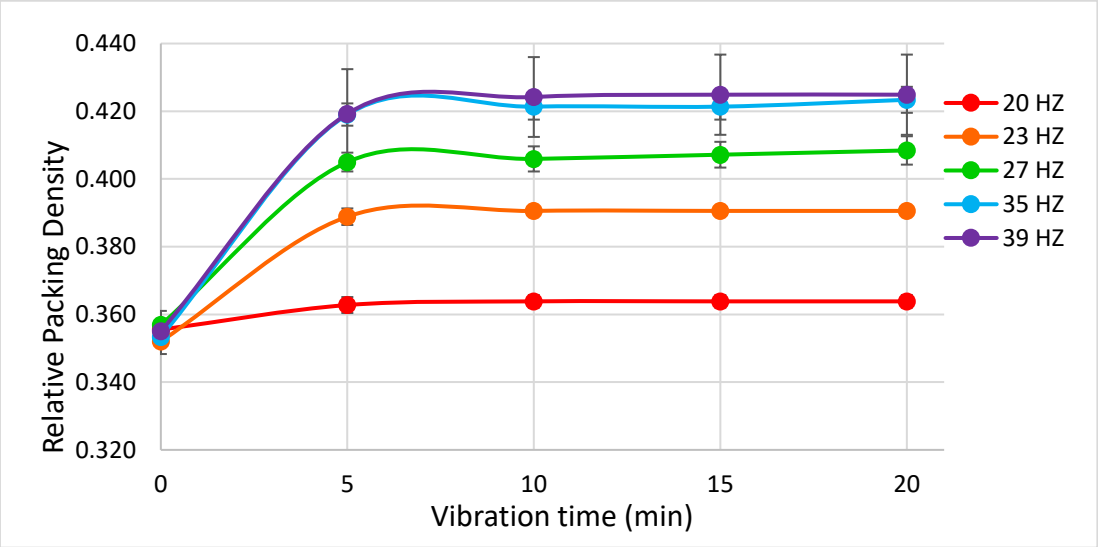

Figure 2.12. The relative packing density of graphite powder (compared to dense graphite) for different vibration times and frequencies.

The relative packing density of samples vibrated at 39 Hz was almost identical to those at 35 Hz. Such frequencies were too aggressive to contain the graphite powder in the CA_6C crucibles, so the next highest frequency of 32 Hz was used. Little difference in the packing density was measured after 5 minutes for each vibration frequency, 8 minutes was used for the multiwall experimental assembly.

2.17 Component Assembly and 24 hr Salt Infiltration Test

An initial bottom layer of the graphite powder (K106 grade, Carbon Graphite Materials) of approximately 0.4 in. thickness was first deposited on the bottom of the outer tank cavity. A photograph of an outer CA_6C crucible with graphite powder deposited on the bottom is shown in Figure 2.14.-a. This powder was vibrated using a flat-deck jogger (J-50 flat deck jogger, Syntron Material Handling, South Saltillo, MS, USA) at a frequency of ~32 Hz (speed 8) for 8 min while inside a closed Ar-filled bag to minimize adsorption of gas to the graphite powder.

The inner crucible was then placed on the packed graphite particle bed and covered with parafilm (Grade M, Bemis PM996, Sheboygan Falls, WI, USA) to prevent graphite from falling into the cavity of this inner crucible. The gap between the crucibles was then filled with the graphite powder and vibrated at speed 3 to add more graphite powder and fill the crucible cavity to the top. The graphite powder was covered with tape to prevent excessive loss of the powder, and the assembly was placed in a closed Ar-filled bag, as shown in Figure 2.13., and vibrated again for 8 min at ~32 Hz. A photograph of the assembly after the vibration-assisted packing of the graphite powder and after removing the tape and parafilm is provided in Figure 2.14.-b.

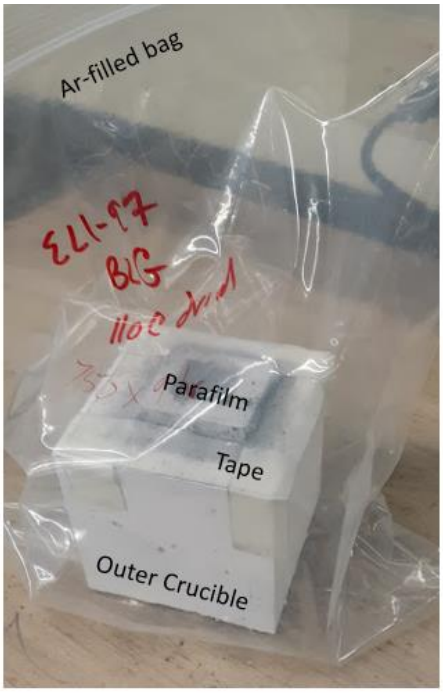

Figure 2.13. Photograph of the multiwall assembly inside an Ar-filled bag with parafilm protecting the inner crucible cavity and tape covering the graphite powder during the vibration-assisted packing of the graphite powder

MKN salt was added to the cavity of the inner crucible (Figure 2.14.-c) inside an Ar-atmosphere glovebox, and then the assembly was placed on a graphite tray that was placed inside a 6-in. diameter stainless steel tube furnace. The tube was purged for 1 hr with industrial-grade Ar (100 ppm O_2) using a flow of 140 cm^3/min. The Ar flow was reduced to 30 cm^3/min, and the temperature was raised at 100°C/hr to the peak temperature of 750°C. This peak temperature was maintained for 24 hr, and then the furnace was cooled down 180°C/hr to room temperature.

The mass of the assembly before and after the heat treatment at 750°C for 24 hr was used to determine the mass of the evaporated salt. After weight evaluation of the assembly, the inner crucible and the graphite powder were removed from the outer crucible. The inner cavity of the outer crucible, and outer wall of the inner crucible were gently brushed with a cotton swab to remove loose graphite from the surface, which was recovered for weight change measurements of the retrieved graphite powder. The inner and outer crucibles were then weighed to evaluate any weight change of the crucibles. The recovered graphite powder was also weighed to determine whether any salt penetrated into this powder.

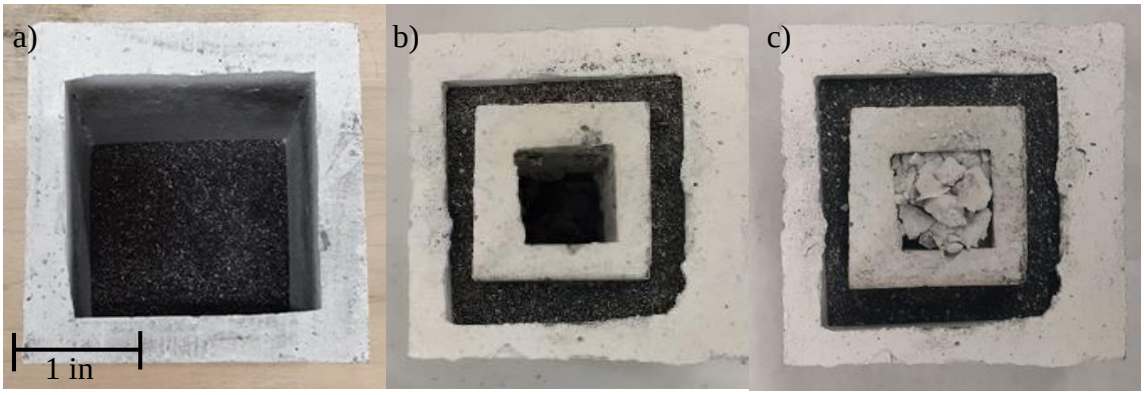

Figure 2.14. Top-down photographs of a) an outer CA_6C crucible with graphite powder deposited on the bottom, b) a multiwall assembly after placing a parafilm-protected inner crucible on the bottom, packed graphite layer, filling the layers between the crucibles with graphite, then covering with tape for vibration-assisted packing, and c) the multiwall assembly with the protective tape and parafilm removed.

2.18 Titration to Determine Chloride Concentration in Graphite Powder

The graphite powder was exposed to 825 ml of ultrafiltered water (18.2 MΩ·cm (25°C), Milli-Q Direct, Millipore Sigma, Burlington, MA, USA) for 45 hr. The resulting water solution was then twice filtered through 11 µm cellulose filter (Whatman Qualitative 55 mm Diameter filter paper, Cytiva, Marlborough, MA, USA) via vacuum-assisted filtration, which included rinsing the vial with an additional 25 ml of water (for 850 ml of total water solution). The solution was then divided into three 100 ml samples. A 0.025M $KCrO_4$ indicator solution was prepared by adding 1 gram of $KCrO_4$ (≥99.0%, ACS grade, BeanTown Chemical, Hudson, NH, USA) to 20 ml of ultrafiltered water and waiting for 24 hr before use (while wrapped in aluminum foil for protection from light-induced degradation). 1 ml of this indicator solution was added to 100 ml of the filtrate solution,

then titrated against 0.1 N $AgNO_3$ aqueous solution (0.995-0.1005 N, VWR International, Radnor, PA, USA) in a 25 ml burette (±0.03 ml accuracy, VWR International, Radnor, PA, USA). This process was repeated 3 times for the filtrate solutions, as well as 3 times for the ultrafiltered water to serve as a background chloride concentration.

3. RESULTS AND DISCUSSION

3.1 Chemical Compatibility Screening

Commonly-used, alumina-bearing refractory ceramics were tested against MKN salt to screen for materials that exhibited good chemical resistance to molten chlorides. Calcium aluminate-based materials were of primary interest due to their success in castable cement and as corrosion-resistant refractories for the aluminum industry. High-alumina-bearing castable compositions may also contain $BaSO_4$ as an antiwetting agent [32]. Hence, $BaSO_4$ was also tested for compatibility with the MKN salt.

MKN salt was prepared as described in Section 2.2, and an XRD pattern obtained after 12 hours at 750^{o}C in industrial-grade Ar ($p_{O2} \leq$ 100 ppm) is shown in Figure 3.2. According to the phase diagram (Figure 3.1.), the 40/40/20 mol% $MgCl_2$/KCl/NaCl is expected to be comprised of mostly $KMgCl_3$ and NaCl, which was consistent with the XRD results. The XRD data revealed major peaks for $KMgCl_3$, NaCl, KCl-doped NaCl ($Na_{0.9}K_{0.1}Cl$), and the hydrated $KMgCl_3$ phase (these salt samples hydrated as they were characterized by XRD analysis, which requires about 20 min for each scan to complete). The absence or presence of MgO was of particular interest, as this oxide can be a reaction product between the salt and Al_2O_3-containing ceramics.

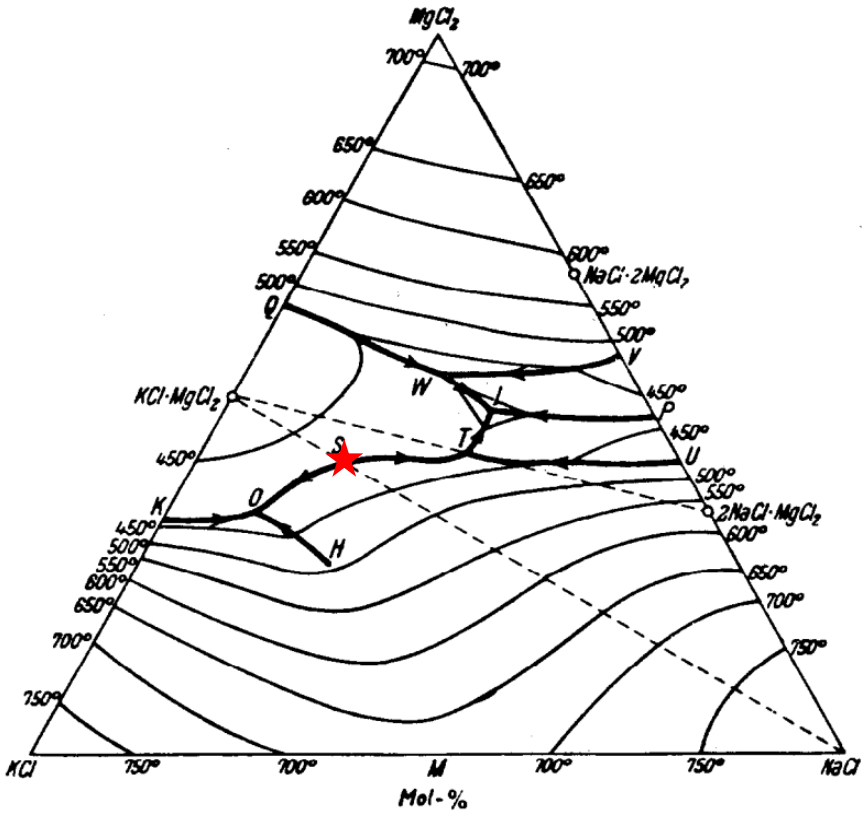

Figure 3.1. Ternary phase for $MgCl_2$-KCl-NaCl showing location of 40/40/20 mol% MKN composition [33].

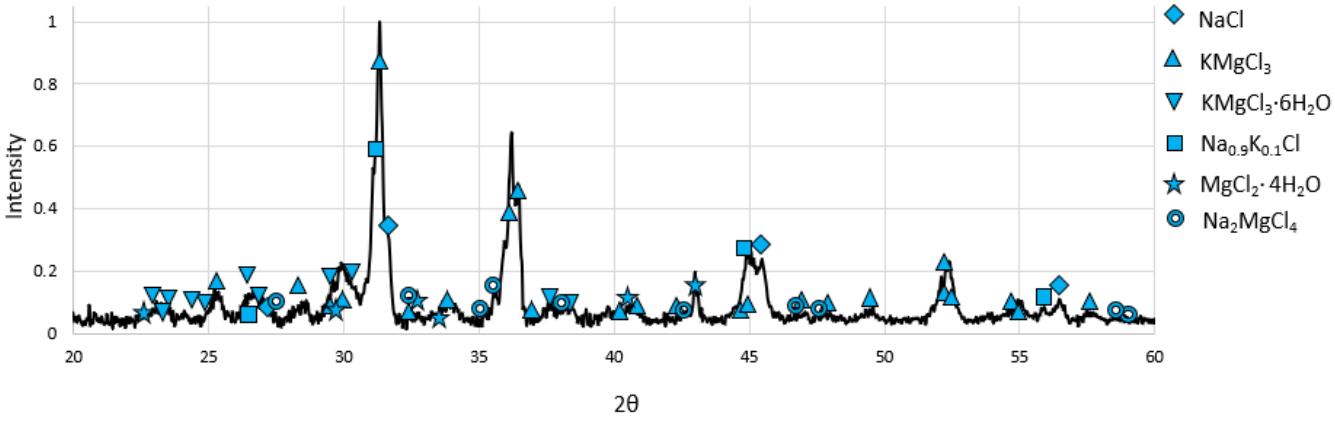

Figure 3.2. XRD pattern obtained from MKN salt after 12 hr at 750°C under flowing industrial-grade Ar ($p_{O2} \leq$ 100 ppm).

The alumina (Al_2O_3), calcium monoaluminate/calcium dialuminate (CA/CA_2), calcium hexaluminate (CA_6), and barium sulfate ($BaSO_4$) powder samples were prepared as described in Section 2.4. Powders were dried at 750°C for 3 hr in industrial-grade Ar ($p_{O2} \leq$ 100 ppm) to remove

free and chemically bound water. In an Ar-atmosphere glovebox, the powder was combined with MKN salt in an approximate 1:1 volume ratio using a leveled scoopula and then mixed by grinding with a mortar and pestle for 30 seconds. The combined powder was then transferred to a graphite crucible and heated at 750°C for 24 hr under industrial-grade Ar. Once cooled, samples were characterized by XRD analysis to evaluate the presence of reaction products.

3.1.1 Al_2O_3-MKN

XRD analyses of the dried alumina powder before and after exposure to MKN salt for 24 hr at 750°C in flowing industrial-grade Ar are provided in Figure 3.3. Alumina was found to react with the MKN salt to yield MgO and $MgAl_2O_4$. The following reactions were considered.

Equation 1.) $Al_2O_{3(s)} + 3MgCl_{2(l)} = 3MgO_{(s)} + 2AlCl_{3(g)}$

$$\Delta G^o_{rxn(750^oC)} = +156.39 \text{ kJ}$$

$$p_{AlCl_3,eqm} = 1.02\text{x}10^{-4} \text{ atm}$$

(meaning a local $AlCl_3$ partial pressure < $1.02\text{x}10^{-4}$ atm would make $\Delta G_{rxn(750^oC)}$ negative and drive the reaction in Equation 1 to the right)

Equation 2.) $Al_2O_{3(s)} + MgO_{(s)} = MgAl_2O_{4(s)}$

$$\Delta G^o_{rxn(750^oC)} = -4.80 \text{ kJ}$$

Equation 3.) $4Al_2O_{3(s)} + 3MgCl_{2(l)} = 3\ MgAl_2O_{4(s)} + 2AlCl_{3(g)}$

$$\Delta G^o_{rxn(750^oC)} = +141.99 \text{ kJ}$$

$$p_{AlCl_3,eqm} = 2.37\text{x}10^{-4} \text{ atm}$$

(meaning a local $AlCl_3$ partial pressure < $2.37\text{x}10^{-4}$ atm would make $\Delta G_{rxn(750^oC)}$ negative and drive the reaction in Equation 3 to the right)

The values used for calculating ΔG^o and the partial pressure of gaseous species for each equation can be found in Appendix A: Thermodynamic Calculations. Such free energy calculations revealed a relatively low equilibrium partial pressure of $AlCl_3$, meaning if the partial pressure exceeds this value, the reaction will not proceed to the right. However, these screening experiments were performed in 30 cm^3/min flowing industrial-grade Ar, which may have reduced the partial pressure enough to make these reactions favorable. It is also possible that the Al_2O_3 reacted with MgO that had been generated by the reaction of the MKN salt and oxygen in the industrial-grade

Ar (p_{O2}= 100 ppm), then this MgO further reacted with the Al_2O_3 to form $MgAl_2O_4$. If the Al_2O_3 did directly react with the $MgCl_2$ to form $AlCl_3$, the absence of $AlCl_3$ in the XRD pattern is expected as $AlCl_3$ possesses a sublimation temperature of just 183°C [34].

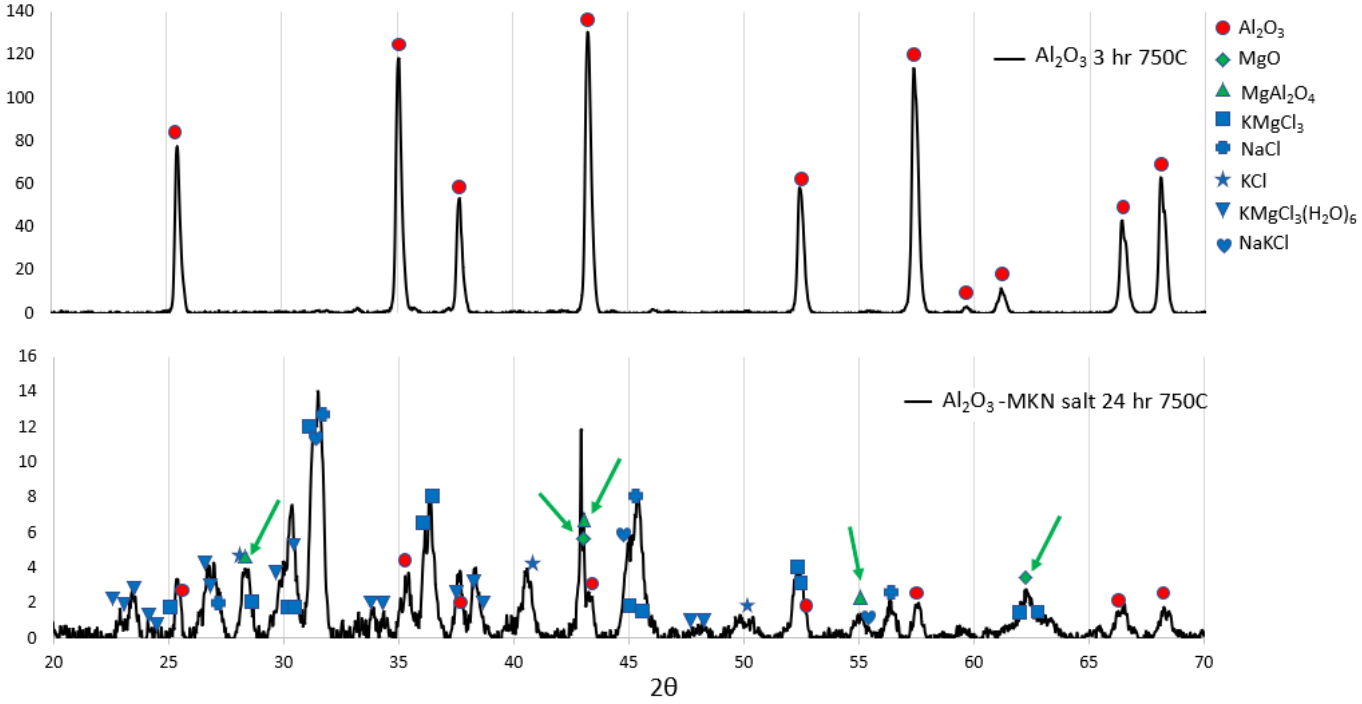

Figure 3.3. XRD pattern obtained from Al_2O_3: top) after drying for 3 hr under flowing industrial-grade Ar, and bottom) after 24 hr exposure to MKN salt at 750°C under flowing industrial-grade Ar ($p_{O2}\leq$ 100 ppm).

3.1.2 CA/CA_2-MKN

XRD analyses of the dried CA/CA_2 powder before and after exposure to MKN salt for 24 hr at 750°C in flowing industrial-grade Ar are provided in Figure 3.4. CA/CA_2 was also found to react with the $MgCl_2$ in the MKN salt to form MgO, $MgAl_2O_4$, and $CaCl_2$ (present as $CaCl_2$ and $CaCl_2$ bearing salts in the XRD pattern). These reaction products are consistent with the following reactions for CA (shown in Equations 4 and 5) and CA_2 (shown in Equations 7 and 8), with the formation of $AlCl_3$ also considered in Equations 6 and 9.

Equation 4.) $CaAl_2O_{4(s)} + MgCl_{2(l)} = MgO_{(s)} + Al_2O_{3(s)} + CaCl_{2(l)}$

$$\Delta G^o_{rxn(750^oC)} = -114.79 \text{ kJ}$$

Equation 5.) $CaAl_2O_{4(s)} + MgCl_{2(l)} = MgAl_2O_{4(s)} + CaCl_{2(l)}$

$$\Delta G^o_{rxn(750^oC)} = -119.59 \text{ kJ}$$

Equation 6.) $4CaAl_2O_{4(s)} + 7MgCl_{2(l)} = 4MgO_{(s)} + 3MgAl_2O_{4(s)} + 4CaCl_{2(l)} + 2AlCl_{3(g)}$

$$\Delta G^{o}_{rxn(750^{o}C)} = -317.15 \text{ kJ}$$

Equation 7.) $CaAl_4O_{7(s)} + MgCl_{2(l)} = MgO_{(s)} + 2Al_2O_{3(s)} + CaCl_{2(l)}$

$$\Delta G^{o}_{rxn(750^{o}C)} = -80.04 \text{ kJ}$$

Equation 8.) $CaAl_4O_{7(s)} + MgCl_{2(l)} = MgAl_2O_{4(s)} + Al_2O_{3(s)} + CaCl_{2(l)}$

$$\Delta G^{o}_{rxn(750^{o}C)} = -84.84 \text{ kJ}$$

Equation 9.) $CaAl_4O_{7(s)} + 4MgCl_{2(l)} = 3MgO_{(s)} + MgAl_2O_{4(s)} + CaCl_{2(l)} + 2\ AlCl_{3(g)}$

$$\Delta G^{o}_{rxn(750^{o}C)} = +71.56 \text{ kJ}$$

$$p_{AlCl_3,eqm} = 0.015 \text{ atm}$$

(meaning a local $AlCl_3$ partial pressure < 0.015atm would make $\Delta G_{rxn(750^{o}C)}$ negative and drive the reaction in Equation 9 to the right)

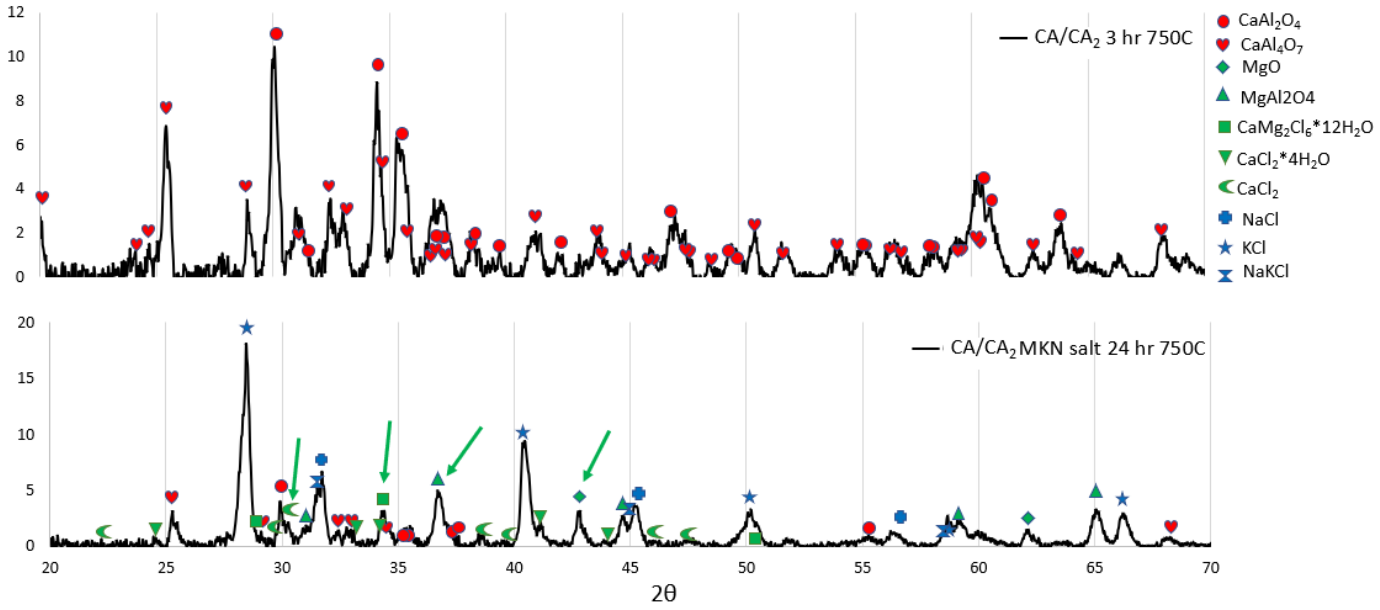

Figure 3.4. XRD pattern obtained from CA/CA2: top) after drying for 3 hr under flowing industrial-grade Ar, and bottom) after 24 hr exposure to MKN salt at 750°C under flowing industrial-grade Ar ($p_{O2} \leq$ 100 ppm).

The Gibbs free energy calculations suggest the reaction of CA and CA_2 with $MgCl_2$ to form $CaCl_2$, MgO, and/or $MgAl_2O_4$ were thermodynamically favorable by a few different routes. As mentioned, the further reaction of the Al_2O_3 with the $MgCl_2$ to form $MgAl_2O_4$ (Equation 2) could also still apply. Additionally, the relatively high equilibrium partial pressure calculated for $AlCl_3$

in Equation 9 suggests $AlCl_3$ may have formed in the flowing Ar system (as discussed in the Section3.1.1.) and evaporated from the sample.

3.1.3 CA_6-MKN

XRD analyses of the dried CA_6 powder before and after exposure to MKN salt for 24 hr at 750°C in industrial-grade Ar are provided in Figure 3.5. CA_6 was found to be less reactive with the MKN salt, as determined by the absence of $MgAl_2O_4$ and likely absence of MgO, which is hard to confirm, however, as the peaks for MgO overlap with peaks from the CA_6. $MgAl_2O_4$ was a more favorable option, as shown between Equation 10 and Equation 11 below.

Equation 10.) $CaAl_{12}O_{19(s)} + MgCl_{2(l)} = MgO_{(s)} + 6Al_2O_{3(s)} + CaCl_{2(l)}$

$$\Delta G^o_{rxn(750^oC)} = -95.68 \text{ kJ}$$

Equation 11.) $CaAl_{12}O_{19(s)} + MgCl_{2(l)} = MgAl_2O_{4(s)} + 5Al_2O_{3(s)} + CaCl_{2(l)}$

$$\Delta G^o_{rxn(750^oC)} = -100.48 \text{ kJ}$$

The Gibbs free energy calculations suggest the reaction of CA_6 with $MgCl_2$ to form $CaCl_2$, MgO, and/or $MgAl_2O_4$ was thermodynamically favorable. While the presence of MgO is inconclusive, the lack of $MgAl_2O_4$, which was more favored to form, suggested that CA_6 did not react with the MKN salt after 24 hr at 750°C. Since the CA_6 showed the most chemical resistance to the MKN salt at 750°C after 24 hr, it was chosen for further exploration as the primary component of a castable composition for infiltration studies with the MKN salt (as described in Section 3.2.).

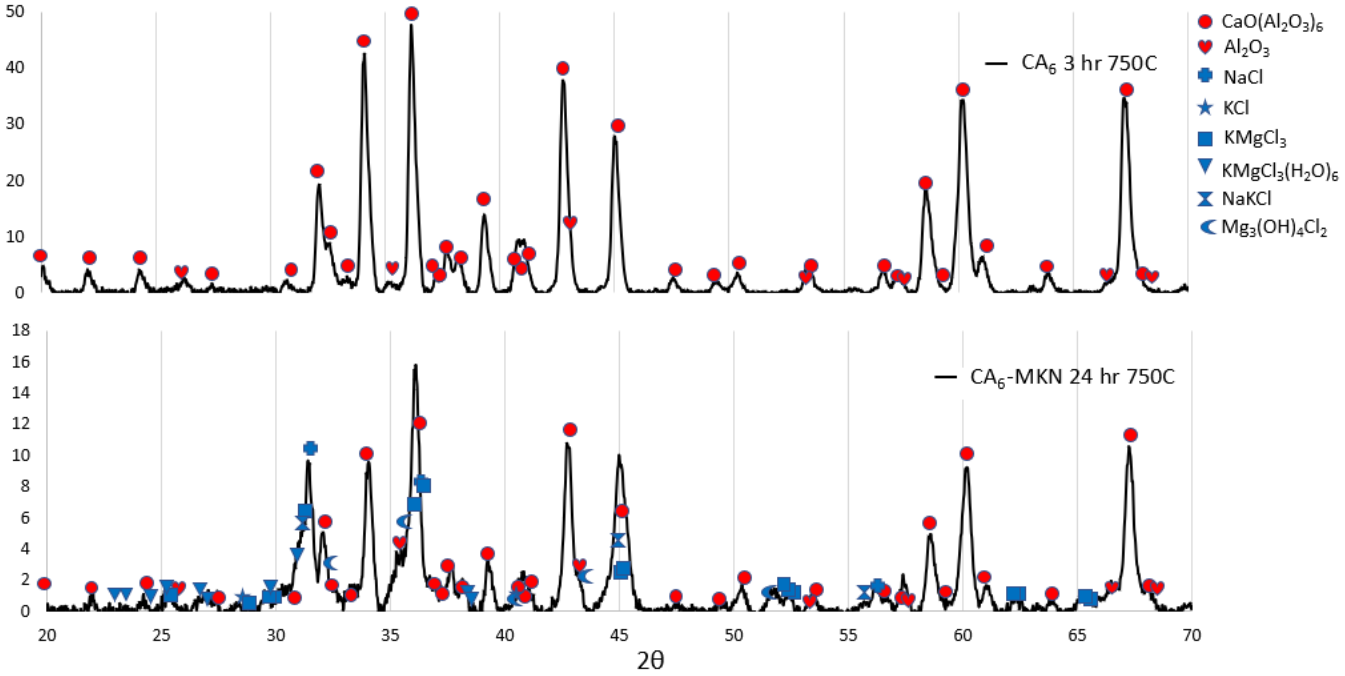

Figure 3.5. XRD pattern obtained from CA_6: top) after drying for 3 hr under flowing industrial-grade Ar, and bottom) after 24 hr exposure to MKN salt at 750°C under flowing industrial-grade Ar ($p_{O2} \leq$ 100 ppm).

3.1.4 $BaSO_4$-MKN

The CA_6 based castable composition provided by Westmoreland Advanced Materials (WAM, Charleroi, PA, USA) also contained $BaSO_4$, and so it was of interest to also test $BaSO_4$ for compatibility with the MKN salt. XRD analysis of the dried $BaSO_4$ powder before and after exposure to MKN salt for 24 hr at 750°C in flowing industrial-grade Ar is provided in Figure 3.6.

$BaSO_4$ was found to be reactive with the $MgCl_2$ in the MKN salt, as indicated by the presence of $BaCl_2$ and $MgSO_4$ (as $MgSO_4 \cdot H_2O$). These reaction products are consistent with the reaction described in *Equation 12*. The apparent presence of $KNaSO_4$ suggested that the $BaSO_4$ or the $MgSO_4$ further reacted to form this product, as was considered in Equations 13-16.

Equation 12.) $BaSO_{4(s)} + MgCl_{2(l)} = BaCl_{2(l)} + MgSO_{4(s)}$

$$\Delta G^o_{rxn(750^oC)} = \text{-17.88 kJ}$$

Equation 13.) $BaSO_{4(s)} + 2NaCl_{(l)} = BaCl_{2(l)} + Na_2SO_{4(s)}$

$$\Delta G^o_{rxn(750^oC)} = \text{+38.82 kJ}$$

Equation 14.) $BaSO_{4(s)} + 2KCl_{(l)} = BaCl_{2(l)} + K_2SO_{4(s)}$

$$\Delta G^{o}_{rxn(750^{o}C)} = +45.53 \text{ kJ}$$

Equation 15.) $MgSO_{4(s)} + 2NaCl_{(l)} = MgCl_{2(l)} + Na_2SO_{4(s)}$

$$\Delta G^{o}_{rxn(750^{o}C)} = +58.70 \text{ kJ}$$

Equation 16.) $MgSO_{4(s)} + 2KCl_{(l)} = MgCl_{2(l)} + K_2SO_{4(s)}$

$$\Delta G^{o}_{rxn(750^{o}C)} = +63.42 \text{ kJ}$$

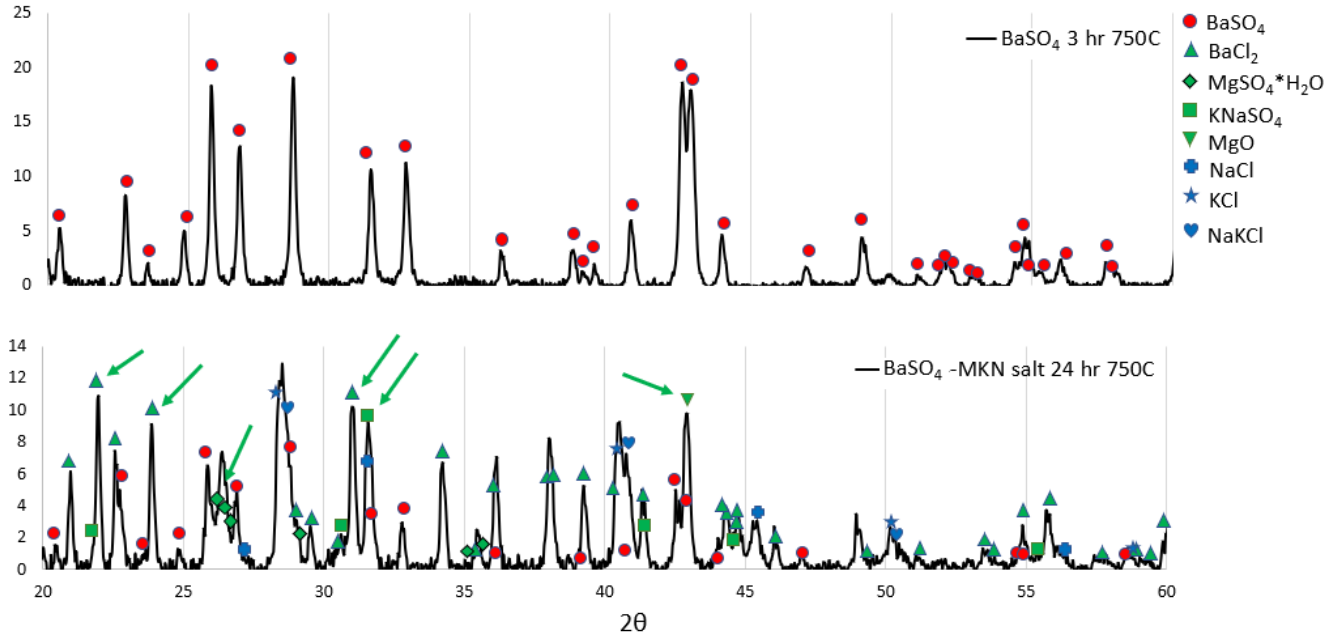

Figure 3.6. XRD pattern obtained from $BaSO_4$: top) after drying for 3 hr under flowing industrial-grade Ar, and bottom) after 24 hr exposure to MKN salt at 750°C under flowing industrial-grade Ar ($p_{O2} \leq$ 100 ppm).

The Gibbs free energy calculations indicated that the reaction of $BaSO_4$ with $MgCl_2$ to form $BaCl_2$ and $MgSO_4$ was favorable. While the formation of Na_2SO_4 and K_2SO_4 were not favorable, it is not unusual for salts to form mixtures with other cations in high-temperature melts that remain present upon solidification [35], such was also seen in the MKN salt composition (e.g., the $Na_{0.9}K_{0.1}Cl$ in Figure 3.2). The following reaction also considered the high presence of MgO in the XRD pattern.

Equation 17.) $BaSO_{4(s)} + MgCl_{2(l)} = BaCl_{2(s)} + MgO_{(s)} + SO_{3(g)}$

$$\Delta G^{o} \ (750^{o}C) = +45.66 \text{ kJ}$$

$$p_{SO_3,eqm} = 4.66 \text{ x} 10^{-3} \text{ atm}$$

(meaning a local SO_3 partial pressure < 4.66 x10^{-3} atm would make $\Delta G_{rxn(750^oC)}$ negative and drive this equation to the right)

The flowing Ar may have lowered the partial pressure of the SO_3 enough to favor the formation of MgO. In conclusion, $BaSO_4$ was found to be reactive with the MKN salt and was recommended to be removed from future castable formulations to be used with MKN salt.

The chemical compatibility screening of Al_2O_3, CA/CA_2, and CA_6 with MKN salt showed reaction products in the Al_2O_3 and CA/CA_2 samples after 24 hr at 750°C in Ar. While the reaction of $MgCl_2$ with CA_6 was calculated to be thermodynamically favored, CA_6 showed the most resistance to the MKN salt at 24 hr at 750°C. CA_6 castable compositions are commercially available and comparable in price to tabular alumina, and so the use of a CA_6-based castable composition was selected for further infiltration studies with the MKN salt.

3.2 Salt Infiltration of a CA_6C Crucible

CA_6C is a castable cement composition from Westmoreland Advanced Materials (CA_6C for "calcium hexaluminate-based castable", WAM, Charleroi, PA, USA) that has a CA_6-based composition, with an overall Al_2O_3:CaO molar ratio of 5.8:1. The precursor material was composed of large CA_6 aggregates with a CA/CA_2-Al_2O_3 cementitious binding matrix, which upon heating to 1500°C, reacts to form a CA_6 matrix.

A CA_6C sample was provided by WAM that was cast as a crucible and fired to 1500°C for 5 hr in ambient air using a heating rate of 25°C/hr. A cavity was then core drilled into the center of the crucible (0.8 in. diameter, 1 in. deep). Upon arrival at Purdue, the sample was heated to 750°C at 50°C/hr and held for 5 hr in air to remove moisture. The cavity was then filled with MKN salt and heated at 100°C/hr to 750°C for 2 hr in industrial-grade Ar (p_{O2} = 10^2 ppm). Top-down optical images of a starting cast/fired CA_6C crucible, and the same crucible after the molten salt test, and after removing residual solidified salt from the crucible cavity, are provided in Figure 3.7. After removing the residual material from the crucible cavity and factoring out the mass loss due to salt evaporation, the CA_6C crucible exhibited a mass gain from 727.34 g to 736.24 g (8.90 g increase), which corresponded to the penetration of 93.2% of the non-evaporated salt into the specimen. Visual inspection of the samples revealed a circular discoloration on the top surface of

the specimen, which was consistent with appreciable infiltration of the MKN salt after only 2 hr at 750°C.

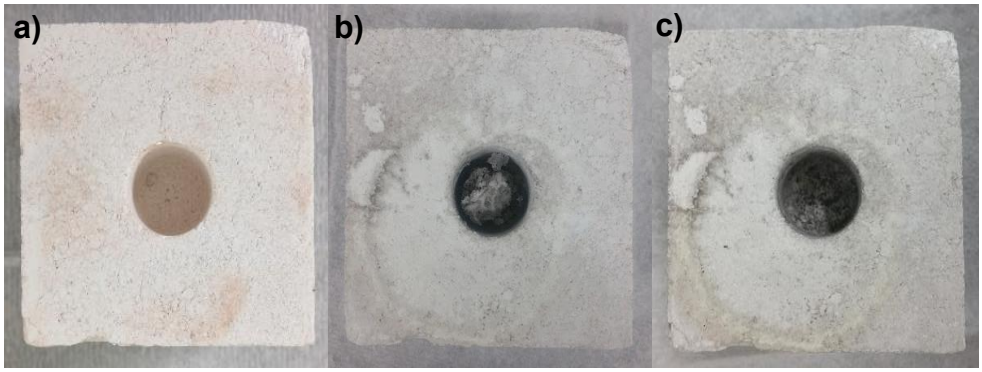

Figure 3.7. Top-down photographs of a cast CA_6C crucible after a) drying for 5 hr at 750°C in air b) after exposure to MKN salt at 750°C for 2 hr in industrial-grade Ar, c) after the non-infiltrated salt was removed from the cavity.

The appreciable infiltration of the fired CA_6C specimen by the MKN salt within only 2 hr at 750°C indicated that additional measures needed to be taken to inhibit such infiltration. The approach of this thesis was to combine the thermally-insulating CA_6C with nonwetting carbonaceous material through two different methods; i) the infiltration of liquid pitch followed by $\geq$ 750°C heat treatment to remove volatile carbonaceous species before exposure to the salt (as discussed in Sections 3.4 and 3.4.9), and ii) a graphite particle bed-multiwall crucible approach where the CA_6C sample was used to provide erosion resistance for the graphite powder, that in turn, prevented penetration of the salt (as discussed in Section 3.6).

3.3 Wetting of Graphite by MKN Salt

Graphite is a carbonaceous material that has shown good resistance to wetting and penetration by molten chloride salts [28] [27]. To confirm carbonaceous materials are not wet by MKN salt, a graphite disk sample was exposed to a pressed tablet of MKN salt for 30 min at 750°C in flowing industrial-grade Ar, as described in Section 2.8. Photographs of the salt-graphite sample before and after 30 min at 750°C are provided in Figure 3.8.-a and -b, respectively.

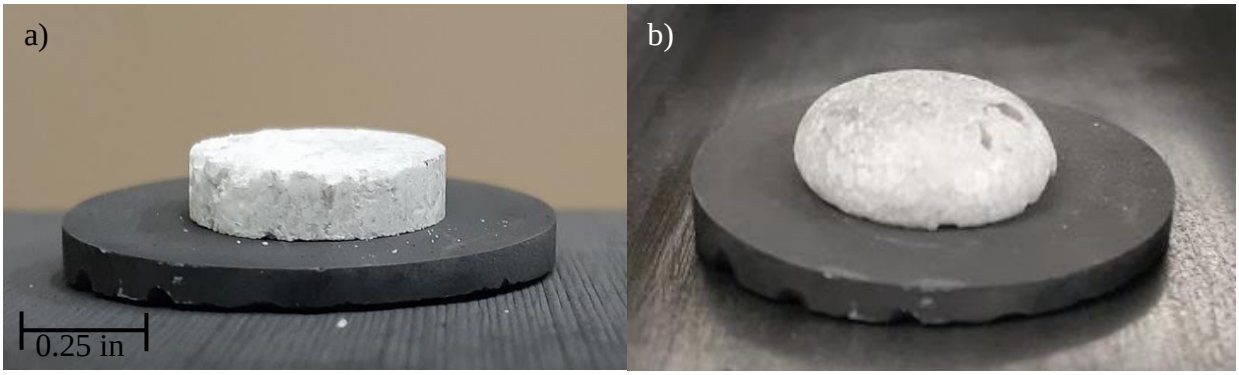

Figure 3.8. Photographs of the MKN salt on a graphite disk sample: a) before and b) after 30 min at 750^{o}C in industrial-grade Ar.

The solidified salt drop did not wet and spread off the graphite disk. Such curvature at the base of the drop indicated poor wetting and weight measurements. The solidified salt was removed freely from the graphite by merely tipping the disk. The salt and graphite disk were weighed before and after exposure to the MKN salt, as summarized in Table 3.1. The graphite disk displayed no weight gain confirming the lack of molten MKN salt penetration into the sample. The small weight change of the salt tablet was due to the evaporation of the salt.

Table 3.1. Weight measurements of salt and graphite disk before and after 30 minutes at 750^{o}C

	Weight Before (g)	Weight After (g)
MKN Salt Tablet	0.032	0.031
Graphite Disk	0.097	0.097

The graphite's resistance to the molten MKN salt wetting and penetration suggested the incorporation of such carbonaceous materials into the CA_6C would improve the penetration resistance of the CA_6C crucible samples.

As discussed in Sections 3.4 and 3.4.9, the incorporation of carbonaceous material into the CA_6C crucible was achieved by liquid pitch infiltration and subsequent thermal treatment at $\geq 750^oC$ in Ar. Such samples displayed an overall 80% reduction in the percentage of salt infiltrated into the crucible compared to the carbon-free test. A comparison of such infiltration results for virgin samples is provided in Figure 3.9., which shows the % infiltration of each sample indicated by its sample type and salt exposure time.

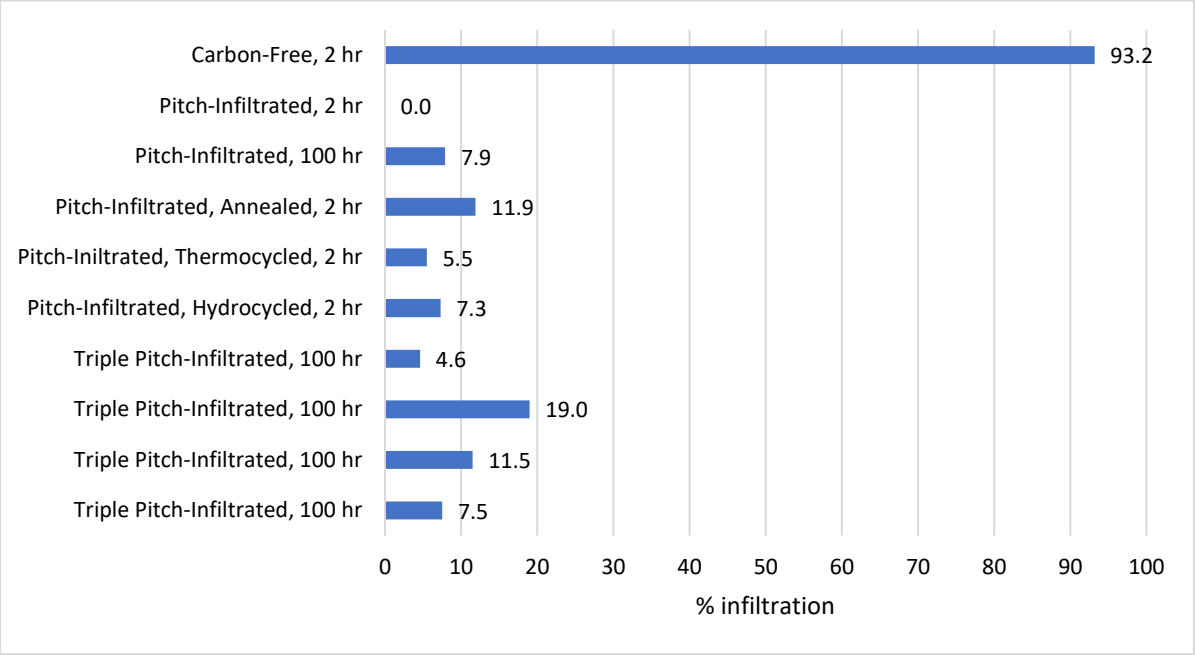

Figure 3.9. Summary of the percentage of salt infiltrated into virgin samples, which are described by their sample type and exposure time to the salt.

3.4 Molten Salt Infiltration of CA_6C Crucibles Exposed to a Single Pitch Infiltration Treatment

CA_6C crucible samples were provided by WAM that were prepared similarly to the CA_6C infiltration test described in Section 3.2 (i.e., cast and fired to 1500^oC in air). Samples were then sent to Servsteel (Merrillville, IN, USA, a company the conducts pitch infiltration on a commercial scale). At Servsteel, crucible samples were placed into a processing chamber and heated to 182^oC using an approximate heating rate of 50^oC/hr. Once at 182^oC, the chamber was evacuated to 49 Torr and held for 45 min. The vessel was then pressurized to 60 psi and held for 45 min, then the furnace was shut off, and the samples were left to cool to room temperature. Pitch-infiltrated

crucible samples were then sent to Purdue, where they were heated at 50°C/hr to 750°C, held at 750°C for 5 hr in 30 cm^3/min flowing industrial-grade Ar (p_{O2} ~ 100 ppm), then cooled to room temperature at 180°C/hr. Samples were then heated at 100°C/hr to 750°C for 2 or 3 additional hrs until the mass stopped changing for each sample (+-0.03g as per the repeatability of the scale and under 0.005% of the total sample mass) for a total time of 7-13 hr at 750°C for each sample. The cavity of a given crucible was then filled with MKN salt and heated at 100°C/hr to 750°C, held for the desired test time, then cooled at 180°C/hr under Ar to room temperature.

Weight change measurements were used to evaluate the global extent of molten salt infiltration into the crucibles, as described in Section 2.7. Such weight change measurements, summarized in Table 3.2, were used to compare the penetration of molten MKN salt into several pitch infiltrated crucibles from Servsteel (as described in Sections 3.4.1- 3.4.8). Each experiment is labeled with the crucible type ("CA_6C" for the carbon-free crucible and "Pitch/CA_6C" for pitch containing crucibles) followed by its crucible number and experiment number (e.g., Pitch/CA_6C 1.1 was the first experiment with pitch-infiltrated Crucible 1 and Pitch/CA_6C 1.2 was the second experiment with pitch-infiltrated Crucible 1).

Table 3.2. Summary of the molten salt infiltration of CA_6C crucible samples provided by WAM and Servsteel

	CA_6C 1.1	Pitch/ CA_6C 1.1	Pitch/ CA_6C 1.2	Pitch/ CA_6C 1.3	Pitch/ CA_6C 2.1	Pitch/ CA_6C 3.1	Pitch/ CA_6C 4.1	Pitch/ CA_6C 5.1	Pitch/ CA_6C 5.2
Sample type	Virgin	Virgin	Reuse of Pitch/ CA_6C 1.1	Reuse of Pitch/ CA_6C 1.2	Virgin	Virgin-annealed	Virgin-thermo-cycled	Virgin-water-cycled	Reuse of Pitch/ CA_6C 5.1
Weight of sample after thermal treatment at 750°C (g)	727.34	560.14	559.94	560.20	565.75	679.82	675.89	677.36	677.62
Weight with salt in the cavity (g)	737.86	570.63	570.30	570.54	575.96	689.62	684.95	687.25	688.6
Exposure time at 750°C	2 hr	2 hr	100 hr	50 hr	100 hr	2 hr	2 hr	2 hr	2 hr
Weight after exposure to salt (g)	736.89	570.48	569.45	568.88	574.91	688.97	684.83	686.89	687.67
Weight of added salt accounting for evaporation (g)	9.52	10.34	9.51	8.68	9.16	9.15	8.94	9.53	10.05
Weight after removing salt (g)	736.24	560.04	560.84	567.96	566.47	680.91	676.38	678.06	686.89
Weight of salt infiltrated (g)	8.87	-0.10	0.90	7.76	0.72	1.09	0.49	0.70	9.27
% infiltration	93.2%	Minor	9.5%	89.4%	7.9%	11.9%	5.5%	7.3%	92.2%

3.4.1 Pitch/CA_6C-1.1 Crucible: 2 hr Molten Salt Test

Top-down optical images of a pitch-infiltrated CA_6C crucible (Pitch/CA_6C 1.1) exposed to the molten MKN salt for 2 hr at 750°C in Ar ($p_{O_2} = 10^2$ ppm atm) are provided in Figure 3.10. The salt did not appear to wet or appreciably infiltrate the sample. After mechanical removal of the salt, the mass gain (after considering the mass loss due to evaporation) was 0.59 g and corresponded to 5.7% infiltration of the salt placed in the central cavity of the crucible. Further removal of the adhered salt on external surfaces using water-soaked cotton swabs revealed a slight mass loss of 0.1 g relative to the starting crucible weight. This was likely due to the loss of some carbon during

the removal with water-soaked cotton swabs. Such a small change in sample weight indicated that negligible infiltration (Table 3.2) of the molten MKN salt occurred during 2 hr at 750°C in Ar.

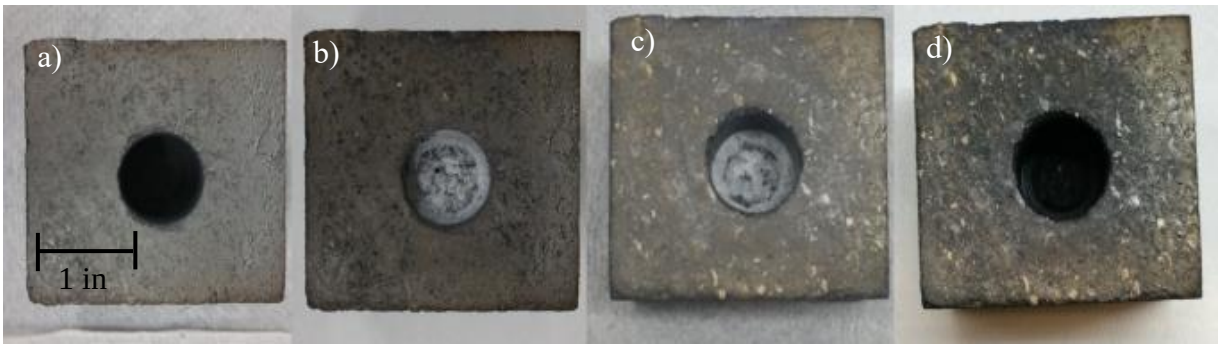

Figure 3.10. Top-down photographs of Pitch/CA_6C 1.1 crucible: a) after firing at 750°C, b) after 2 hr exposure to MKN salt at 750°C in Ar, c) after mechanical removal of the residual solidified salt in the cavity, and d) using water-bearing cotton swabs to dissolve adhered salt to the outer surface of the crucible cavity.

3.4.2 Pitch/CA_6C-1.2 Crucible: 100 hr Molten Salt Test

Due to limited sample availability at the time, it was advantageous to determine if crucible samples could be reused for further testing. After the 2 hr test described in Section 3.4.1, the salt-exposed, pitch-infiltrated CA_6C specimen was soaked in 500 ml of ultrafiltered water for 14 hr at room temperature to remove any remaining solidified salt within the sample, then dried for 5 hr at 750°C in industrial-grade Ar. The crucible was then refilled with salt and exposed at 750°C for 100 hr in Ar. Top-down optical images of the pitch-infiltrated CA_6C crucible, and the same crucible after a molten MKN salt test for 100 hr at 750°C in Ar and removal of residual solidified salt from the crucible cavity, are shown in Figure 3.11. After mechanical removal of the residual solidified salt in the specimen cavity (Figure 3.11.-c) and additional salt removal with water-bearing cotton swabs (Figure 3.11.-d), a net mass gain (after considering the mass loss due to salt evaporation) was obtained (Table 3.2) corresponding to the penetration of 9.6% of the non-evaporated salt into the specimen.

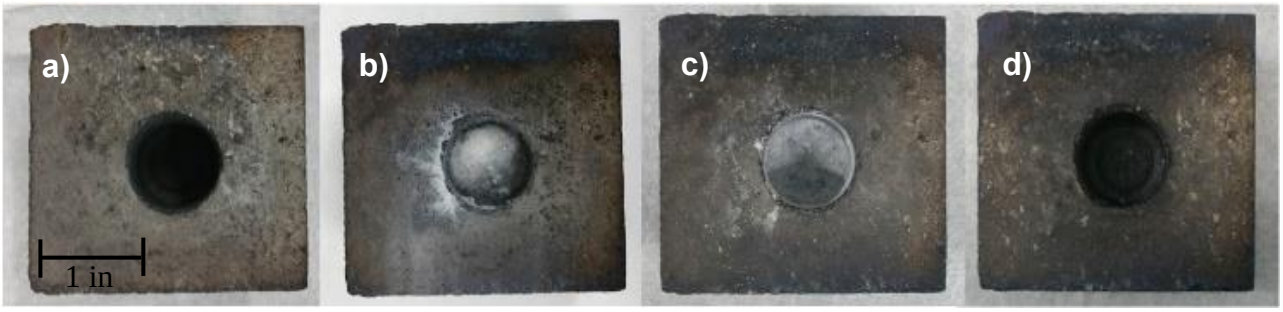

Figure 3.11. Top-down photographs of Pitch/CA_6C 1.2 crucible: a) after soaking the Pitch/CA_6C 1.1 sample for 2 hr in water followed by drying at 750°C in Ar, b) after exposure to MKN salt at 750°C for 100 hr in Ar, c) after mechanical removal of the non-infiltrated salt in the cavity, d) after dissolving the remaining salt with water-bearing cotton swabs.

It was hypothesized that the increase in salt penetration after 100 hr of additional salt exposure relative to the first 2 hr salt exposure test might have resulted from the loss of some carbonaceous material within the specimen near the cavity surface in the salt removal/dissolution process. As shown by later tests, this mass change value was within the range for a molten salt infiltration, possibly due to the lack of even or complete carbon coverage and/or due to potential ineffective dissolution of salt before reuse of the sample, creating a pathway for further salt infiltration (see Section 3.4.8).

In both the first 2 hr and second 100 hr tests, the samples showed no signs of cracking or obvious external discoloration associated with infiltration. The global infiltration of a virgin pitch-infiltrated CA_6C crucible specimen (Pitch/CA_6C 2.1 crucible specimen) exposed to MKN salt for 100 hr was then examined to determine if a non-recycled, pitch-infiltrated CA_6C specimen exhibited strong resistance to molten MKN infiltration after such prolonged exposure.

3.4.3 Pitch/CA_6C-2.1 Crucible: 100 hr Molten Salt Test

A virgin pitch-infiltrated CA_6C crucible (pitch/CA_6C -2.1) was exposed to molten MKN salt for 100 hr at 750°C in Ar. Top-down optical images of the pitch-infiltrated CA_6C-2.1 crucible, and the same crucible after the molten MKN salt test and then after removing residual solidified salt from the crucible cavity, are provided in Figure 3.12. Mass change measurements (Table 3.2.) indicated that the Pitch/CA_6C -2.1 crucible was penetrated by 7.9% of the non-evaporated salt that had been placed in the crucible cavity. This value for the pitch/CA_6C-2.1 crucible was not far from the 9.6% salt penetration value exhibited by the previous pitch/CA_6C-1.2 crucible that had been

exposed twice to the molten salt for a total of 102 hr (2 hr, then 100 hr), which suggested that the exposure of the latter crucible specimen to water and to drying prior to retesting did not have an appreciable effect on the subsequent salt penetration behavior. Thus, the pitch/CA_6C-1.2 crucible specimen was reused again for additional infiltration studies, as discussed below.

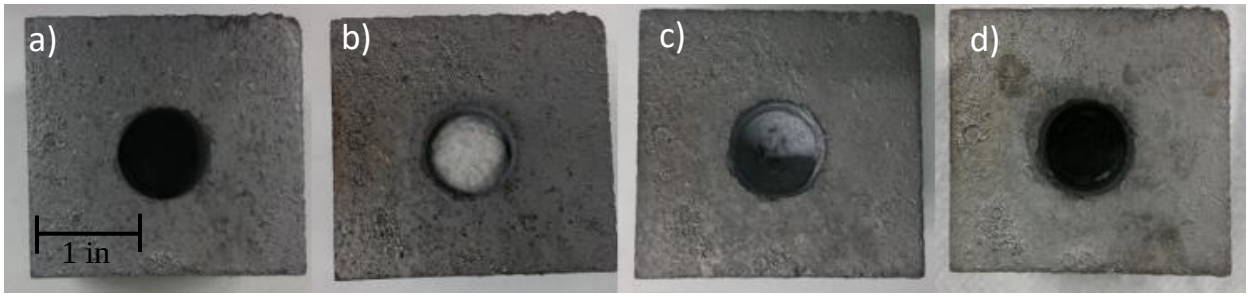

Figure 3.12. Top-down photographs of the pitch/CA_6C-2.1 crucible after a) firing to 750^oC, b) loading with MKN salt and exposing for 100 hr at 750^oC in Ar, c) mechanical removal of the residual solidified salt from the crucible cavity, and d) after the dissolution of the residual solidified salt that was adhered to the cavity wall.

3.4.4 Pitch/CA_6C-1.3 Crucible: 50 hr Molten Salt Test

The pitch/CA_6C-1.2 crucible specimen was immersed in 500 ml of ultrafiltered water for 14 hr at room temperature, dried at 750^oC for 5 hr in industrial-grade Ar, and then re-exposed to the molten MKN salt for an additional 50 hr. Top-down photographs of the pitch/CA_6C-1.2 crucible specimen and this pitch-infiltrated crucible after further 50 hr exposure to molten MKN salt at 750^oC (pitch/CA_6C-1.3) are provided in Figure 3.13. Mass change measurements (Table 3.2) indicated that the pitch/CA_6C-1.3 crucible was penetrated by 82.4% of the non-evaporated salt that had been placed in the crucible cavity. This dramatic increase in the global molten MKN salt penetration upon the third salt re-exposure of this same crucible suggested that a significant change occurred within the specimen between the second (100 hr) and the third (50 hr) salt exposures, which was believed to have resulted from a critical change in the internal surface coverage by the carbonaceous material.

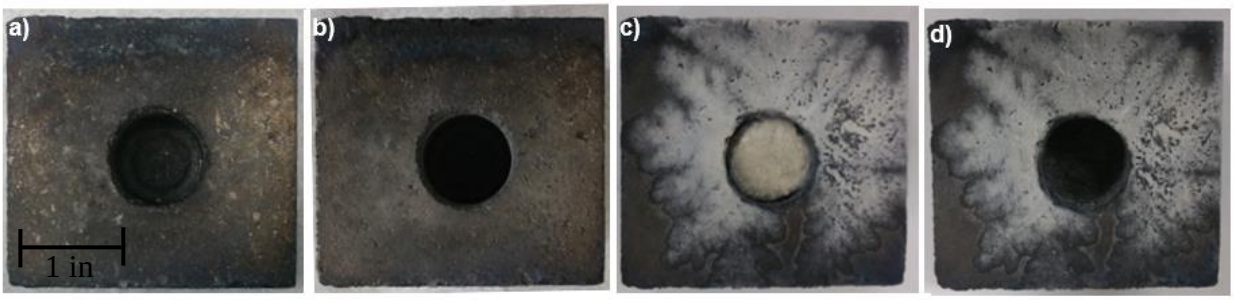

Figure 3.13. Top-down photographs of the same pitch-infiltrated CA_6C crucible after repeated exposure to the MKN salt at 750°C in Ar: a) pitch-infiltrated CA_6C-1.2 after 100 hr exposure to the MKN salt at 750°C in Ar (and after removal of residual solidified salt from the crucible cavity) b) pitch-infiltrated CA_6C-1.2 after soaking for 14 hr in water followed by drying for 5 hr at 750°C in Ar. c) pitch-infiltrated CA_6C-1.3 after exposure of the sample to MKN salt at 750°C for 50 hr in Ar, and d) pitch-infiltrated CA_6C 1.2 sample after removing the residual solidified salt from the crucible cavity.

A change in coverage of internal ceramic surfaces by carbonaceous material in the pitch/CA_6C crucibles could change the molten MKN salt penetration pathway along exposed ceramic surfaces. Further studies were conducted with samples Pitch/CA_6C-3.1, Pitch/CA_6C-4.1, and Pitch/CA_6C-5.1 to investigate the potential causes of such alteration in the carbon coverage.

- Pitch/CA_6C-3.1: a pitch-infiltrated CA_6C crucible specimen annealed at 750°C in Ar for 150 hr to investigate if the carbon coverage was altered due to dewetting of the carbonaceous material from internal ceramic surfaces within the crucible specimen over 750°C annealing time
- Pitch/CA_6C-4.1: a pitch-infiltrated CA_6C crucible specimen thermocyled 5 times to 750°C, held for 30 hr at 750°C for each cycle, to investigate if carbon coverage was altered due to delamination of the carbonaceous material from the internal ceramic surfaces upon thermal cycling (due to the thermal expansion mismatch between the carbonaceous material and the ceramic phases)
- Pitch/CA_6C-5.1: a pitch-infiltrated CA_6C crucible specimen repeatedly exposed to water for 14 hr followed by heating to 750°C for 5 hr in Ar to determine if carbon coverage was altered due to delamination of carbonaceous material from the internal ceramic surfaces due to the repeated formation and decomposition of hydrated or hydroxide-bearing ceramic phases upon repeated exposure to water and heating

Each sample then underwent a 2 hr salt infiltration test at 750°C to study the effect of each process separately on the salt infiltration.

3.4.5 Pitch/CA_6C-3.1 150 hr -Annealed Crucible: 2 hr Molten Salt Test

A pitch/CA_6C crucible was annealed for 150 hr at 750°C in Ar, then was filled with MKN salt and exposed for 2 hr at 750°C in Ar. After removing the solidified salt from the central crucible cavity for global mass change measurements, the pitch/CA_6C-3.1 crucible was found to be penetrated by 11.9% of the non-evaporated salt placed in the crucible cavity (Table 1.1). This was higher than Pitch/CA_6C-1.1 specimen's infiltration, which was annealed for only 8 hr at 750°C prior to 2 hr exposure to molten MKN salt at 750°C. This result suggested that prolonged 750°C annealing prior to molten salt testing altered the coverage of internal ceramic surfaces so as to enhance MKN infiltration. Top-down optical images of the 150 hr-annealed pitch/ CA_6C-3.1 crucible before salt exposure, after 2 hr of exposure to salt, and after removing the salt are provided in Figure 3.14.

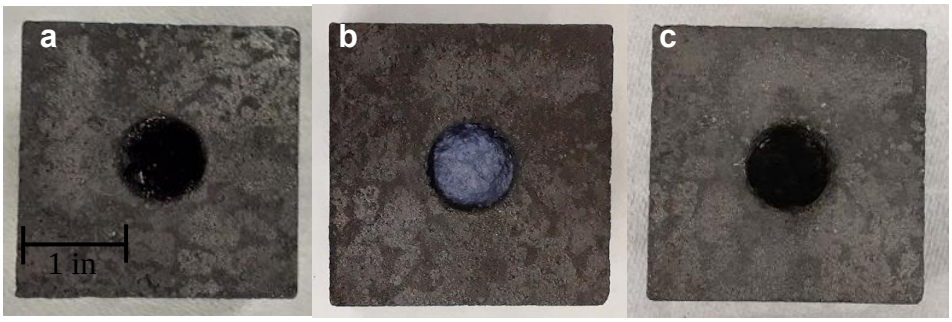

Figure 3.14. Top-down photographs of the pitch/CA_6C-3.1 crucible after: a) annealing for 150 hr at 750°C, b) after loading with MKN salt and exposing for 2 hr at 750°C in Ar, and c) after mechanical removal of the residual solidified salt from the crucible cavity.

3.4.6 Pitch/CA_6C-4.1 Thermocycled Crucible: 2 hr Molten Salt Test

A pitch/CA_6C-4.1 sample was thermally cycled five times between room temperature and 750°C under industrial-grade Ar. A heating rate of 50°C/hr for the first cycle and a heating rate of 100°C/hr for the following 4 cycles. Once the furnace reached 750°C, it was held for 30 hr before moving to the next cycle. (Note: during the 4th cycle, the sample may not have seen a full 30 hr anneal at 750°C due to a furnace malfunction). The pitch/CA_6C-4.1 crucible was then exposed to the molten MKN salt for 2 hr at 750°C in Ar (Figure 3.15). This pitch/CA_6C-4.1 crucible was

found to have been penetrated by 5.5% of the non-evaporated salt placed in the crucible cavity (Table 3.2). Such a modest 5.5% MKN infiltration for the thermally-cycled pitch/CA_6C-4.1 specimen was not greater than the MKN infiltration (11.9%) for the 150 hr annealed Pitch/CA_6C-3.1 sample, which was exposed to the same total time at 750°C (150 hr) but without the thermal cycling. These experiments indicated that thermal cycling between room temperature and 750°C did not appreciably degrade the molten salt penetration resistance of the pitch/CA_6C specimens.

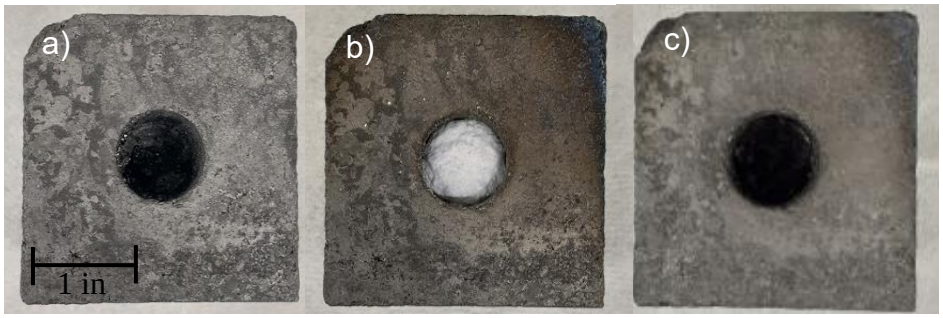

Figure 3.15. Top-down photographs of the pitch/CA_6C 4.1 crucible after: a) 5 thermal cycles between room temperature and 750°C (each with 30 hr anneals at 750°C), b) after loading with the MKN salt and exposing for 2 hr at 750°C, and c) after mechanical removal of the residual solidified salt from the crucible cavity.

3.4.7 Pitch/CA_6C-5.1 Hydration-Cycled Crucible: 2 hr Molten Salt Test

A pitch-infiltrated CA_6C-5.1 crucible was first heated to 750°C for 5 hr in industrial-grade Ar, and then heated for an additional 2 hr at 750°C to confirm there was no additional change in the crucible weight. The sample was then soaked for 14 hr in water at room temperature, followed by heating at 50°C/hr to 750°C in Ar, holding at 750°C for 5 hr, and cooling at 180°C/hr to room temperature. Such water exposure/thermal treatment cycling was repeated five times. The crucible was heated for an additional 3 hr at 750°C to ensure no further mass change and then exposed to molten MKN salt for 2 hr at 750°C in Ar (Figure 3.16). This pitch/CA_6C-5.1 crucible was penetrated by 7.3% of the non-evaporated salt placed in the crucible cavity (Table 3.2.). The modest 7.3% MKN infiltration for this hydration-cycled pitch/CA_6C-5.1 specimen was not greater than the MKN infiltration (11.9%) of the non-hydration-cycled pitch/CA_6C-3.1 crucible that was annealed at 750°C for 150 hr. These experiments indicated that hydration cycling between room temperature and 750°C did not appreciably degrade the molten salt penetration resistance of the pitch/CA_6C specimens.

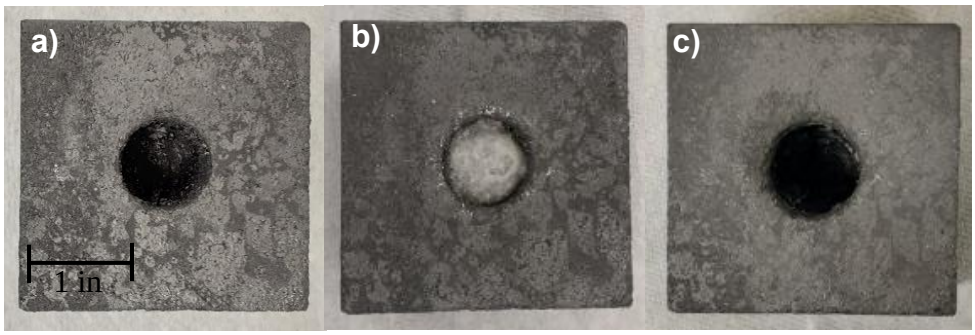

Figure 3.16. Top-down photographs of the pitch/CA_6C-5.1 crucible after a) firing at 750°C for 7 hr, b) after 5 cycles of soaking in water for 14 hr followed by a 5 hr thermal treatment at 750°C, and c) after mechanical removal of the residual solidified salt from the crucible cavity.

The similar and relatively modest values of molten salt infiltration (5.5%-11.9% or 8.7$\pm$3.2%) for these pitch-infiltrated CA_6C specimens (Table 3.2) suggested that 750°C annealing, thermocycling, and hydration-cycling had minimal effect on carbon coverage and did not explain the dramatic infiltration of the twice reused sample, Pitch/CA_6C-1.3. It was hypothesized that the tapping procedure during salt removal between tests may have caused a decrease in carbon coverage or introduced microcracks inside of the sample. This process usually takes over an hour and suggests the sample sees over 4000 taps concentrated by the screwdriver's small tip. The hydration-cycled sample, Pitch/CA_6C-5.1, was then reused for an additional MKN salt exposure to test if an increased salt infiltration was observed.

3.4.8 Pitch/CA_6C-5.2 Crucible: 2 hr Molten Salt Test

The Pitch/CA_6C-5.1 crucible sample that was previously hydration-cycled and exposed to MKN salt for 2 hr was then immersed in water for 14 hr at room temperature, dried at 750°C for 5 hr in industrial-grade Ar, and then re-exposed to the molten MKN salt for an additional 2 hr at 750°C. This pitch/CA_6C-5.2 crucible was penetrated by 92.2% of the non-evaporated salt placed in the crucible cavity (Table 3.2). Photographs of the pitch/CA_6C-5.2 crucible after 2 hr exposure to the MKN salt are provided in Figure 3.17.

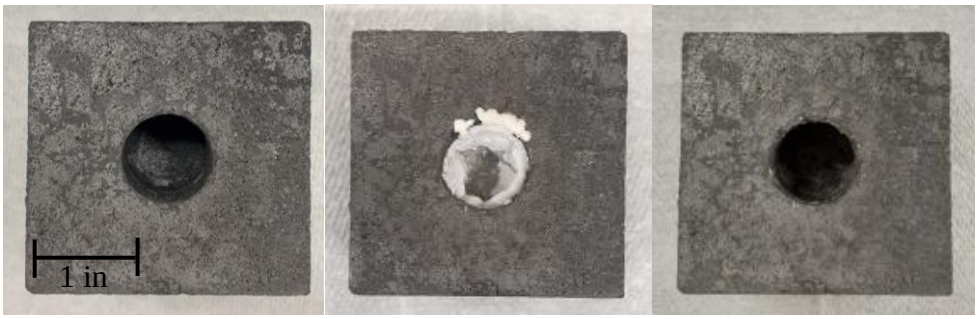

Figure 3.17. Top-down photographs of the pitch/CA_6C-5.2 crucible a) after soaking in water for 14 hr followed by thermal treatment for 5 hr at 750°C, b) after 2 hr exposure to the MKN salt at 750°C, c) after removal of the residual solidified salt from the crucible cavity.

This drastic increase in the salt penetration suggested that the tapping procedure could have affected the internal carbon/CA_6C structure and reduced the carbon's effectiveness in preventing penetration. However, such a drastic increase was not observed between the reuse of the pitch/CA_6C-1.1 crucible for experiment pitch/CA_6C-1.2 (Table 3.2), which saw a similar salt removal procedure. Further evaluation of the crucible weight before exposure to the salt shows a small weight increase for pitch/CA_6C-1.3 and -5.2 before re-exposure to the MKN salt, whereas pitch/CA_6C-1.2 did not. It is possible that the process of dissolving the salt in the water did not provide a dilute enough solution to fully remove the salt inside the crucible cavities. Such salt remaining inside the cavity walls could provide a pathway for fresh salt to penetrate through the crucible in later experiments. While 500 ml of water for less than 1 gram of salt should have been sufficient for dissolution (solubilities of salts in water are $\geq$ 342 g/l [36]), the water was stagnant during this process and may have locally saturated the solution inside the crucible cavity or pores of the crucible, leaving salt behind inside the crucible after firing to 750°C for 5 hr in Ar.

3.4.9 Casting of CA_6C Crucibles

CA_6C crucibles were cast according to the vibration-assisted procedure used by WAM and described in Section 2.6. Plexiglas molds were designed to create a cube-shaped crucible with 2.8 in. outer dimensions and a central cavity in the shape of a truncated cone (0.8 in. diameter on the top, 0.625 in. on the bottom, and 1 in. depth). This design was constrained by the diameter of the tube furnace and the desire to have a crucible wall thickness >3x the largest aggregate in the CA_6C composition. The casting and curing of such samples followed the procedure described in Section 2.6. Once the samples finished drying at 110°C for 24 hr in ambient air, crucibles were then fired

to 850°C for 11 hr in air using a heating rate of 50°C/hr. Photographs of a CA_6C crucible after firing at 850°C are provided in Figure 3.18.

This change in peak firing temperature of crucibles from 1500°C to 850°C was conducted to lower the cost of the final tank solution, as 1500°C firing in the field for a large tank (on the order of 10 m height x 30 m diameter) can be especially challenging and costly. Rather, the components were heated to 100°C above the operation temperature of 750°C, as specified in regular protocols for tank installation [37].

Figure 3.18. Top-down photographs of a cast CA_6C crucible after firing at 850°C for 11 hr.

3.5 Molten Salt Infiltration of Multi-Pitch Infiltrated Samples

Pitch-infiltrated samples provided by Servsteel showed promising results but displayed a range of molten salt infiltration, possibly due to incomplete coverage of the internal ceramic surfaces with carbonaceous material. Efforts were then shifted to creating an in-house pitch infiltration process to control the carbonaceous content and coverage in the sample and understand the effects of increasing the carbon coverage via multiple pitch infiltrations on the resistance to molten salt penetration.

3.5.1 Pitch Infiltration Pressure Vessel Design

To conduct controlled pitch infiltration, a pressure vessel and sample holder were designed to achieve and exceed the temperature/pressure conditions used by Servsteel. The minimum thickness of the pressure vessel was computed by the following formula obtained from the *ASME Boiler and Vessel Pressure Code VIII - Rules for Construction of Pressure Vessel Division 1* [38]:

$$t = \frac{PR}{SE - 0.6P}$$

where,

t = minimum required thickness of shell (in inches)

E = weld joint efficiency factor, determined by joint location and degree of examination

P = internal design pressure (psi)

R = inside radius of the shell course under consideration (in.)

S = maximum allowable stress value (psi)

For the tube to fit inside the furnace, the pressure vessel's outer diameter was designated to be 6.625 in. Hence, the inside radius of the vessel, R, needed to be: R = ½ × (6.625-2t) in. The values of other parameters used in the equation above are:

P = 150 psi (maximum pressure to be used for pitch infiltration at 371^{o}C)

E = 0.5 (weld joint efficiency for a 300 series stainless decreases with temperature, so a worst-case scenario was considered with the use of E= 0.5, though below 510^{o}C a more representative value would be 0.85-1 [39])

S = 12,100 psi (at 700^{o}F (371^{o}C), ASME BVPC. II. D.C-2015 for 316 stainless steel)

Insertion of those values into the equation above yielded a vessel wall thickness of t = 0.0813 in. Hence, for a rough safety factor value of 2.5, the vessel's wall thickness needed to be at least 0.203 in.

Therefore, a 316 stainless steel pipe with an outer diameter of 6.625 in. and thickness of 0.28 in. was purchased, and a 316 stainless steel plug was welded into one end. A flange was then welded on the other end of the tube to allow a seal plate to be added with ports for an inlet, outlet, pressure relief valve, and thermocouple. A schematic illustration of the pressure vessel that highlights components on the endcap (and is not to scale with the illustration of the sample holder) is shown in Figure 3.19. An illustration with the dimensions to scale is provided in Figure 3.21.

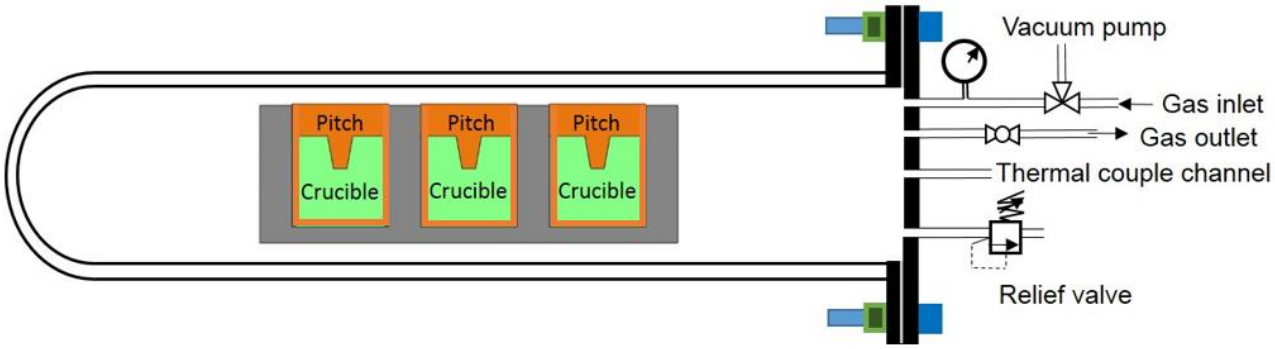

Figure 3.19. A schematic illustration of the pressure vessel containing an aluminum sample holder for the pitch infiltration of CA_6C crucibles (modified schematic originally by Dr. Liangjuan Gao).

A finite element simulation using SolidWorks® was performed by Dr. Saeed Bagherzadeh to determine the stress distribution on the system up to 150 psi and at 371°C, which were the extreme conditions considered for pitch infiltrations. The results of the simulation are included in Figure 3.20. A safety factor of 5 was calculated under operating conditions of 182°C and 60 psi from the simulation and was considered satisfactory.

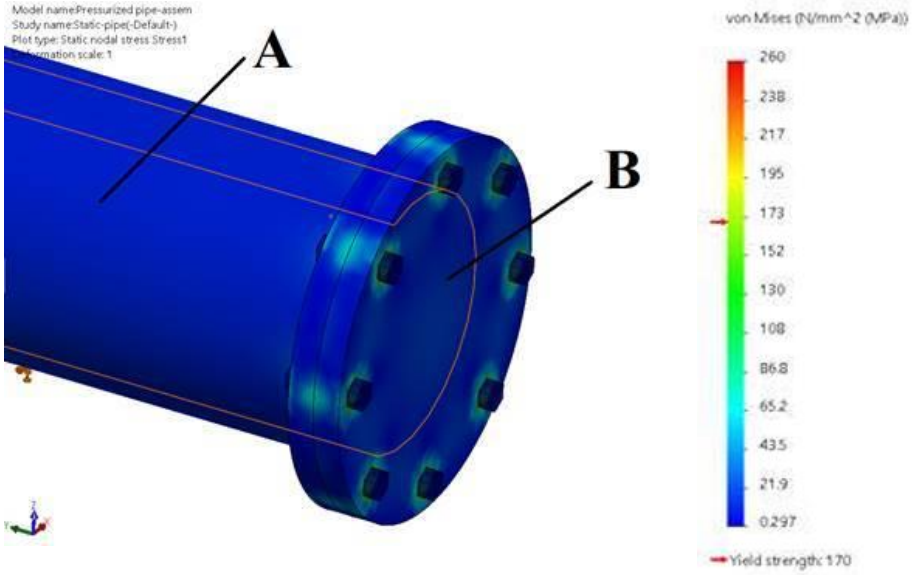

Figure 3.20. The stress distribution in the pressure vessel derived from a finite element simulation up to 150 psi at 371°C.

The pressure vessel was inserted into a horizontal furnace, as shown previously in Figure 2.7. An aluminum sample holder was designed for holding 3 cube-shaped crucible specimens within the pressure vessel for each pitch infiltration trial, as described in Section 2.8. A schematic illustration of the infiltration tube assembly with the dimensions of items to scale is provided in Figure 3.21.

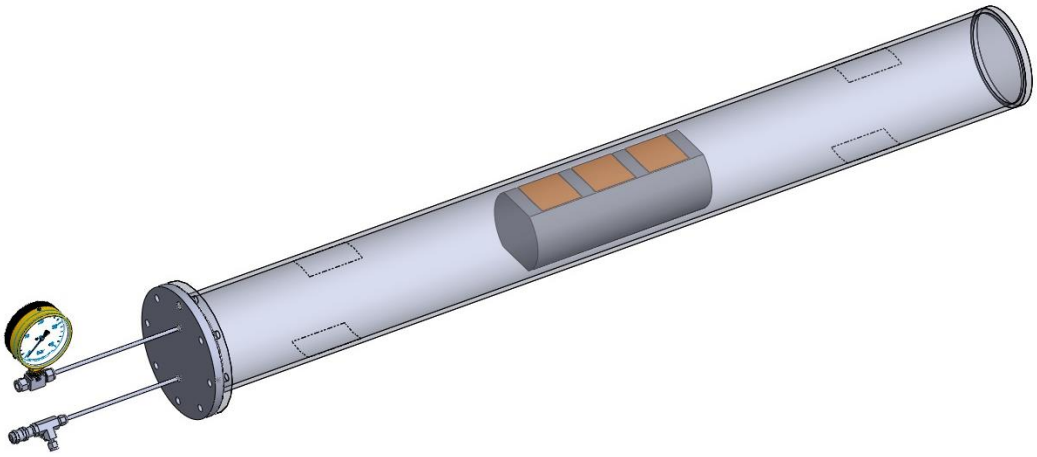

Figure 3.21. a) A schematic illustration of the pressure vessel and sample holder used for pitch infiltration (illustration courtesy of Dr. Saeed Bagherzadeh).

3.5.2 Pitch Infiltration of CA_6C Crucibles

The pressure-aided infiltration procedure described by Servsteel was replicated as closely as possible in initial trials but resulted in samples that were incompletely covered with pitch. Experimental details of modifications made to our pitch infiltration can be read in more detail in Appendix B: Pitch Infiltration Trials. CA_6C samples used for the study with multiple pitch infiltration cycles all followed the procedure described in Section 2.8, which is summarized below.

CA_6C samples were placed in a stainless steel mesh basket, then lowered into the aluminum sample holder. The same pitch used by Servesteel (CTF-19, a petroleum-based, coal-tar-free, with a melting point of 104-124^{o}C from Lone Star Specialties, LLC) was heated to 120^{o}C for at least 1 hr before being poured over the crucible samples in the aluminum holder. The assembly was then placed in the pressure vessel, heated to 120^{o}C, held for 1 hr to allow the assembly to heat uniformly and ensure the pitch viscosity was low enough to allow gas bubbles to outgas freely through the pitch. The pressure vessel was evacuated with a roughing pump and backfilled with Ar three times to remove gas from the CA_6C crucible sample and liquid pitch. This purging and backfilling was a modification to the commercial Servsteel pitch infiltration process, which involved dunking the

sample into a vat of pitch (which was not possible to replicate in our horizontal tube furnace). The chamber was returned to vacuum and actively pumped as it heated to 182^{o}C at 50^{o}C/hr, and then held for 45 min under vacuum. The chamber was then pressurized at 182^{o}C to 60 psi using Ar and held for 45 min. The pressure was held at 60 psi as the sample cooled down to 100^{o}C, then the pressure was slowly released, and the sample holder was removed from the pressure vessel. The mesh basket was used to remove the CA_6C crucible from the pitch, and the warm pitch remaining in the central crucible cavity was poured out. The sample was cooled to room temperature in ambient air for 3-4 hrs before weight change measurements were conducted. Photographs of the first sample to undergo three pitch infiltration cycles are provided in Figure 3.23. Samples are labeled with their crucible number followed by the pitch infiltration cycle such that Sample 1.1 refers to the first test crucible after the first infiltration cycle (Figure 3.23.-a), Sample 1.2 refers to the first test crucible after the second infiltration cycle (Figure 3.23.-c), and Sample 1.3 after the third infiltration cycle (Figure 3.23.-e). Side view images of a CA_6C crucible after pitch infiltration and subsequent firing at 850^{o}C in Ar are provided in Figure 3.22.

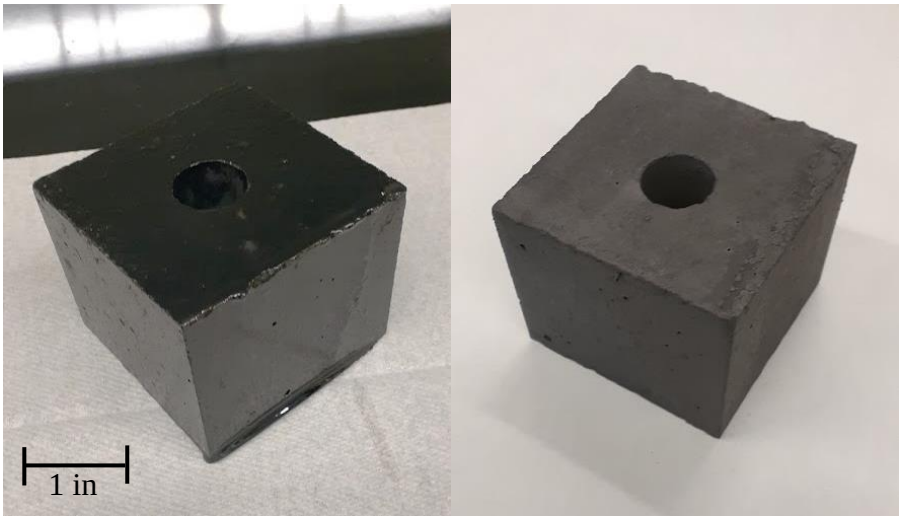

Figure 3.22. Side-view images of a CA_6C crucible after: a) a pitch infiltration and b) subsequent firing at 850^{o}C in Ar.

The pitch-infiltrated samples were then heated at 850^{o}C in Ar for 11-13 hr (i.e., until no further mass loss is detected). This process of pitch infiltration and 850^{o}C firing was repeated 3 times for each sample. As shown in Figure 3.24., no further appreciable mass gain of the pitch-

infiltrated CA_6C specimen was detected after three pitch infiltrations and subsequent heat treatments at 850°C.

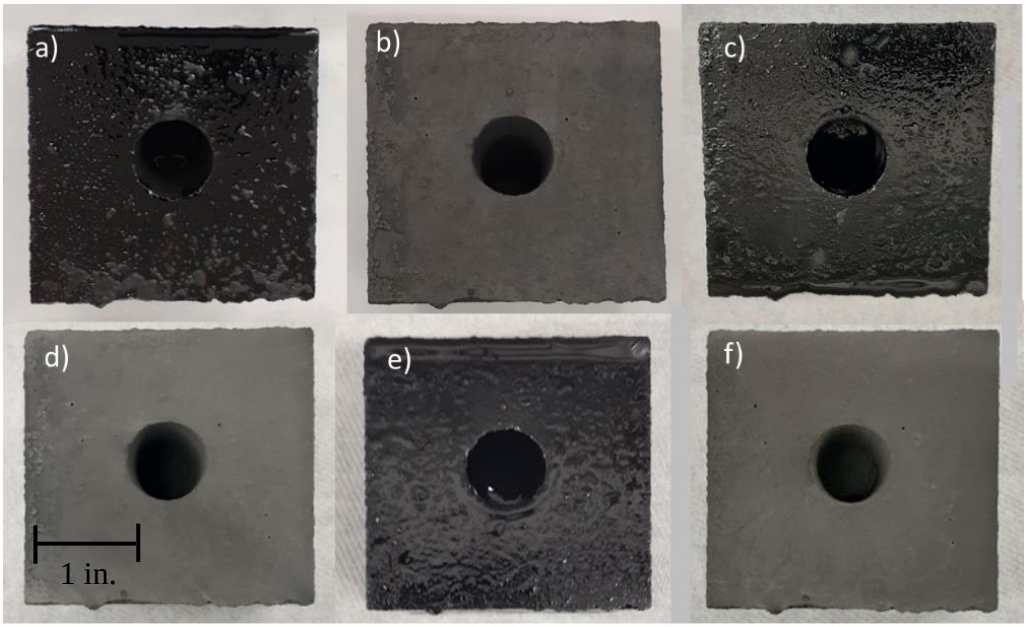

Figure 3.23. Top-down photographs of the crucible Sample 1 after: a) the first pitch infiltration (Sample 1.1), b) firing Sample 1.1 at 850°C for 11 hr in Ar, c) the second pitch infiltration (Sample 1.2), d) firing Sample 1.2 at 850°C for 11 hr in Ar, e) the third pitch infiltration (Sample 1.3), and f) firing sample 1.3 at 850°C for 11 hr in Ar.

Three additional samples, named Samples 2, 3, and 4, were also infiltrated three times following the same procedure as for Sample 1. A summary of the weigh change measurements for samples after each infiltration cycle is provided in Table 3.3

Table 3.3. Summary of the sample weights, relative weight gains, and cumulative weight gain after each pitch infiltration cycle

	Sample 1	Sample 2	Sample 3	Sample 4	Average
Infiltration Cycle 1					
Starting weight of sample (no carbon)	816.05	772.20	802.79	799.00	
Weight after first pitch infiltration	907.27	855.34	887.27	882.65	
Weight gain of sample	91.22	83.14	84.48	83.65	
% weight gain	11.18%	10.77%	10.52%	10.47%	10.74%
Weight after 11 hr at 850ºC	839.32	795.46	825.87	821.75	
Cumulative weight gain after 850ºC	23.27	23.26	23.08	22.75	
Cumulative % weight gain of sample	2.85%	3.01%	2.87%	2.85%	**2.90%**
Infiltration Cycle 2					
Weight after second pitch infiltration	868.88	815.12	858.29	843.02	
Weight gain relative to start of Cycle 2	29.56	19.66	32.42	21.27	
Relative % gain relative to start of Cycle 2	3.52%	2.47%	3.93%	2.59%	3.13%
Weight after 11 hr at 850ºC	851.21	803.52	838.06	830.73	
Weight gain relative to start of Cycle 2	11.89	8.06	12.19	8.98	
% weight gain relative to start of Cycle 2	1.42%	1.01%	1.48%	1.09%	1.25%
Cumulative weight gain after 850ºC	35.16	31.32	35.27	31.73	
Cumulative % weight gain of sample	4.30%	4.06%	4.39%	3.97%	**4.18%**
Infiltration Cycle 3					
Weight after third pitch infiltration	865.57	808.29	844.19	835.79	
Weight gain after third pitch infiltration	14.36	4.77	6.13	5.06	
Relative % gain relative to start of Cycle 3	1.69%	0.59%	0.73%	0.61%	0.91%
Weight after 11 hr at 850ºC	856.6	805.26	840.53	832.82	
Weight gain relative to start of Cycle 3	5.39	1.74	2.47	2.09	
% weight gain relative to start of Cycle 3	0.63%	0.22%	0.29%	0.25%	0.35%
Cumulative weight gain after 850ºC	40.55	33.06	37.74	33.82	
Cumulative % weight gain of sample	4.97%	4.28%	4.70%	4.23%	**4.55%**

The pitch infiltration process yielded relatively consistent carbon incorporation for each sample after the first infiltration cycle (2.90 g ±0.08 g). The spread in the cumulative weight gain values increased with each infiltration but remained under 0.5%, with values of 4.18 ±0.20% and 4.55 ±0.36% after the second and third infiltration cycles, respectively. As shown in Figure 3.24.

the cumulative amount of carbonaceous material continued to increase over each infiltration and the relative amount gained each cycle decreased with each successive infiltration cycle.

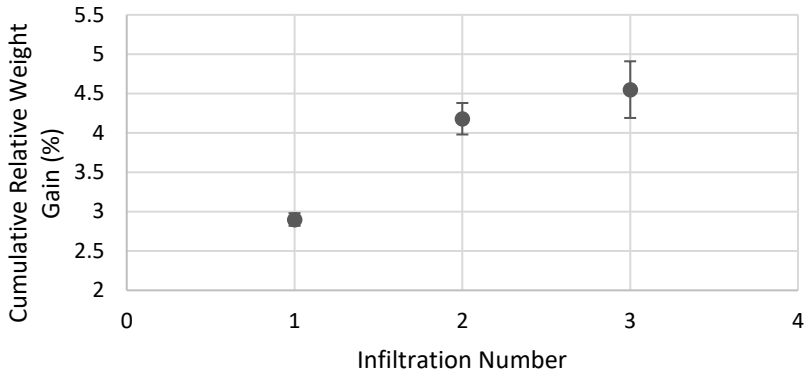

Figure 3.24. The average cumulative weight gain and standard deviation of pitch-infiltrated samples after successive pitch infiltration cycles and heat treatments at 850°C.

3.5.3 Estimate of Pores Filled with Carbonaceous Material

The percentage of pores filled with carbonaceous material after infiltration and after thermal treatment at 850°C was estimated by comparing the calculated volume of the carbonaceous material in the sample to the open pore volume of the sample, as indicated by the following equation:

$$\%\ of\ pores\ filled = \frac{100 \times (m_{c1} + m_{c2})}{(\rho_{c1} + \rho_{c2})V_s P}$$

where m_{c1} is the mass of the pitch infiltrated into the sample (as determined by the weight gain of the sample after infiltration, Table 3.3), and m_{c2} is the mass of 850°C-fired carbonaceous material (as determined by the cumulative weight gain of the sample after firing at 850°C, Table 3.3); ρ_{c1} is the density of CTF 19 pitch as provided in the datasheet (1.22 g/cm^3) [40], and ρ_{c2} is the density of the carbonaceous material as determined by Helium pycnometry (1.89 g/cm^3, as discussed in Section 2.10). V_s is the sample's external volume (obtained by the dimension measurements of the crucible), and P is the apparent porosity of the CA_6C crucible sample. The measured average porosity of CA_6C samples (P= 0.251) was used, as described in Section 2.11. Table 3.4. summarizes the resulting % pores filled calculated for each sample after each pitch infiltration and subsequent heat treatment at 850°C for 11 hr.

Table 3.4. Summary of the percent pores filled as calculated using values from Table 3.3

	Pitch Infiltration 1	Pitch Infiltration 1 after 850°C	Pitch Infiltration 2	Pitch Infiltration 2 after 850°C	Pitch Infiltration 3	Pitch Infiltration 3 after 850°C
Sample 1	91.9	15.1	44.9	22.9	37.2	26.4
Sample 2	89.9	16.2	37.4	21.9	27.1	23.1
Sample 3	89.6	15.8	50.2	24.1	30.6	25.8
Sample 4	87.4	15.3	37.6	21.4	26.7	22.8

3.5.4 100 hr Molten Salt Tests with CA_6C Crucibles Exposed to Three Pitch Infiltration Cycles

Sample 1 was filled with an MKN salt sample provided by MIT that was purified in a large, 8 kg batch of salt using an Ar sparging process, and tested separately for MKN infiltration after 100 hr at 750°C in Ar. Samples 2, 3, and 4 were filled with the MKN salt prepared in Section 2.2, then heated together to 750°C for 100 hr under Ar for salt infiltration studies.

Once cooled to room temperature, samples were removed from the furnace and weighed to determine how much salt evaporated from the sample, then the crucibles were placed in an Ar-atmosphere-controlled glovebox prior to salt removal from the cavity of each sample. It was noticed that more salt evaporated for each sample (2.7 g ±0.19 g) compared to the 100 hr test with sample Pitch/CA_6C-2.1 (1.05 g, see Table 3.2). Salt was mechanically removed from each cavity as described in Section 2.7, then dabbed with water-soaked cotton swabs to remove the remainder of the salt, and dried under vacuum for 3 hr. It was observed that an apparent product remained adhered to the surface of the sample and needed to be removed to obtain accurate weight change measurements.

The surface of Sample 1 was lightly sanded with 180 grit SiC paper, which resulted in a small 0.02 g decrease in the sample weight. The apparent product was then dabbed with 0.8 M acetic acid, which resulted in no weight change in the sample after drying under vacuum. This was followed by dabbing with 0.1 M HCl, which visually appeared to have removed some of the apparent product from the sample (Figure 3.25.-h), but also resulted in no further weight loss of the sample. The resulting weight for Sample 1 displayed a weight gain of 0.36 g, which corresponded to 4.55% infiltration of the MKN salt. Photographs of Sample 1 after 3 pitch

infiltration and 850°C thermal treatment cycles, after being loaded with the MKN salt and exposed the MKN salt for 100 hr at 750°C in Ar, and after each step of removing the solidified salt and apparent product from the surfrace of the crucible are provided in Figure 3.25.

Table 3.5. Summary of weight change measurements of multi-pitch infiltrated samples after 100 hr exposure to MKN salt at 750°C in Ar.

	Sample 1	Sample 2	Sample 3	Sample 4
Weight of sample after final thermal treatment at 850°C (g)	856.6	805.26	840.53	832.82
Weight with salt in the cavity (g)	867.32	814.75	849.38	840.74
Exposure time at 750°C	100 hr	100 hr	100 hr	100 hr
Weight after exposure to salt (g)	864.51	811.96	846.6	838.32
Weight of added salt accounting for evaporation (g)	7.91	6.70	6.07	5.50
Weight after removing salt (g)	856.96	806.53	841.23	833.25
Weight of salt infiltrated (g)	0.36	1.27	0.70	0.43
% infiltration	4.55%	18.96	11.53	7.82

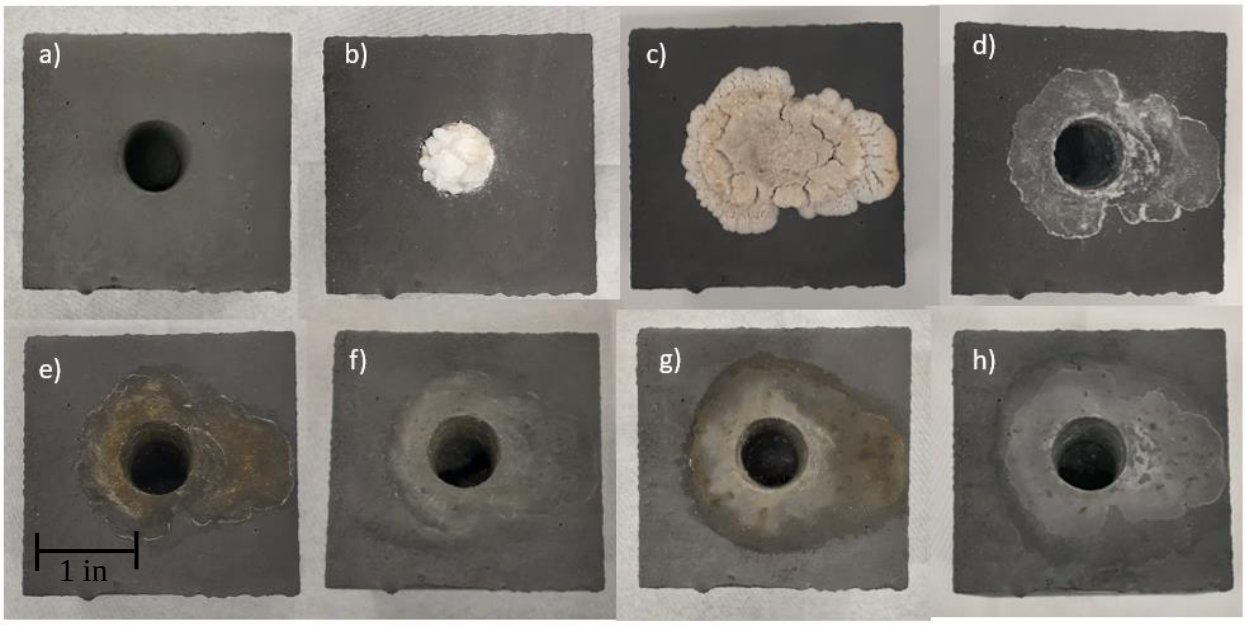

Figure 3.25. Top-down photographs of Sample 1.3 after: a) thermal treatment at 850C for 11 hr b) being filled with MKN salt from MIT, c) after 100 hr exposure at 750°C in Ar, d) after mechanically removing salt from the surface, e) using water-soaked cotton swabs to remove the remaining salt and drying under vacuum for 1 hr, f) After lightly sanding the surface with SiC paper, after dabbing with acetic acid, followed by water and drying under vacuum for 1 hr, and g) after dabbing with 0.1 M HCl, followed by water and drying under vacuum for 1 hr.

Samples 2, 3, and 4 followed a similar salt and apparent product removal procedure. Dissolution of the salt with water-soaked cotton swabs was directly followed with HCl-soaked cotton swabs. The sample was dabbed with water-soaked cotton swabs again to dilute acid on the surface, then dried under vacuum. In an attempt to dissolve more product, the acid-soaked cotton swab procedure was repeated with HCl that was heated to 60^{o}C; however, no further weight loss was observed for the samples. The tops of samples were then lightly sanded with a 180 grit SiC paper, which resulted in a small weight loss (0.01-0.02 g for the samples, which is within the accuracy of the scale). Care was taken to minimize any removal of the carbonaceous material, and as shown in the photographs (Figure 3.26.-f, Figure 3.27.-d, and Figure 3.28-d) some product remained on the surface.

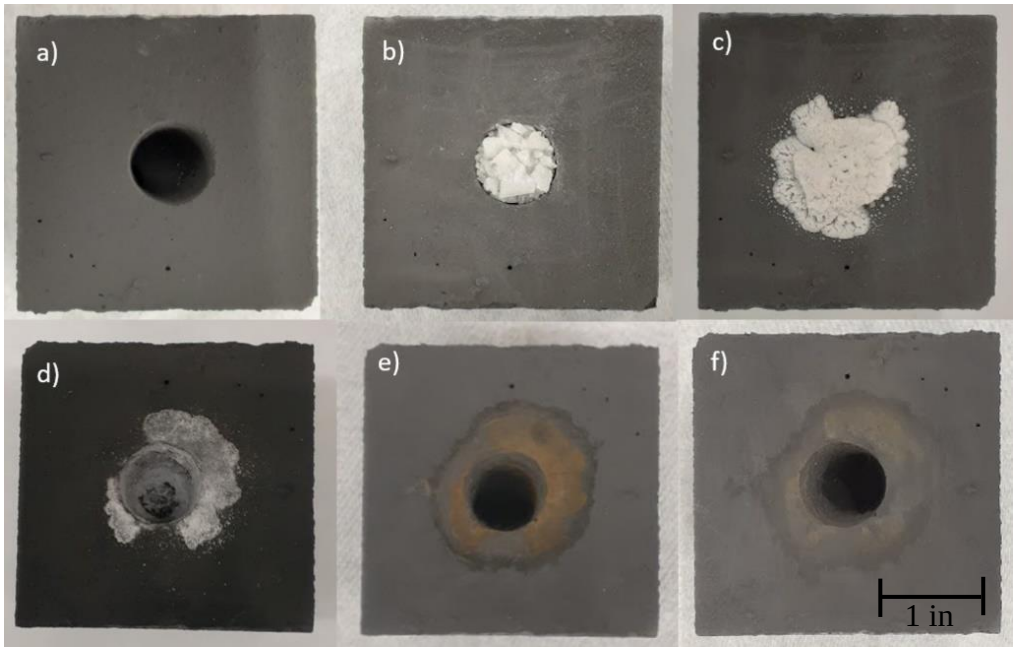

Figure 3.26. Top-down photographs of Sample 2.3 after: a) 11 hr at 850^{o}C in Ar, b) filled with MKN salt, c) after 100 hr exposure at 750^{o}C in Ar, d) after mechanically removing the salt from the cavity, e) after dabbing with water-soaked cotton swabs, followed by removal with heated HCl, and drying under vacuum for 3 hr, and f) after lightly sanding the apparent product on the surface with SiC paper.

After removing the salt and apparent product from the surface of the crucible cavity, Sample 2 showed a weight increase of 1.27 g, which corresponded to 18.96% infiltration of the MKN salt (Table 3.5). Sample 3 showed a weight increase of 0.70 g, and Sample 4 showed a weight increase of 0.43 g (11.53% and 7.82% infiltration of the MKN salt, respectively).

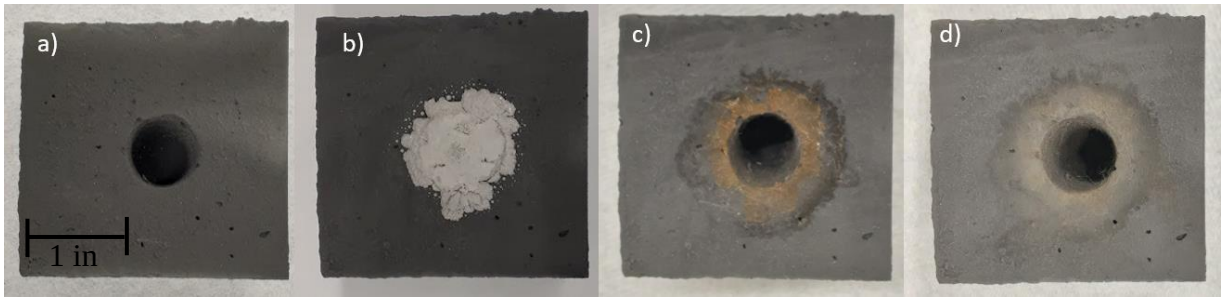

Figure 3.27. Top-down photographs of Sample 3.3 after: a) 11 hr at 850^{o}C in Ar, b) after 100 hr exposure to MKN salt at 750^{o}C in Ar, c) after mechanically removing the salt from the cavity followed by dabbing water-soaked and heated HCl-soaked cotton swabs, followed by drying for 3 hr under vacuum and d) after lightly sanding the apparent product with SiC paper.

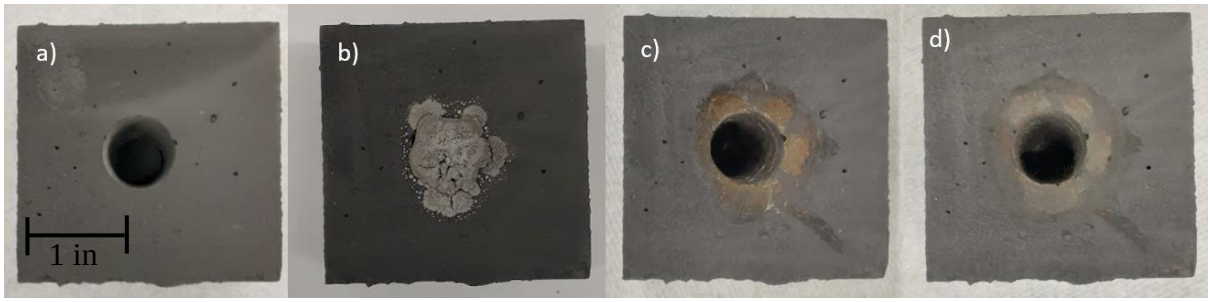

Figure 3.28. Top-down photographs of Sample 4.3 after: a) 11 hr at 850^{o}C in Ar, b) after 100 hr exposure to MKN salt at 750^{o}C in Ar, c) after mechanically removing the salt from the cavity followed by dabbing water-soaked and heated HCl-soaked cotton swabs, followed by drying for 3 hr under vacuum and d) after lightly sanding the apparent product with SiC paper.

It was noticed that Samples 2, 3, and 4 showed an increased weight gain as the position of the sample moved closer to the endcap in the furnace. However, all samples were within the hot-zone of the furnace (6 in. of ± 2^{o}C and 8 in. of ±5^{o}C at 750^{o}C), which should not have resulted in any of the samples drastically cooling relative to each other, as to result in condensation of salt vapor onto the samples. Even if such condensation on a sample occurred, the vapor pressures of the individual molten salts are < 1 Torr, at 750^{o}C [41], which corresponded to a concentration of just 0.01g in the tube volume (by applying PV=NRT).

While multi-pitch infiltrated crucibles ranged from 4.55-18.96% infiltration of the molten salt, such penetration was still improved by 80-95% compared to the molten salt infiltration of carbon-free CA_6C samples. As shown in the weight gain measurements (Table 3.3), more carbon can still be introduced into the sample. While a fourth infiltration is expected to result in a relatively small increase in the weight of carbonaceous material, it may provide the coverage necessary to coat the inner surfaces and prevent salt infiltration. Sample 1 was cross-sectioned to observe the distribution of carbon and MKN salt in the sample.

3.5.5 Cross Section SEM-EDX Analysis

Sample 1 was cross-sectioned using a wafering diamond blade on a slow speed saw with mineral oil as the cutting fluid, as described in Section 2.12. The large size of the crucible required cutting the sample into multiple small pieces before obtaining a cross-section of the bottom portion, where the salt was in contact the longest with the MKN salt. Photographs of Sample 1.3 (after 100 hr exposure to the MKN salt) during the cross-sectioning process are provided in Figure 3.29. Cross-sections did not show any obvious signs of salt infiltration, as would be indicated by a region of discoloration around the central cavity.

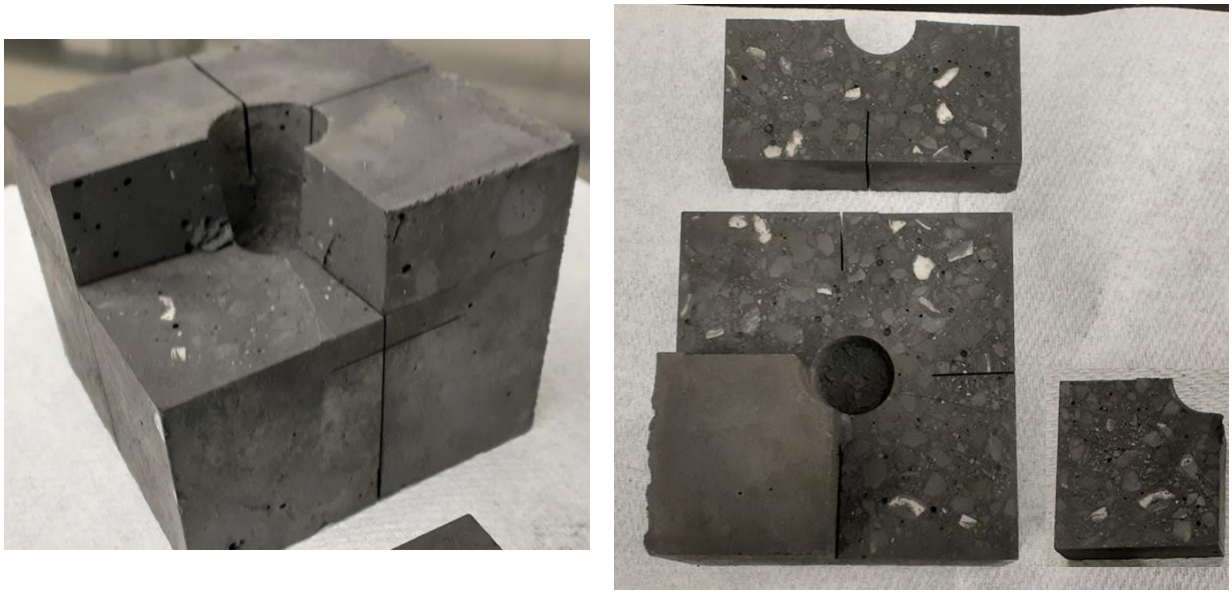

Figure 3.29. Side-view and top-down optical images when cross-sectioning Sample 1.3 after exposure to the MKN salt from MIT for 100 hr.

Cross-sections of Sample 1.3 also showed that the pitch infiltration process described in Section 3.5.2 was successful in fully infiltrating through the thickness of the sample, but not successful in fully infiltrating through all of the large CA_6 grains, as indicated by the white regions in the cross-section (Figure 3.29. and Figure 3.30.). These grains did not appear to be interconnected in Sample 1, and it is of interest to compare the distribution of infiltrated grains to the cross-section of Sample 2, which had the highest salt infiltration of the 4 samples. Continued studies of Sample 2 will include cross-sectioning the crucible and inspecting the sample for any uncoated, interconnected CA_6 grains near the crucible cavity, as such grains could provide regions for the salt to wet and infiltrate. Future pitch infiltrations could benefit from increasing the infiltration pressure or lowering the pitch viscosity to successfully infiltrate these CA_6 grains and investigate the effect on the resistance to molten salt infiltration.

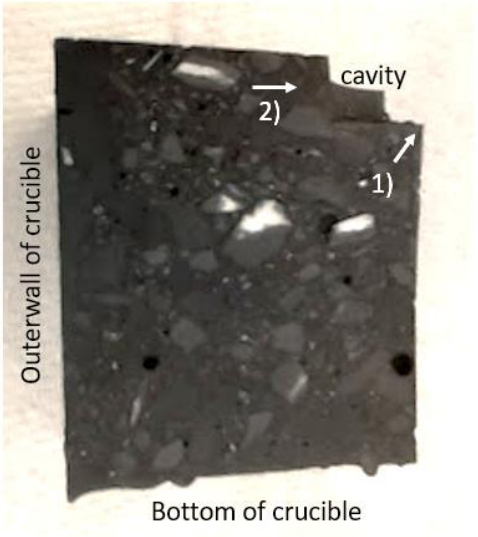

Figure 3.30. A photograph of the cross-section from the bottom of the crucible below the central cavity, indicating the regions where SEM images (in Figure 3.31 and Figure 3.32.) were analyzed.

A cross-section was obtained from the bottom of the crucible cavity, as shown in Figure 3.30, to observe the salt penetration into the sample with SEM/EDX analysis. Once dried, the cross-section was first analyzed without polishing the surface for two reasons: (i) samples containing a large amount of salt have prevented the mounting epoxy from curing properly, which has ruined cross-sections of earlier samples, (ii) salt and carbon tends to pull out of the sample and smear across the surface, making it difficult to determine which regions truly had salt present before polishing. Continued studies will include polishing the cross-sections to perform better EDX analysis in regions of interest.

The cross-section from the bottom of the salt-infiltrated crucible cavity was analyzed by SEM and preliminary EDX to observe the presence of chlorides. SEM and EDX images at Location 1 in Figure 3.30. are provided in Figure 3.31. Data collected near the surface was compared to images collected approximately 3 mm away from the cavity surface, as indicated by Location 2 in Figure 3.30. SEM and EDX analysis at Location 2 is provided in Figure 3.32. Chlorides were evident from the surface of the crucible cavity (Location 1), to approximately 1 mm from the cavity walls.

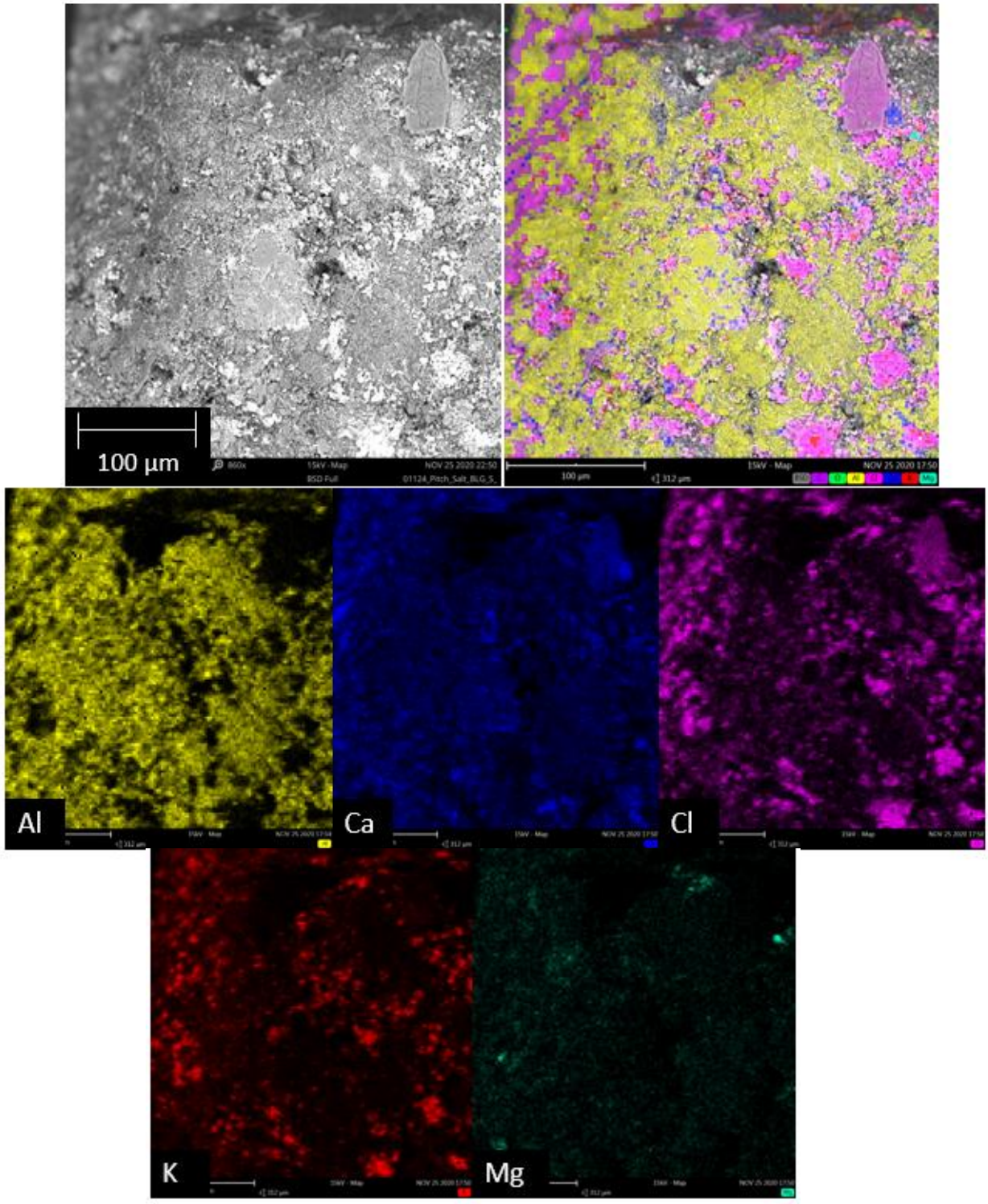

Figure 3.31. An SEM/Backscattered image at the bottom of the crucible cavity, marked as Location 1 in Figure 3.30., and preliminary EDX maps of Al, Ca, Cl, K, and Mg, showing the infiltration of salt into the crucible sample.

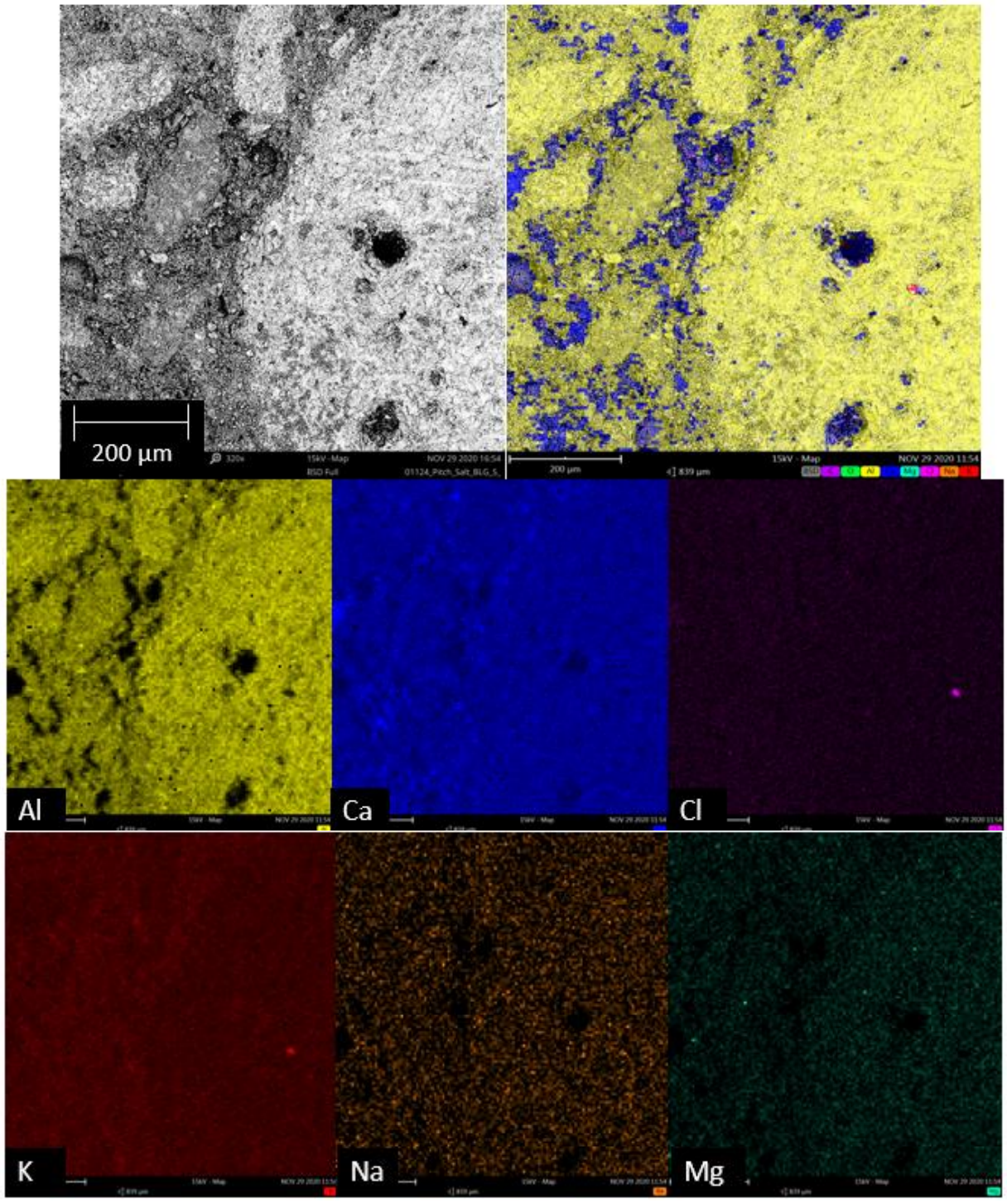

Figure 3.32. An SEM/Backscattered image further away from the cavity at the bottom of the crucible, marked as Location 2 in Figure 3.30., and preliminary EDX maps of Al, Ca, Cl, K, Na, and Mg showing the likely lack of infiltration of salt into the crucible sample.

The EDX spectra obtained during the analysis of Locations 1 and 2 are provided in Figure 3.33. There was some overlap between Ca and K peaks, which will make it difficult to confirm the absence of salt in polished samples and will require the use of better EDX analysis techniques that allow individual peaks to be selected, such as at 3.2 keV for the potassium peaks and 3.9 keV for the calcium.

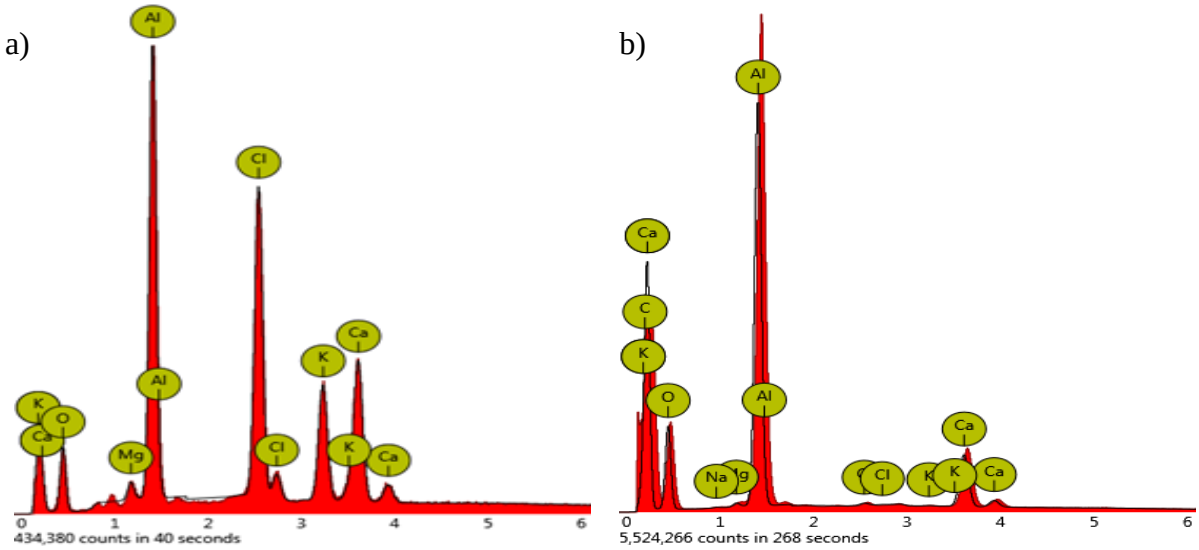

Figure 3.33. EDX patterns obtained at: a) Location 1, which was near the crucible cavity, and b) Location 2, which was about 3 mm from Location 1.

The apparent distribution of salt by SEM/EDX analysis was consistent with modest salt penetration into Sample 1 (4.55%, Table 3.5). It will be of interest to cross-section Sample 2, which had the highest infiltration (18.96%), to observe the distribution of non-pitch infiltrated grains and salt penetration throughout the sample. It was hypothesized that the high penetration was caused by the distribution of non-pitch-infiltrated grains near the crucible cavity, which may not be captured in a single cross-section of the sample. Continued work may include the removal of such CA_6 grains, which would remove the non-pitch infiltrated surface that can be wet and penetration by the molten salt.

3.6 Multiwall (Porous Ceramic/ Packed Graphite Powder) Approach

While the pitch infiltration approach showed promise and certainly has improved the containment of molten salts compared to non-pitch infiltrated CA_6C samples, this approach can also be challenging to implement in the field. Bricks or large sections would need to be cast and

repeatedly fired under an inert atmosphere to remove volatile pitch constituents, introducing additional cost and complexity. While certainly not impossible and still a potential solution, a second carbon particle-based approach was also explored, as discussed in the following section.

Graphite was confirmed to show good resistance to wetting and penetration of molten MKN salt in Section 3.3. However, a tank comprised of shaped, rigid graphite walls at the scale required for CSP would be relatively expensive. Additionally, the poor erosion resistance of graphite is unattractive for flowing salt systems (as is the case for CSP thermal storage tanks that are continually being filled and emptied). This second approach takes advantage of the salt's high infiltration into porous CA_6C to create an erosion barrier backed with a packed graphite particle bed that serves as a non-wetting barrier to hinder further salt penetration. A schematic illustration of the multiwall layers as applied to a thermal energy storage tank is provided in Figure 3.34.

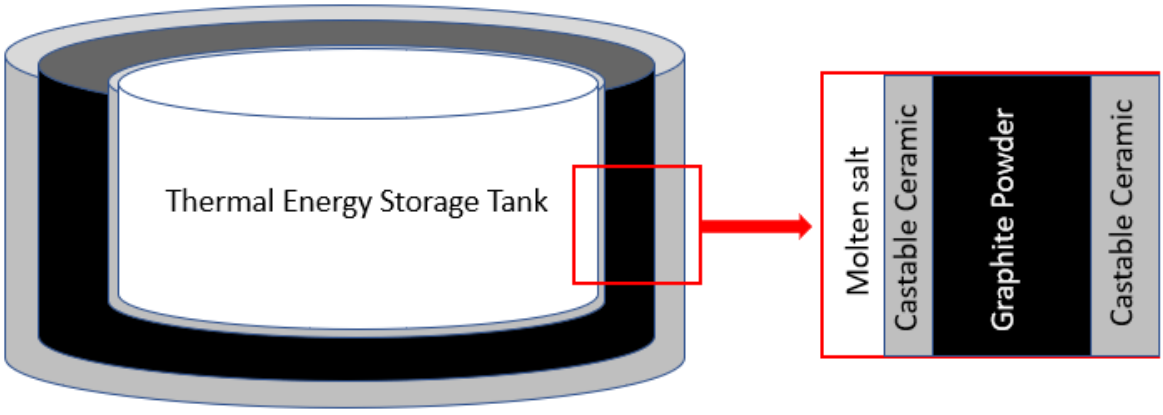

Figure 3.34. Schematic illustration showing the proposed layers of the multiwall approach to contain molten chlorides in thermal energy storage tanks.

3.6.1 Component Assembly and 24 hr Salt Infiltration Test

The multiwall test crucible was assembled as described in Section 2.17. A photograph of the crucible assembly is provided in Figure 3.35.-a. The graphite powder's relative packing density after the vibration-assisted packing was calculated to be 0.405 (0.92 g/cm^3 compared to 2.26g/cm^3 for dense graphite). The tape and parafilm were then removed, and the cavity of the inner crucible cavity was filled with additional MKN salt (Figure 3.35.-a). The assembly was then placed on a graphite tray, then placed in the STT-1500C-6-36 furnace under Ar (100 ppm O_2) and exposed at

750^{o}C for 24 hr. A photograph of the multiwall assembly after 24 hr exposure at 750^{o}C in Ar is provided in Figure 3.35.-b.

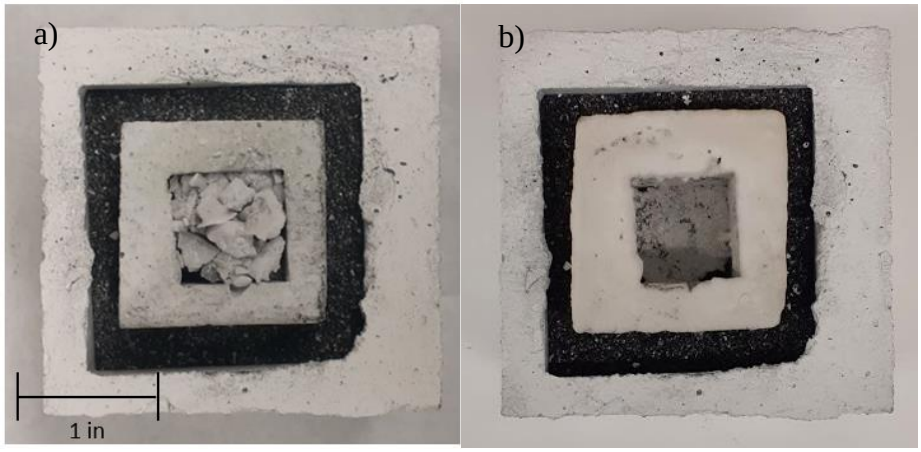

Figure 3.35. Top-down photographs of the multiwall assembly: a) before and b) after 24 hr at 750^{o}C in Ar.

3.6.2 Assembly Weight Change Calculations

Once removed from the furnace, the entire assembly was weighed. This weight was compared to the assembly weight before the 24 hr test at 750^{o}C to determine how much salt had evaporated. The inner crucible was easily lifted out of the surrounding graphite powder and was gently tapped to remove loose graphite powder. It was observed that some graphite remained attached to the outer surfaces of the inner CA_6C crucible (Figure 3.36.-b). It was also observed that the graphite between the crucibles remained relatively loose and free-flowing. The loose graphite powder was carefully recovered and weighed. Graphite adhering to the inner surfaces of the outer crucible (Figure 3.36.-a) was collected by careful tapping of the outer crucible over a collection tray and using cotton swabs to help remove the remaining graphite.

If the multiwall approach was ineffective at preventing the penetration of the molten salt through the assembly then an increase in the weight of the graphite of about 12 g was expected (12 g is the difference between salt used to fill the pores of the inner crucible and the total salt added once taking into account the evaporation of the salt). Instead, a small 2.97 g weight loss of the graphite powder was detected. This alone suggested that little salt infiltrated into the graphite, and

as shown in Table 3.6, this weight loss was mostly accounted for by the weight gain of the outer and inner crucibles due to adhering of the graphite powder.

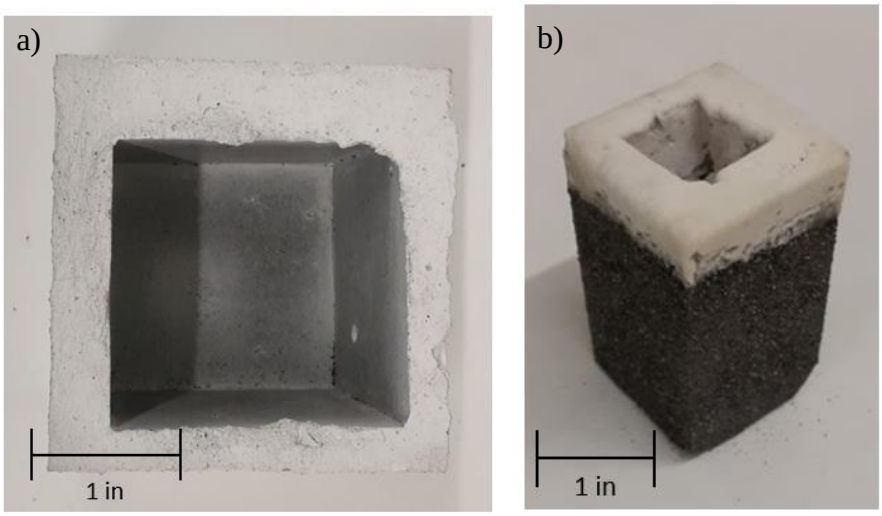

Figure 3.36. Photographs of: a) the outer CA_6C crucible and b) the inner CA_6C crucible after recovery of the graphite after 24 hr exposure to MKN salt at 750°C in Ar.

Table 3.6. Summary of the weight change values for each component in the multiwall assembly before and after the MKN salt penetration test at 750°C in Ar

	Associate Weight Before (g)	Associate Weight After (g)	Weight change (g)	Expected weight change (g)	Difference (g)
Graphite powder	83.88	80.91	-2.97	0	-2.97
Inner crucible	145.20	185.41[a]	40.21	37.77[b]	2.44
Outer crucible	546.82	547.29	0.47	0	0.47
a: weight with non-infiltrated salt remaining in the cavity	b: weight of total salt added (accounting for evaporation)			Total:	-0.06

To further confirm the low penetration of the salt into the graphite powder, XRD analysis of the graphite powder was conducted and described in Section 3.6.3. Due to the apparent low concentration of salt in the graphite powder, additional titration studies of the chloride solution obtained through prolonged water exposure of the graphite powder was performed to measure the chloride concentration and is described in Section 3.6.4.

3.6.3 XRD Analysis of Salt-Exposed Graphite Powder

The graphite powder was analyzed by XRD to observe if solidified salt peaks were detected in the sample. Since the salt signal was expected to be weak compared to the graphite, a longer scan time of 1.2 sec per step was used to distinguish the salt diffraction peaks from the background. Three samples were analyzed, and as shown in Figure 3.37., none of the samples exhibited evidence of solidified salt.

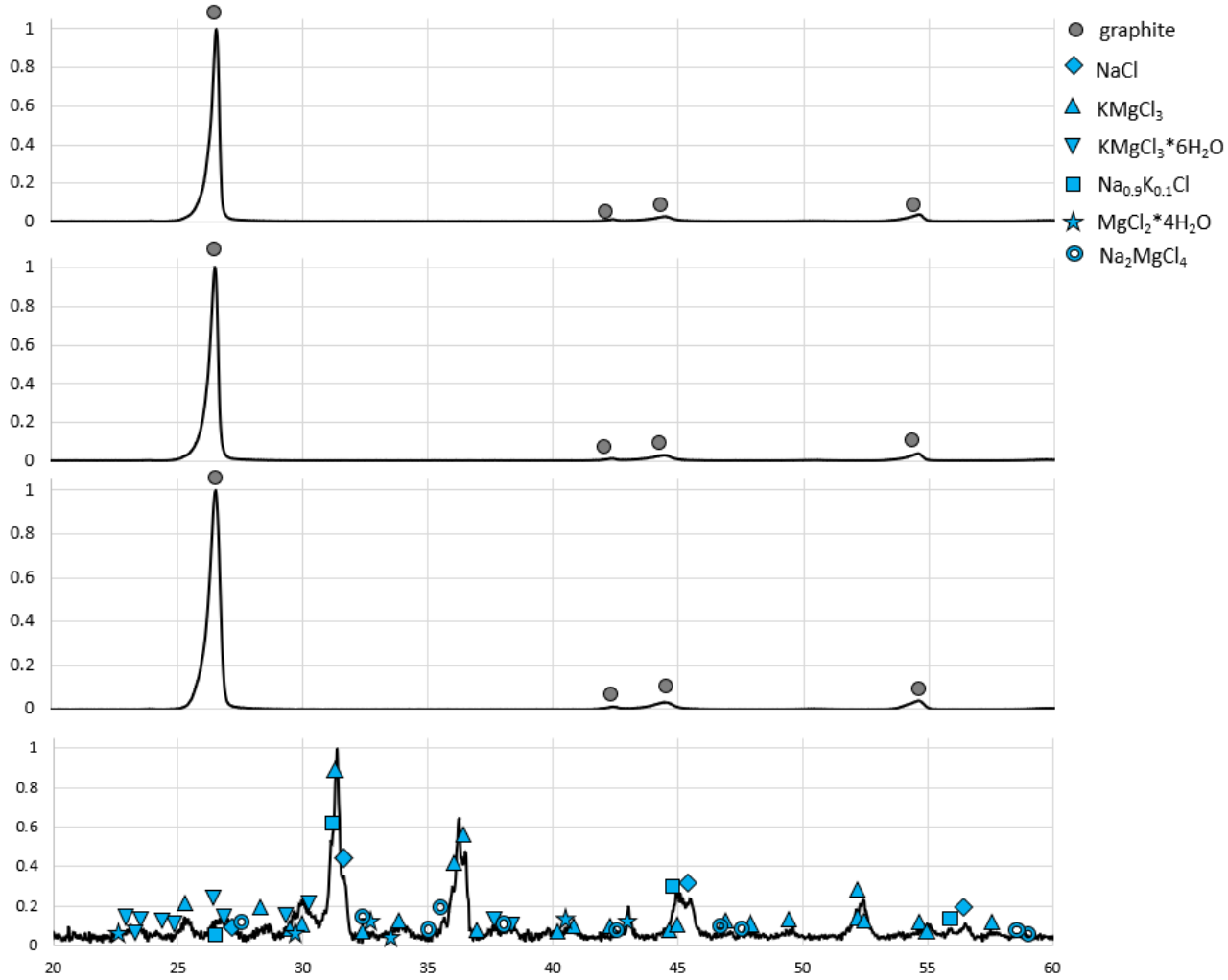

Figure 3.37. X-ray diffraction patterns: a), b), and c) of the graphite powder extracted from the multiwall assembly after exposure to MKN salt for 24 hr compared to d) solidified MKN salt as prepared in Section 2.2.

3.6.4 Titration to Determine Chloride Concentration in the Graphite Powder

The graphite powder (80.91 g) was immersed in 850 ml of ultrafiltered water (as described in Section 2.18) and stirred for 48 hr to dissolve potential salt adhering to the powder. The mixture

was then filtered through 11µm cellulose filter paper in a porcelain Buchner funnel. The collected solution was divided into three 100 ml vials and reserved for titration with silver nitrate ($AgNO_3$).

The collected filtrant solutions were titrated against a 0.1 N $AgNO_3$ solution, as described in Section 2.18. To each 100 ml sample, 1 ml of the indicator was added, then actively stirred with a magnetic stir bar while titrated with the $AgNO_3$ solution until the indicator changed from light yellow to orange. The titration was repeated three times for the water solution as well as the ultrafiltered Millipore water (which served as a control for the chloride concentration measurement). The resulting chloride concentration of the ultrafiltered water was 0.0027 ± 0.0006 M, which was consistent with the reported chlorine concentration in Milli-Q Direct Systems [42]. The resulting chloride concentration in the filtrant solutions was .0047 ± 0.0006 M. The difference between these values provided the chloride concentration of the graphite powder filtrate, which was 0.0020 M Cl^-. Assuming all the salt dissolved from the graphite, this would correspond to just 3 mg of salt in the 80.91 g of recovered graphite powder.

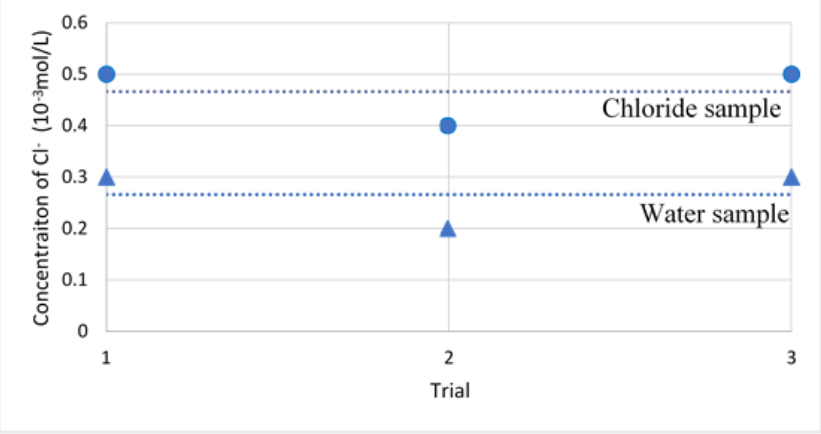

Figure 3.38. Titration results of ultrafiltered water compared to the solution obtained from the recovered graphite powder that contained solidified salt.

3.6.5 Cross-Section SEM-EDX Analysis

The inner and outer crucibles were cross-sectioned with a slow speed wafering blade in mineral oil, as described in Section 2.12. The mineral oil was refreshed between samples to prevent cross-contamination. As mentioned in Section 3.5.5, continued studies will include polishing these cross-sections to obtain more accurate EDX analysis in regions of interest.

The inner crucible was cross-sectioned to examine the bottom of the crucible, where salt was in contact with the MKN salt for the longest time. Photographs of the cross-sections are shown

in Figure 3.40.(a-c). Cross Section 1 shows the surface of the graphite powder adhered to the outer surface of the crucible. In the thickest region, the graphite layer was about 1 mm thick. SEM/BSE images combined with preliminary EDX point analysis showed chloride salt adhered around the graphite, with small grains of salt scattered throughout the entire graphite surface. The EDX spectra for the salt and graphite point analysis are provided in Figure 3.39.

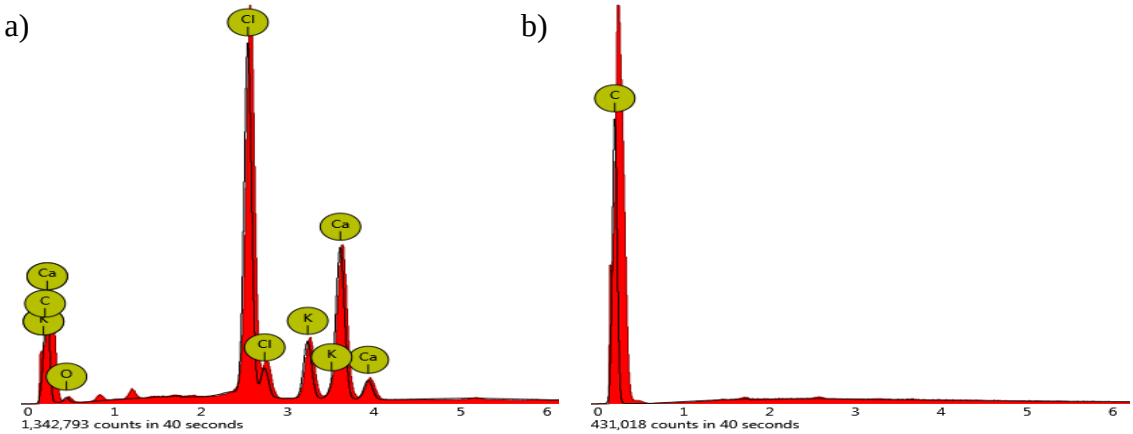

Figure 3.39. EDX patterns obtained from point analysis at: a) a white (salt) region and b) a dark (graphite) region.

The presence of small salt grains everywhere was consistent with graphite grains breaking off with some of the adhered salt during the analysis of the crucible. The adhered graphite thickness can be used to estimate the salt infiltration zone into the graphite powder, which would be about 1 mm thick at the bottom of the crucible.

The inner crucible was also cross-sectioned through the wall thickness at the bottom of the crucible. SEM and preliminary EDX analysis of Cross Section 2 (Figure 3.40.-e) showed salt at the crucible's outer wall with graphite adhered to the salt, which confirmed that salt fully penetrated through the inner crucible and interfaced with the graphite.

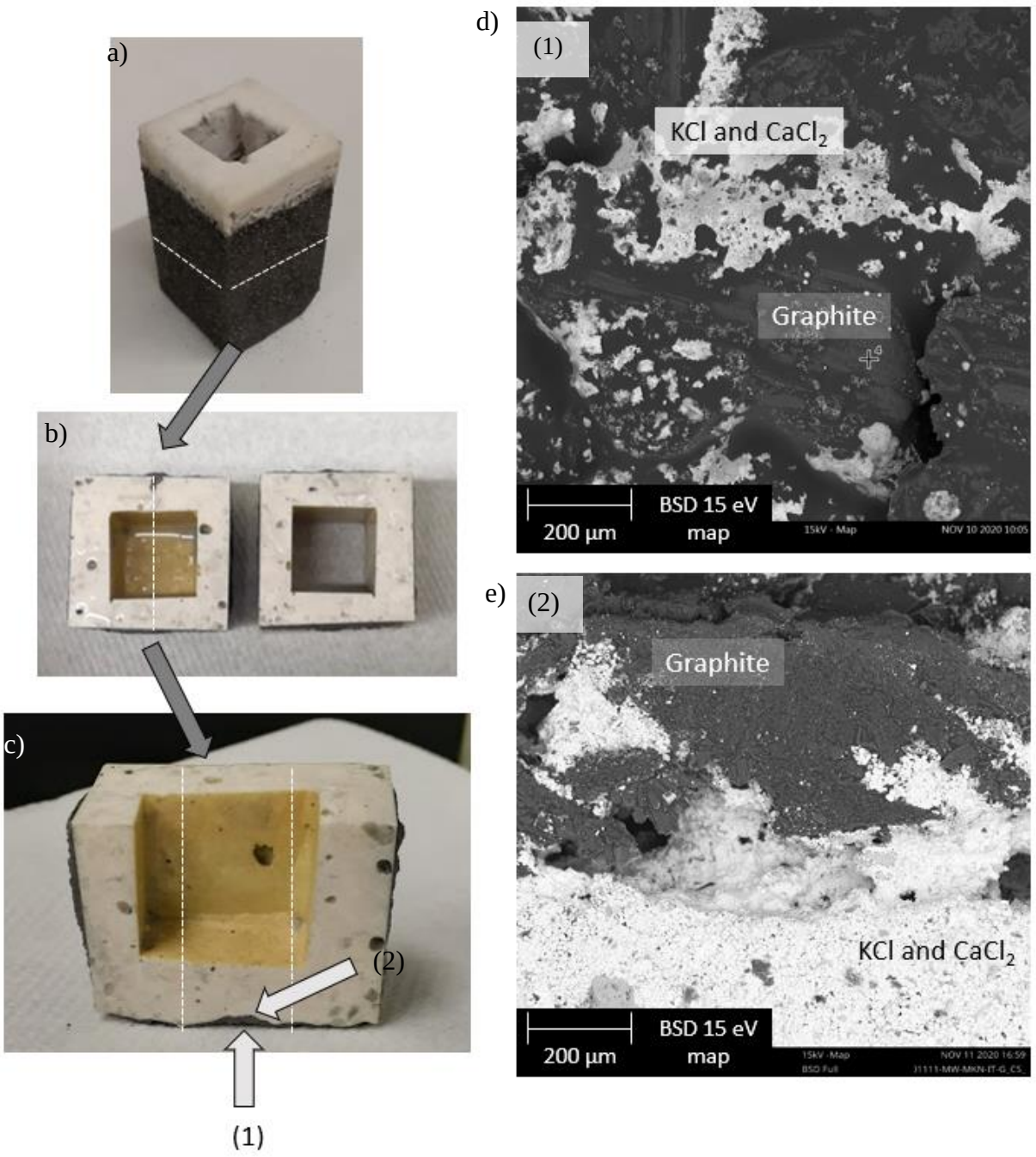

Figure 3.40. Photographs a)-c) show the inner crucible after 24 hr exposure to the MKN salt showing where samples were cross sectioned for SEM-EDX analysis, d) An SEM- Backscattered image of the graphite surface with apparent KCl and some $CaCl_2$ as determined by preliminary EDX analysis, and e) SEM-Backscattered image of graphite/crucible interface at the outer wall of the inner crucible.

The low penetration of the MKN salt through the graphite powder was consistently observed during characterization of the multiwall test after being filled with MKN salt and heated

to 750°C for 24 hr in Ar. Weight change measurements indicated a 2.97 g decrease in the recovered graphite powder, which was accounted for in the inner and outer CA_6C crucibles' weight gains. The salt infiltration depth into the graphite powder was estimated to be about 1 mm as determined by the SEM analysis of the adhered graphite layer thickness on the outer surface of the inner crucible. XRD analysis of the recovered graphite powder indicated a lack of MKN salt peaks in the spectra. This low concentration was confirmed through titration studies of the chloride solution obtained by soaking the graphite powder in water to remove the salt. Such titration studies indicated a small, 2 mM chloride concentration, which corresponded to 3 mg of salt in the graphite powder (out of 12 g of excess salt added). These characterization results suggest that a multiwall CA_6C crucible with a packed graphite powder bed was successful in preventing the penetration of the MKN salt. Such a multiwall design can offer low-cost carbon incorporation with castable ceramic that still allows the castable ceramic to be installed as one piece, removing mortar joints and decreasing transportation costs. Future studies of this design could include testing the infiltration with cheaper forms of carbon powder, which could reduce the cost of CSP thermal energy storage even further. Studies to determine the minimum thickness for a particular molten salt pressure head would also be necessary to use this method.

4. CONCLUSIONS

The objective of this thesis was to determine if the incorporation of carbonaceous materials with a castable ceramic cement could significantly decrease the penetration of molten MKN salt, as to identify a cost-effective solution for the containment of molten chloride salts at 750°C. Two types of carbon-ceramic composites were tested for their resistance to MKN salt infiltration at 750°C, and both displayed promising improvement of the molten MKN salt containment.

Powdered samples of Al_2O_3, CA/CA_2, CA_6, and $BaSO_4$ were screened for their chemical compatibility with molten MKN salt at 750°C. Of these materials, CA_6 showed the most resistance to the MKN salt after 24 hr at 750°C. A commercially available CA_6-based castable ceramic composition (CA_6C) was selected for further study as the ceramic component in the carbon-ceramic composites. Salt infiltration studies with a CA_6C crucible exhibited significant penetration (93.2%) after 2 hr of exposure to the MKN salt at 750°C, which indicated the need to modify the material if the CA_6C castable ceramic is to be used in thermal energy storage. A wetting experiment with the MKN salt on a graphite disk confirmed the salt's weak wetting behavior on a carbonaceous material. To incorporate carbonaceous material with the CA_6C crucibles, two methods were investigated: (i) through the direct incorporation of liquid pitch into the sample via pitch infiltration, which was followed by thermal treatment at $\geq$ 750°C to remove volatile carbonaceous materials, and (ii) by combining the CA_6C crucible with a packed-graphite powder bed to prevent the penetration of molten MKN salt.

Commercially pitch-infiltrated CA_6C crucibles were heat-treated at 750°C to remove volatile species, then used for infiltration studies with the MKN salt at 750°C. These studies revealed $\leq$12% infiltration of the molten salt into virgin samples after $\leq$100 hr exposure at 750°C. Additional studies with these samples revealed that annealing the crucible samples for 150 hr, thermocycling, and hydration-cycling the crucible samples did not significantly affect the molten salt infiltration into the samples.

To better control the carbon content and coverage, CA_6C crucibles were cast, and a pitch infiltration vessel was built at Purdue. CA_6C crucibles underwent three cycles of repeated pitch infiltration and subsequent firing at 850°C to remove volatile species. Each pitch infiltration cycle resulted in an increased cumulative weight gain and corresponding increased percentage of pores filled with carbonaceous material.

These multi-pitch infiltrated crucibles revealed ≤ 19% infiltration of the molten salt into samples after 100 hr exposure at 750°C. While these salt infiltration results were higher than the commercially-infiltrated crucibles, samples still displayed an 80-95% decrease in molten salt penetration compared to a carbon-free CA_6C crucible. Cross-sections of a multi-pitch infiltrated sample revealed uninfiltrated CA_6 grains, which could provide a surface salt to wet and penetrate if located near the crucible cavity. Future studies can be dedicated to infiltrating these CA_6 grains with higher pressure infiltration or use of lower viscosity pitch. Removing these large grains from the CA_6C composition could also enable the complete pitch infiltration of a crucible. Such studies could reveal that any aggregate can be used as long as enough pitch is present to thoroughly coat ceramic phases. This could enable the use of even cheaper castable ceramic compositions to further reduce the cost of thermal energy storage for CSP. Further work to estimate these carbon-castable ceramics' lifetime would progress their use in thermal energy storage.

Such pitch-infiltrated ceramics would likely require pre-infiltrated and fired bricks, which introduces costs associated with the brick transportation and assembly. While still a promising option, a multiwall-packed graphite powder bed approach would enable the use of a monolithic tank design and significantly simplify the incorporation of carbon with the castable cement, ultimately offering a more feasible option for CSP thermal energy storage.

An inner and outer CA_6C crucible were cast and fired to 750°C, then assembled with a packed graphite powder bed between them. This assembly was exposed to molten MKN salt at 750°C for 24 hr. Weight change measurements revealed no weight gain of the graphite powder or outer CA_6C crucible due to the salt. The low penetration of salt into the graphite powder was confirmed by XRD analysis and titration studies with the graphite powder. These measurements were consistent with SEM analysis of the graphite adhered to the inner crucible, which estimated an infiltration depth of about 1 mm into the graphite powder. Such characterization all pointed to low penetration of the salt into the graphite powder.

These studies of molten salt infiltration into the carbon-ceramic composites revealed that combining nonwetting carbonaceous materials with castable ceramics indeed displayed improved containment of the MKN salt at 750°C, suggesting a potential cost-effective containment solution for molten chlorides can be found in such carbon/ceramic composites to bring low-cost thermal energy storage for CSP to fruition.

APPENDIX A. THERMODYNAMIC CALCULATIONS

The standard Gibbs free energy of each reaction at 750°C was calculated based on the standard Gibbs Energy of Formation at 750°C (ΔG_f^o) of each compound involved. A summary of the values used in each calculation is provided in Appendix Table. 1.

Appendix Table. 1. A summary of standard enthalpy of formation and standard entropy for each substance used in the standard Gibbs free energy of reaction calculations

Compound	$\Delta G^o_{f,(750^oC)}$ (kJ/mole)	Reference
$MgCl_{2(l)}$	-479.900	[43]
$NaCl_{(l)}$	-316.743	[43]
$KCl_{(l)}$	-339.027	[43]
$Al_2O_{3(s)}$	-1353.698	[43]
$MgAl_2O_{4(s)}$	-1882.688	[44]
$MgO_{(s)}$	-524.190	[43] [45]
$CaCl_{2(s)}$	-638.821	[43]
$AlCl_{3(g)}$	-532.218	[43]
$CaAl_2O_{4(s)}$	-1922.024	[43]
$CaAl_4O_{7(s)}$	-3310.472	[43]
$CaAl_{12}O_{19(s)}$	-8709.624	[46]
$BaSO_{4(s)}$	-1075.809	[43]
$MgSO_{4(s)}$	-877.487	[43]
$BaCl_{2(s)}$	-696.103	[43]
$Na_2SO_{4(s)}$	-974.375	[43]
$K_2SO_{4(s)}$	-1012.230	[43]
$SO_{3(g)}$	-289.759	[43]

To calculate the Gibbs free energy, the following equation was used,

$$\Delta G^o_{rxn(750^oC)} = \sum n\Delta\, G^o_{f,products(750^oC)} - \sum m\Delta G^o_{f,reactants(750^oC)}$$

In the cases where $\Delta G^o_{rxn} > 0$, if a gaseous product was formed, then the following equation was used to calculate the minimum partial pressure needed to make $\Delta G^o_{rxn} < 0$

$$\Delta G^o_{rxn,eqm} = -RTlnK$$

where K is the equilibrium reaction quotient such that $K = (p_x)^n$ and p_x is the partial pressure of the gas. Such equations assume only gas is ideal and that any condensed phases present are present in their pure component reference states such that their activities are equal to 1. The resulting Gibbs free energy for reactions considered in Section 3.1 are summarized below.

Equation 1.) $Al_2O_{3(s)} + 3MgCl_{2(l)} = 3MgO_{(s)} + 2AlCl_{3(g)}$

$\Delta G^o_{rxn(750^oC)}$= +156.39 kJ

$p_{AlCl3,eqm}$= 1.02x10^{-4} atm

Equation 2.) $Al_2O_{3(s)} + MgO_{(s)} = MgAl_2O_{4(s)}$

$\Delta G^o_{rxn(750^oC)}$= -4.80 kJ

Equation 3.) $4Al_2O_{3(s)} + 3MgCl_{2(l)} = 3\ MgAl_2O_{4(s)} + 2AlCl_{3(g)}$

$\Delta G^o_{rxn(750^oC)}$= +141.99 kJ

$p_{AlCl3,eqm}$= 2.37x10^{-4} atm

Equation 4.) $CaAl_2O_{4(s)} + MgCl_{2(l)} = MgO_{(s)} + Al_2O_{3(s)} + CaCl_{2(l)}$

$\Delta G^o_{rxn(750^oC)}$= -114.79 kJ

Equation 5.) $CaAl_2O_{4(s)} + MgCl_{2(l)} = MgAl_2O_{4(s)} + CaCl_{2(l))}$

$\Delta G^o_{rxn(750^oC)}$= -119.59 kJ

Equation 6.) $4CaAl_2O_{4(s)} + 7MgCl_{2(l)} = 4MgO_{(s)} + 3MgAl_2O_{4(s)} + 4CaCl_{2(l)} + 2AlCl_{3(g)}$

$\Delta G^o_{rxn(750^oC)}$= -317.15 kJ

Equation 7.) $CaAl_4O_{7(s)} + MgCl_{2(l)} = MgO_{(s)} + 2Al_2O_{3(s)} + CaCl_{2(l)}$

$\Delta G^o_{rxn(750^oC)}$= -80.04 kJ

Equation 8.) $CaAl_4O_{7(s)} + MgCl_{2(l)} = MgAl_2O_{4(s)} + Al_2O_{3(s)} + CaCl_{2(l)}$

$\Delta G^o_{rxn(750^oC)}$= -84.84 kJ

Equation 9.) $CaAl_4O_{7(s)} + 4MgCl_{2(l)} = 3MgO_{(s)} + MgAl_2O_{4(s)} + CaCl_{2(l)} + 2\ AlCl_{3(g)}$

$\Delta G^o_{rxn(750^oC)}$= +71.56 kJ

$p_{AlCl3,eqm}$= 0.149 atm

Equation 10.) $CaAl_{12}O_{19(s)} + MgCl_{2(l)} = MgO_{(s)} + 6Al_2O_{3(s)} + CaCl_{2(l)}$

$\Delta G^o_{rxn(750^oC)}$= -95.68 kJ

Equation 11.) $CaAl_{12}O_{19(s)} + MgCl_{2(l)} = MgAl_2O_{4(s)} + 5Al_2O_{3(s)} + CaCl_{2(l)}$

$\Delta G^o_{rxn(750^oC)}$= -100.48 kJ

Equation 12.) $BaSO_{4(s)} + MgCl_{2(l)} = BaCl_{2(l)} + MgSO_{4(s)}$

$\Delta G^{o}_{rxn(750^{o}C)}$ = -17.88 kJ

Equation 17.) $BaSO_{4(s)} + MgCl_{2(l)} = BaCl_{2(s)} + MgO_{(s)} + SO_{3(g)}$

ΔG^{o} (750°C)= +45.66 kJ

$p_{AlCl3,eqm}$ = 4.66x10^{-3} atm

Equation 13.) $BaSO_{4(s)} + 2NaCl_{(l)} = BaCl_{2(l)} + Na_2SO_{4(s)}$

$\Delta G^{o}_{rxn(750^{o}C)}$ = +38.82 kJ

Equation 14.) $BaSO_{4(s)} + 2KCl_{(l)} = BaCl_{2(l)} + K_2SO_{4(s)}$

$\Delta G^{o}_{rxn(750^{o}C)}$ = +45.53 kJ

Equation 15.) $MgSO_{4(s)} + 2NaCl_{(l)} = MgCl_{2(l)} + Na_2SO_{4(s)}$

$\Delta G^{o}_{rxn(750^{o}C)}$ = +56.70 kJ

Equation 16.) $MgSO_{4(s)} + 2KCl_{(l)} = MgCl_{2(l)} + K_2SO_{4(s)}$

$\Delta G^{o}_{rxn(750^{o}C)}$ = +63.42 kJ

APPENDIX B. PITCH INFILTRATION TRIALS

Proceeding the multi-pitch infiltrated samples used in Section 3.4.9, multiple pitch infiltration trials were necessary to develop a procedure that successfully coated the CA_6C crucible samples inside the pressure vessel assembly at Purdue. The initial, general procedure was designed to replicate the process used by Servsteel as closely as possible. Cast CA_6C samples that had been fired at 850^{o}C for 11-13 hr in air were placed on stainless steel baskets in the cube-shaped cavities of the aluminum sample holder. Pitch was warmed to 70^{o}C or 120^{o}C in an oven, then deposited on the top of the crucibles until the cavities were filled. After sealing the assembly in the pressure vessel, the vessel was evacuated using a roughing pump (capable of achieving a vacuum pressure of 30 mTorr), held at this pressure for 2 min, and then backfilled with Ar to 1 atm. This process of evacuation and Ar backfilling was conducted three times. The vessel was then actively evacuated with the roughing pump while it was heated at either 50^{o}C/hr or 100^{o}C/hr to 182^{o}C. The temperature was held at 182^{o}C under vacuum for 45 min, then pressurized with industrial-grade Ar to 60 psi. The vessel was held for 45 min at 60 psi; then the furnace was cooled at 180^{o}C/hr to 100^{o}C while maintaining the Ar pressure at 60 psi. Upon reaching 100^{o}C, the pressure was reduced to 1 atm, and the pressure vessel was opened for removal of the crucible specimens. The mesh baskets were used to pull the CA_6C crucible specimens out of the remaining excess pitch in the aluminum sample holder's cavities, and the non-infiltrated pitch remaining in the central cavity of each CA_6C crucible specimen was poured out. The CA_6C crucibles were then placed on a stainless steel tray to continue cooling to room temperature in ambient air. A summary of the conditions used for each pitch infiltration trial and the resulting % weight gain is summarized in Appendix Table. 2.

.

Appendix Table. 2. Summary of the conditions used and resulting % weight gain of the samples during initial pitch infiltration trials

	Infiltration Trial 3.1	Infiltration Trail 4.1	Infiltration Trial 5.1	Infiltration Trial 6.1	Infiltration Trial 7.1
Temperature of preheated pitch (^oC)	70	120	120	120	120
Heating rate (^oC/hr)	100	100	100	50	50
Outgassing temperature of the pitch (^oC)	25	25	25	25	120
Volume of pitch in holder cavity (cm^3)	280	280	570	280	280
% weight gain of sample	3.0	3.8	2.8	4.7	11.2

Pitch Infiltration 3.1: 70^{o}C Preheated Pitch

For the preparation of the pitch for Infiltration Trial 3.1, the pitch was preheated to 70^{o}C, and the resulting viscous pitch was dolloped onto a CA_6C crucible sample within the aluminum sample holder. After cooling to room temperature, the specimen holder containing the pitch/ CA_6C crucible was sealed in the stainless-steel pressure vessel, and the vessel was evacuated and backfilled 3 times with industrial-grade Ar at room temperature (as discussed above). The vessel was then evacuated and heated at 100^{o}C/hr to 182^{o}C. The sample saw the 45 min vacuum and pressure treatments followed by cooling as described above. A photograph of the CA_6C crucible 3.1 exposed to this trial is provided in Appendix Figure 2**.**-a. Visual inspection of this crucible's external faces indicated that the crucible had not been completely coated with pitch (i.e., much of the area of the top face and the upper regions of the side faces of this crucible did not exhibit a dark black color). The mass gain of the crucible after such pitch infiltration was a modest 3.0%. An appreciable amount of pitch had also accumulated outside of (and below) the aluminum crucible holder (i.e., significant outward flow of the pitch occurred away from the crucible and aluminum sample holder). The relatively high viscosity of the pitch at 70^{o}C may have prevented the sample holder from being filled with enough pitch to coat the CA_6C crucible.

Pitch Infiltration 4.1 and 5.1: 120^{o}C Preheated Pitch and a Larger Sample Holder

For the setup of infiltration trials 4.1 and 5.1 (and subsequent trials), pitch was preheated to 120^{o}C, and the more fluid pitch was poured over the CA_6C crucibles. For infiltration trial 5.1, a larger stainless-steel container (4.1 in. internal diameter x 3.98 in. internal height, Appendix Figure

1.-b) was used to provide a greater volume of pitch over and around the CA_6C crucible; that is, the volume available for pitch above and around this crucible was about two times larger than for the CA_6C crucible in the aluminum sample holder for trial 4.1. After cooling to room temperature, the pitch/CA_6C crucible assemblies for trial 4.1 and 5.1 were sealed together in the pressure vessel and exposed to the same infiltration conditions as for trial 3.1. (i.e., the pitch was pushed out of the holder by expanding gas trying to escape from below the pitch).

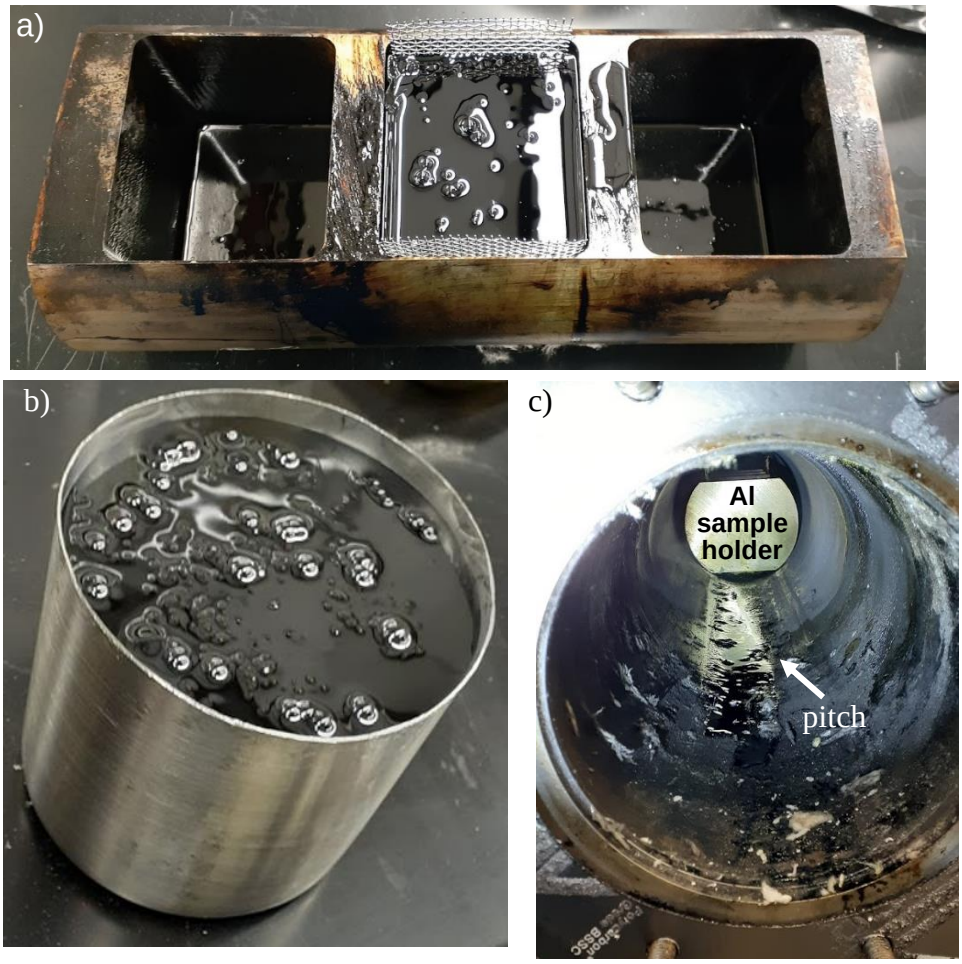

Appendix Figure 1. Photographs of: a) the aluminum sample holder containing the sample used in Trial 4.1, b) the stainless steel crucible holder used for the pitch infiltration trial 5.1 with pitch poured over the CA_6C crucible, and c) the inside of the stainless steel pressure vessel after the infiltration of 4.1, showing a large accumulation of pitch at the bottom of the tube.

The crucible mass gain after pitch infiltration trial 4.1 (3.8%) was slightly higher than for infiltration trial 3.1. The mass gain for pitch infiltration trial 5.1 was only 2.8%. Visual inspection of the faces of crucibles 4.1 and 5.1 (Appendix Figure 2.-b, and -c, respectively) again indicated that these crucibles had not been completely coated with pitch. Pitch was again detected outside

of (and below) the aluminum crucible holder and the stainless steel holder, as shown in Appendix Figure 1.-c). The migration of pitch out of the aluminum sample holder during evacuated heating was attributed to pressure applied by the expansion of gas trapped below the viscous pitch

Pitch Infiltration 6.1 50°C/hr heating rate

To slow the rate of such gas expansion and provide more time for the gas to migrate through the heated pitch (instead of pushing the pitch out of the holder), infiltration trial 6.1 was conducted under vacuum with a heating rate of 50°C/hr (instead of 100°C/hr) between room temperature and 182°C. The mass gain of the CA_6C crucible for pitch infiltration trial 6.1 was higher than for trials 3.1 and 4.1, but still only 4.7%. Visual inspection of the faces of this crucible 6.1 (Appendix Figure 2.-d) again indicated incomplete coating with pitch, and the pitch was again found to have been displaced from the aluminum sample holder.

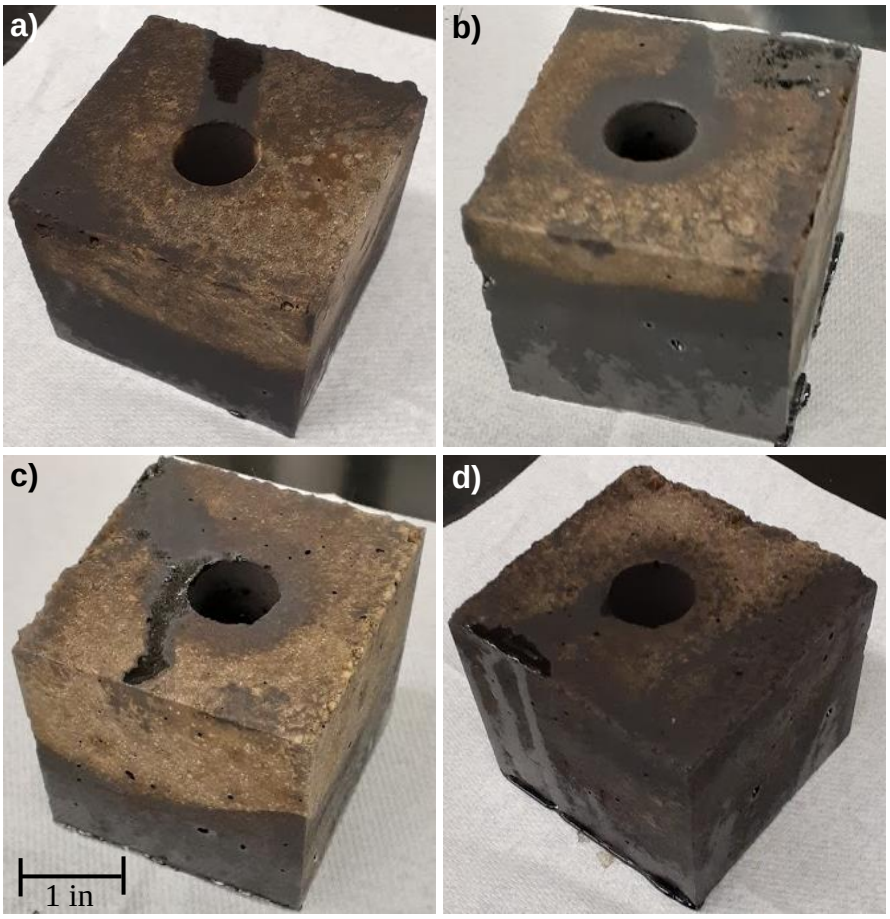

Appendix Figure 2. Photographs of CA_6C crucibles are pitch infiltration trials: a) 3.1, b) 4.1, c) 5.1, and d) 6.1.

Pitch Observations in a Vacuum Oven

To directly observe the flow behavior of the pitch, experiments were then conducted within an evaluable oven with a transparent window. Pitch-loaded CA_6C crucibles were evacuated at room temperature using a roughing pump. Large gas bubbles were observed to form and burst at the surface of the viscous pitch, as shown in Appendix Figure 3.-a, although the pitch did not overflow the aluminum sample holder during evacuation at room temperature. After 3 cycles of evacuation and backfilling with industrial-grade Ar (1 atm pressure), the oven was evacuated and heated at 60°C/hr. At temperatures between 40°C and 80°C, significant gas bubbling through the pitch and appreciable flow of pitch out of the aluminum sample holder were observed (Appendix Figure 3.-b). Upon further heating to temperatures between 110°C and 120°C, a modest rate of gas bubble formation in the pitch, without additional pitch flow out of the specimen holder, was observed. Further heating to temperatures between about 140°C and 182°C resulted in a noticeably higher gas bubble formation rate.

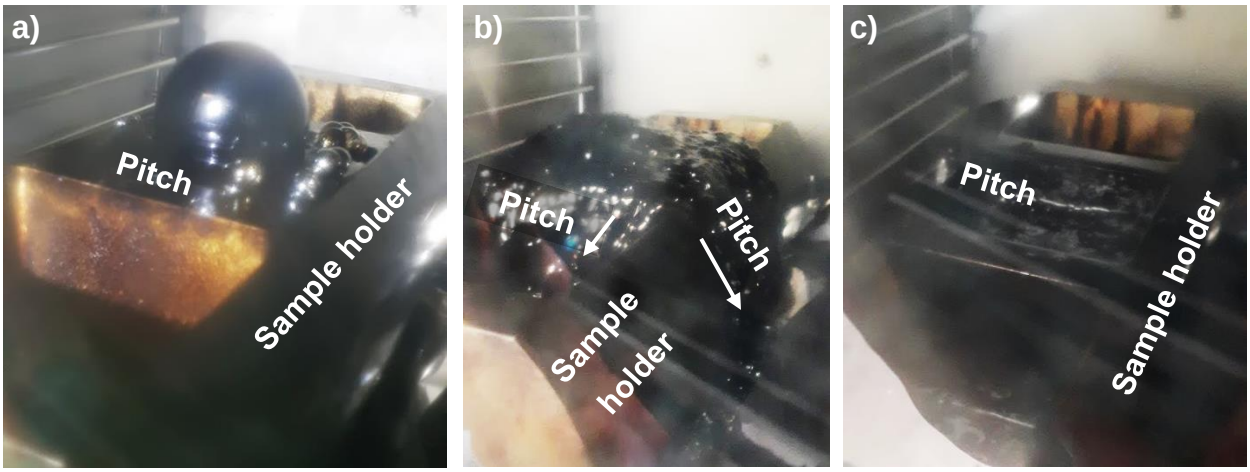

Appendix Figure 3. Photographs through the window of a vacuum oven during: a) evacuation at 22°C for a pitch-loaded CA_6C crucible in the aluminum sample holder, b) heating of the same sample to 62°C while under vacuum, and c) heating the same sample under vacuum to 112°C.

A second experiment in this vacuum oven was then conducted by heating a pitch-loaded CA_6C crucible in the aluminum sample holder to 120°C at 1 atm pressure and holding under this condition for 1 hr. Three cycles of evacuation at 120°C and backfilling with industrial-grade Ar (1 atm pressure) at 120°C were then conducted, followed by evacuation and holding at 120°C. With this treatment, a relatively modest rate of gas bubbling through the pitch, without overflow of the pitch out of the aluminum sample holder, was observed. These direct observations indicated that

evacuation should be conducted after the pitch was heated to 120°C to avoid appreciable displacement of the viscous pitch from the aluminum specimen holder upon gas expansion from below the pitch.

Pitch Infiltration 7.1: Outgassing through 120°C Pitch

Pitch infiltration trial 7.1 was then conducted using the procedure discussed in Section 2.8, where pitch-loaded samples were placed in the pressure vessel and heated 120°C in ambient air for 1 hr before conducting the three cycles of evacuation/backfilling at 120°C. The crucible mass gain after this trial (11.2%) was significantly higher than for the previous infiltration trials, and overflow of the pitch out of the aluminum specimen holder was not observed. Visual inspection of this crucible (Appendix Figure 4.) indicated that the pitch had coated, and infiltrated into, the crucible from all 6 faces. Indeed, this pitch-infiltrated crucible exhibited a similar appearance as the pitch-infiltrated CA_6C crucibles previously provided by Servsteel (which were generated by complete immersion of the CA_6C crucibles in liquid pitch).

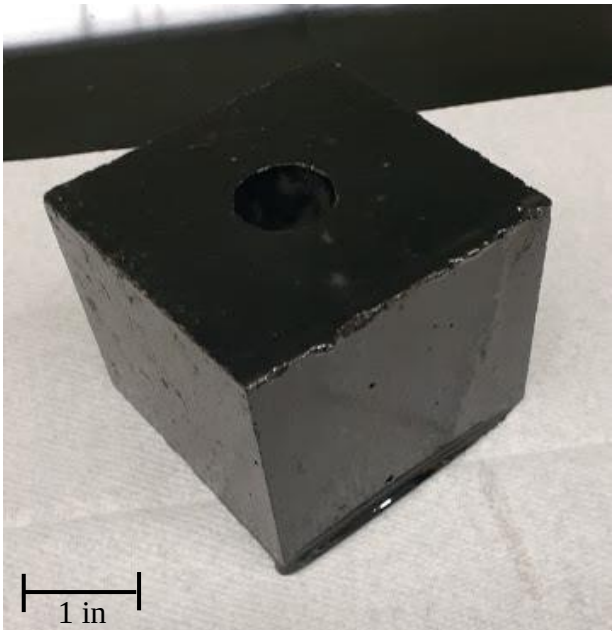

Appendix Figure 4. A photograph of CA_6C crucible after pitch infiltration trial 7.1.

A Note About Gaskets

Due to an unfortunate miscommunication with Servsteel, pitch infiltration trials 1.1 and 2.1 at Purdue were conducted at a peak temperature of 360°C, rather than 360°F (182°C) as used at Servsteel. During these high-temperature infiltration trials, a Viton gasket was used to seal the pressure vessel, and during both cases, the gasket blew out while approaching or holding at 60 psi. These Viton gaskets were replaced with graphite gaskets, which were found to be more mechanically robust. All subsequent trials were conducted at a peak temperature of 182°C with such graphite gaskets and the pressure vessel has operated without failure.

REFERENCES

[1] U.S Energy Information Administration DOE/EIA, "International Energy Outlook 2016," U.S. Energy Information Administration, Washington DC, 2016.

[2] U.S. Energy Information Administration, "U.S. energy facts explained," U.S. Energy Information Administration, 7 May 2020. [Online]. Available: https://www.eia.gov/energyexplained/us-energy-facts/. [Accessed 18 11 2020].

[3] U.S. Department of Energy, "SunShot Vision Study," U.S. Department of Energy, 2012.

[4] National Renewable Energy Laboratory, "The Potential Role of Concentrating Solar Power within the Context of DOE's 2030 Solar Costs Target," NREL, Golden, 2019.

[5] U.S. Department of Energy, "On the Path to Sunshot; Executive Summary," Solar Energy Technologies Office: DOE, 2016.

[6] S. Kuravi, J. Trahan, D. Y. Goswami, M. M. Rahman and E. K. Stefanakos, "Thermal energy storage technologies and systems for concentrating solar power plants," *Progress in Energy and Combustion Science,* vol. 39, pp. 285-319, 2013.

[7] G. Mohan, M. B. Venkararaman and J. Coventry, "Sensibile energy storage options for concentrating solar power plants operating above 600^{o}C," *Renewable and Sustainable Energy Reviews,* vol. 107, pp. 319-337, 2019.

[8] Lazard, "Lazard's Levelized Cost of Energy Analysis- Version 14.0," October 2020. [Online]. Available: https://www.lazard.com/media/451419/lazards-levelized-cost-of-energy-version-140.pdf. [Accessed 12 11 2020].

[9] E. Karatairi and A. Ambrosini, "Improving the efficiency of concentrating solar power systems," *MRS Bulletin,* vol. 43, no. 12, pp. 920-921, 2018.

[10] U. Pelay, L. Luo, Y. Fan, D. Stitou and M. Rood, "Thermal energy storage systems for concentrated solar power plants," *Renewable and Sustainable Energy Reviews,* pp. 82-100, 2017.

[11] W. Ding, A. Bonk and T. Bauer, "Corrosion behavior of metallic alloys in molten chloride salts for thermal energy storage in concentrated solar power plants: A review," *Frontiers of Chemical Science and Engineering,* vol. 12, no. 3, pp. 564-576, 2018.

[12] K. Vignarooban, X. Xu, A. Arvay, K. Hsu and A. M. Kannan, "Heat Transfer Fluids for Concentrating Solar Power Systems- A Review," *Applied Energy,* vol. 146, pp. 383-396, 2015.

[13] W. Ding, H. Shi, A. Jianu, Y. Xiu, A. Bongk, A. Weisenburger and T. Bauer, "Molten Chlorides for Next Generation Concentrated Solar Power Plants: Mitigation Strategies Against Corrosion of Structural Materials," *Solar Energy Materials and Solar Cells,* vol. 193, pp. 298-313, 2019.

[14] P. D. Myers and D. Y. Goswami, "Thermal Energy Storate Using Chloride Salts and Their Eutectics," *Applied Thermal Engineering,* Vols. 109, Part B, pp. 889-900, 2016.

[15] Y. Zhao and J. Vindal, "Potential Scalability of a cost-effective purification method for MgCl2-Containing Salts for Next-Generation Concentration Solar Power Technologies," *Solar Energy Materials and Solar Cells,* vol. 215, p. 110663, 2020.

[16] G. Y. Lai, "Molten Salt Corrosion," in *High-Temperature Corrosion and Materials Applications,* ASM International, 2007, pp. 409-421.

[17] W. Ding, J. G.-. Vindal, A. Bonk and T. Bauer, "Molten Chloride Salts for Next Generation CSP Plats: Electrolytical Salt Purification for Reducing Corrosive Impurities," *Solar Energy Materials and Solar Cells,* vol. 199, pp. 8-15, 2019.

[18] Solar Energy Technologies Office, "Thermal Storage R&D for CSP Systems," DOE: Office of Energy Efficiency & Renewable Energy, [Online]. Available: https://www.energy.gov/eere/solar/thermal-storage-rd-csp-systems. [Accessed 21 11 2020].

[19] M. Takeuchi, T. Kato, K. Hanada, T. Koizumi and S. Aose, "Corrosion REsistance of Ceramic Materials in Pyrochemical reprosessing condition by suing molten salt for spent nuclear oxide fuel," *Journal of Physics and Chemsitry of Solids,* vol. 66, pp. 521-525, 2004.

[20] D. F. Mclaughlin, C. E. Sessions and J. E. Marra, "Corrosion Behavior of Silicon Nitride, Magnesium Oxide, and Several Metals in Molten Calcium Chloride and Chlorine," *Nuclear Technology,* vol. 99, pp. 242-250, 1992.

[21] C. E. Rense, K. W. Fife, D. F. Bowersox and M. D. Ferran, "Materials Compatability During the Chlorination of Molten $CaCl_2$·CaO Salts," Loa Alamos National Laboratory, Los Alamos, 1987.

[22] W. E. Lee and S. Zhang, "Principles of Corrosion Resistance: Hot Liquids," *International Materials Review,* vol. 44, no. 3, pp. 77-104, 1999.

[23] P. Sengupta, Refractories for the Cement Industry, Cham, Switzerland: Springer Nature, 2019.

[24] W. E. Lee, W. Vieire, S. Zhang, K. G. Ahari, H. Sarpoolaky and C. Parr, "Castable Refractory Concretes," *International Materials Review,* vol. 6, no. 3, pp. 145-167, 2001.

[25] Y. Grosu, L. Gonzalez-Fernandez, U. Nithiyanantham and A. Faik, "Wettability Control for Correct Thermophysical Properties Determination of Molten Salts and Their Nanofulids," *Energies,* vol. 12, no. 19, 2019.

[26] E. Grambaloba, J. Petrik and P. Vadasz, "Interaction of Molten Salts in the System SiO_2-Al_2O_3," *Ceramica,* vol. 59, no. 352, pp. 570-575, 2013.

[27] P. Baumli and G. Kaptay, "Wettability of carbon surfaces by pure molten alkali chlorides and their penetration into a porous graphite substrate," *Materials Science and Engineering A,* vol. 495, pp. 192-196, 2008.

[28] P. Baumli and G. Kaptay, "Wettability of carbon surfaces by Molten Alkali Chloride Mixtures," *Materials Science Forum,* vol. 2008, pp. 355-359, 2008.

[29] B. Cullen, Interviewe, *Email Correspondance Based on WAM Test Method #1 (revision No. 1, 6-18-17).* [Interview]. 19 11 2018.

[30] Westmoreland Advanced Materials, *Typical Technical Data WAM BLG,* Monessen, PA: Westmoreland Advanced Materials, LLC, 2019.

[31] Carbon Graphite Materials, Inc., "Products: Synthetic Graphite," Carbon Graphite Materials, Inc., 2020. [Online]. Available: http://cgm-inc.net/products/. [Accessed 27 11 2020].

[32] P. Koshy, S. Gupta, P. Edwards and V. Sahajwalla, "Effect of $BaSO_4$ on the Interfacial Phenomena of High-Alumina Refractories with Al-Alloy," *Journal of Materials Science,* vol. 46, no. 2, pp. 468-478, 2011.

[33] H. Fink and H. J. Seifert, "Quarternary Compounds in the System KCl/NaCl/$MgCl_2$," *Thermochimia Acta*, vol. 72, no. 1-2, pp. 195-200, 1984.

[34] National Center for Biotechnology Information, " PebChem Compound Summary for CID 24012, Alumunium Chloride," 2020. [Online]. Available: https://pubchem.ncbi.nlm.nih.gov/compound/Aluminum-chloride. [Accessed 23 11 2020].

[35] L. Wang, B. Oye, M. Becidan, J. Stuen and O. Skreiberg, "Ash Deposites Characterization in a Large-Scale Municipal Waste-to-Energy Inceineration Plant," *Chemical Engineering Transactions*, vol. 50, pp. 25-30, 2016.

[36] NIST Materials Management Laboratory, "IUPAC-NIST Solubility Database, Version 1.1 NIST Standard Reference Database 106," IUPAC-NIST Solubility Data Series, 18 Februrary 2015. [Online]. Available: https://srdata.nist.gov/solubility/index.aspx. [Accessed 11 11 2020].

[37] "Proceedings of the Raw Materials for Refractories Conference: A Collection of Papers Presented at the Raw Materials for Refractroies Conference," in *American Ceramic Society*, Columbus, OH, 1983.

[38] ASME, Process Piping: ASME Code for Pressure Piping, B31, New York: The American Society of Mechanical Engineers, 2017.

[39] Little P. Eng. for Engineers Training, "ASME B31.3 2014 Process Piping- Weld Joint Strength Reduction Factors," 10 7 2017. [Online]. Available: https://www.littlepeng.com/single-post/2017/07/13/asme-b313-weld-joint-strength-reduction-factors. [Accessed 28 11 2020].

[40] Lonestar, *Safety Data Sheet Petroleum PItch*, Texas: Lonestar Specialties LLC, 2019, shared by email correspondance.

[41] U.S. Department of Commerce/National Bureau of Standards, "Physical Properties Data Compilations Relevant to Energy Storage," in *IV. Molten Salts: Data on Additional Single and Multi-Component Salt Systems*, Washington, DC, U.S. Government Printing Office Washington, 1981, pp. 371-378.

[42] Millipore Sigma, "Milli-Q Direct Water Purification System," 2020. [Online]. Available: https://www.emdmillipore.com/US/en/product/Milli-Q-Direct-Water-Purification-System,MM_NF-C85358?CatalogCategoryID=#specifications. [Accessed 13 November 2020].

[43] I. Barin, Thermochemical Data of Pure Substances, Weinheim, Germany: Velt Verlogsgesellschaft, 1995.

[44] R. Robie and D. Waldbaum, Thermodynamic Properties of Minerals, Washinton: Geological Survey Bulletin, United States Government Printing Office, 190.

[45] K. V. gourishankar, M. Karamineshad Ranjbar and G. R. S. Pierre, "Revision of the Enthalpies and Gibbs Energies of Formation of Calcium Oxide and Magnesium Oxide," *Journal of Phase Equilibria,* vol. 14, no. 5, pp. 601-611, 1993.

[46] B. Hallstedt, "Assessment of the $CaO-Al_2O_3$ System," *Journal of the American Ceramic Society,* vol. 73, no. 1, pp. 15-23, 1990.

[47] I. E. Agency, "Concentrating Solar Power, IEA Technology Roadmaps," *OECD Publishing,* 2010.

[48] R. Musi, B. Grange, S. Sgouridis, R. guedez, P. Armstrong, A. Slocum and N. Calvet, "Techno-economic analysis of concentrated solar power plants in terms of levelized cost of electricity," *AIP Conference Proceedings 1850,* 2017.

[49] C. Guo, S. Shang, Z. Du, M. C. Gao, P. D. Jablonski and Z.-K. Liu, "Thermodynamic modeling of the $CaO-CaF_2-Al_2O_3$ system aided by first-principles calcuations," *Calphad,* vol. 48, pp. 113-122, 2015.

VITA

Elizabeth Laskowski was born in Madison, Wisconsin, on May 19, 1996. She attended Osseo-Fairchild Elementary, Middle, and High School, where she graduated with highest honors in May 2014. The following fall she attended the University of Wisconsin-Eau Claire, where she spent 4 years studying thermo-responsive smart polymers and was a Goldwater Scholarship Honorable Mention. In the Summer of 2017, Elizabeth also worked for the Extreme Light Lab at the University of Nebraska-Lincoln as a research assistant studying gas density profiles through interferometry techniques. In May 2018, she graduated from UW-Eau Claire magna cum laude with university honors and a bachelor's degree in Materials Science, with an emphasis in the chemistry of materials. In the fall of 2018, she attended Purdue University in the Materials Engineering Ph.D. program, where she was awarded a Ross Fellowship and spent 2 years investigating ceramic-based containment solutions for molten chloride salts. In December 2020, she received a master's degree in Materials Engineering from Purdue University and is excited for the next chapters in her career.